Flexibility Provisions from Energy Storage Systems and Loads in Smart Grid

by

Omar Alrumayh

A thesis
presented to the University of Waterloo
in fulfillment of the
thesis requirement for degree of
Doctor of Philosophy
in
Electrical and Computer Engineering

Waterloo, Ontario, Canada, 2021

Examining Committee Membership

The following served on the Examining Committee for this thesis. The decision of the Examining Committee is by majority vote.

External Examiner:	Bala Venkatesh, Professor, Dept. of Electrical and Computer Engineering, Ryerson University
Supervisor:	Kankar Bhattacharya, Professor, Dept. of Electrical and Computer Engineering, University of Waterloo
Supervisor:	Steven Wong, Adjunct Associate Professor, Dept. of Electrical and Computer Engineering, University of Waterloo, Home Affiliation: Natural Resources Canada
Internal Member:	Magdy Salama, Professor, Dept. of Electrical and Computer Engineering, University of Waterloo
Internal Member:	Ramadan El-Shatshat, Lecturer, Dept. of Electrical and Computer Engineering, University of Waterloo
Internal-External Member:	Ali Elkamel, Professor, Dept. of Chemical Engineering, University of Waterloo

Author's Declaration

I hereby declare that I am the sole author of this thesis. This is a true copy of the thesis, including any required final revisions, as accepted by my examiners.

I understand that my thesis may be made electronically available to the public.

Abstract

Electric power systems are experiencing a movement toward increasing the share of renewable energy sources (RESs), while having to cope with the retirement of conventional generating units to facilitate an eco-friendly system. However, the uncertainty and variability associated with RESs and the demand, call for additional sources of flexibility. Residential, commercial, and industrial loads are a potential source of flexibility in power systems. In addition, recent deployments of energy storage systems (ESSs) can contribute significantly to power system flexibility. Therefore, the effective management of flexible sources can lead to an improved power system operation.

This thesis investigates options for capturing the flexibility of residential loads and ESSs in a power distribution system. A two-stage optimization framework is developed wherein multiple home energy management systems (HEMSs) simultaneously optimize their respective energy consumption patterns, and determines their flexibility provisions, which are communicated to the local distribution company (LDC). A flexibility evaluation approach is developed to estimate the residential energy hub (REH) flexibilities at each bus in the distribution system. Intra-hour flexibility indices are calculated to represent the REHs' willingness to alter their consumptions. Different clusters of residential customers are considered, classified by their ownership of photovoltaic (PV) panels and ESSs, and their preferred objectives. The LDC aggregates the controllable demand profiles and the flexibilities of each HEMS to optimize its operational performance and hence determines peak reduction signals that are sent to the HEMSs. Studies are carried out considering a 33-bus distribution system coordinating with 1,295 houses connected at different buses, with varying customer preferences and objectives, to demonstrate the applicability of the proposed scheme.

ESSs can improve the energy management in distribution systems, especially with the increasing penetration of HEMSs that schedule household appliances and render them as smart loads. A large number of uncoordinated HEMSs can result in significant changes to the aggregated load profile of the distribution system. Therefore, a new framework and mathematical model for integrating ESSs in the distribution grid is proposed to minimize the operation cost of the LDC and to alleviate the impact of uncoordinated HEMS

operation on the distribution grid. A novel neural network (NN) based state-of-health (SoH) estimator for a lithium-ion (Li-ion) battery based ESS is proposed, which is incorporated within the LDC's planning problem. The results show that the proposed estimation model is an accurate estimation of the SoH of the ESS. Also, the LDC's ESS investment plan decisions are compared considering the proposed SoH of the ESS vis-á-vis a linear degradation model, and when degradation of ESS is not considered in planning.

The third research problem addressed in the thesis investigates the ESS's role in providing the LDC with flexibility services. A novel flexibility service framework is developed based on the battery energy storage system (BESS)s' capability in providing different levels of charge rate (C-Rate). This work proposes a cooperative game theory based approach to determine the allocation of monetary benefits among flexible BESSs. The proposed model ensures a fair distribution of monetary gains among the coalition members and proposes a novel flexibility pricing scheme.

Acknowledgements

First and foremost, I shall praise and thank Allah Almighty for giving me the strength, patience, knowledge, ability and opportunity to undertake this research journey and to persevere the successful completion of this chapter of my life.

Then, I would like to take this opportunity to express my sincere gratitude and appreciation to Prof. Kankar Bhattacharya and Dr. Steven Wong, for the invaluable guidance, continuous support and encouragement which they provided throughout my graduate studies at the University of Waterloo. Without their knowledge, enthusiasm, availability for discussions at any time and, most importantly, patience, I could not have made my way through this journey. They will continue to be my role models in their exceptional professionalism and commitment to a high standard of quality throughout my academic career.

My appreciation and thanks are also extended to Prof. Ali Elkamel, Prof. Magdy Salama, and Prof. Ramadan El-Shatshat from the University of Waterloo, for serving on my doctoral Advisory Committee, and for their insightful comments and feedback. I am also very thankful to Prof. Bala Venkatesh from Ryerson University, for serving as the external thesis examiner and for his careful reading, wise comments and insightful observations. Furthermore, I would like to thank Prof. Stacey Acker for chairing my thesis examination committee.

With deep appreciation, I would to thank Qassim University, Saudi Arabia, for granting me the scholarship to pursue my graduate studies. I would like to thank the Ministry of Education, Saudi Arabia, and the Saudi Arabian Cultural Bureau in Canada for their support. I also acknowledge the partial funding from Natural Sciences and Engineering Council of Canada (NSERC) through the NSERC Energy Storage Technology (NEST) Network.

My appreciation also goes to all the administrative staff at the University of Waterloo and in the Department of Electrical and Computer Engineering for their assistance and cooperation throughout my PhD studies.

I would like to express my heartfelt gratitude to mother Ruqayyah Alodhayb, my father

Nasser Alrumayh, my brothers, and my sisters all of whom have constantly given me endless love, support, encouragement, and sincere prayers.

My deepest appreciation goes to my lovely wife Hajar and my son Walied for their endless love, unfailing understanding, support and encouragement during my PhD journey. They tolerated the stressful times and shared both the ups and downs of my PhD studies. Their precious love, care, and patience made my journey toward my thesis completion possible.

I would like to thank all my colleagues in the Power and Energy Systems Group at the University of Waterloo, and to the lab mates in the the Electricity Market Simulation and Optimization Laboratory (EMSOL) for their valuable discussions and creating a pleasant and friendly working environment. Special thanks to my colleagues and officemates Talal Alharbi, Hisham Alharbi, Nitin Padmanabhan, and Muhammad Umar Azam.

Finally, this thesis would not have been possible without the help, support and guidance of so many friends who shared happiness and tough times with me throughout various stages of this study and for making my stay memorable. Among them, Abdulaziz Almutairi, Nizar Alsharif, Badr Lami, Rayed Alyousef, Hisham Alabduljabbar, Abdulaziz Alaskar, Omar and Abdullah Bin Humaid, Majed Alotaibi, Nawaf Almutairi, Walied Alharbi, Omar Alarafj, Yasser Assolami, Abdulrahman Alorinan, and Dawood Alsaedi.

Dedication

To my parents

To my wife and my son

To my Brothers and Sisters

To my supervisors

Table of Contents

List of Tables

List of Figures

List of Abbreviations

BESS	battery energy storage system
C-Rate	charge rate
DR	demand response
DER	distributed energy resource
DG	distributed generator
DoD	depth of discharge
ESS	energy storage system
EMS	energy management system
EV	electric vehicle
FERC	Federal Energy Regulatory Commission
HEMS	home energy management system
HVAC	heating, ventilation and air-conditioning
HF	high flexibility
IESO	Independent Electricity System Operator
LDC	local distribution companies
Li-ion	lithium-ion
LF	low flexibility
MILP	mixed integer linear programming

MINLP	mixed integer non-linear programming
MF	moderate flexibility
NaS	sodium sulphur technologies
NPV	net present value
NN	neural network
O&M	operation and maintenance cost
PEV	plug-in electric vehicle
PV	photovoltaic
PRR	peak reduction requests
RCA	Rainflow Counting Algorithm
RES	renewable energy source
REH	residential energy hub
SOC	State of Charge
SoH	state-of-health
TOU	time-of-use

Chapter 1

Introduction

1.1 Motivation

With continuously increasing demand for energy, globally, and which is expected to grow by 12% from its 2019 levels by the year 2030 [1], there has been serious concerns on the long-term adequacy, availability and supply of energy. Traditional fossil fuel-based energy sources are detrimental to the environment and are not the favoured options by governments for new capacity. Thus, it is necessary to investigate other eco-friendly energy resources and solutions to meet the demand in the long-run.

To address this issue, governments have introduced new strategies, policies and dynamic pricing tools in order to reduce the peak demand and hence defer capacity investment costs. The Peaksaver Plus [2] and the Global Adjustment Program in Ontario, Canada [3] are examples of policies to reduce the peak demand of the local distribution companies (LDC); while the time-of-use (TOU) tariff applicable in Ontario is a pricing instrument seeking the same objective of lowering the peak demand. The development of demand response (DR) programs and the smart use of customers' flexibility can help the LDC enhance grid reliability and operational efficiency.

According to the US Federal Energy Regulatory Commission (FERC), DR is defined as [4], "*Changes in electric usage by end-use customers from their normal consumption*

patterns in response to changes in the price of electricity over time, or to incentive payments designed to induce lower electricity use at times of high wholesale market prices or when system reliability is jeopardized". On the other hand, flexibility is the ability of the power system to respond to fast changes in supply and demand, and in the balance of the two [5]. Increased flexibility needs refer to increased fast response requirements from generators and loads, though not increasing the overall capacity.

In 2018, the peak demand in Ontario was 23,240 MW; this lower than expected level was partially attributed to the deployment of various DR programs in the province. The estimates reveal that around 7% of the demand reduction was from DR programs such as Industrial Conservation Initiative, capacity-based DR, and the Peaksaver Plus residential DR program [2].

Effective implementation of DR programs relies on the availability of smart grid infrastructure, where deployment of two-way communication technologies between the LDC and end-users is crucial. Smart meters pass information to the LDC on customers' consumption levels and their readiness to participate in DR programs, by altering their consumption patterns based on price signals received from the LDC. The LDC can hence achieve a considerable degree of flexible operation by coordinating the controllable loads of retail customers, individually.

The effective participation of residential customers in DR programs can be achieved using a home energy management system (HEMS) which is a residential controller that determines the optimal ON/OFF decisions of the household appliances/devices based on the customer's objectives and preferences. According to a study by Hydro One [6], the display of electricity rates in real time, such as TOU rates, can increase load shifting on typical days from 3.7% to 5.5%, while on hot days, up to 8.5%, and bring about 13% reduction in energy consumption. The concept of energy hubs has been proposed in the last decade [7] where various energy system activities are performed within a hub, namely, energy production, conversion, storage, and consumption of different energy carriers [8]. The integration of renewable energy sources (RESs), energy storage systems (ESSs), and smart loads at the residential customer's end have transformed these loads to a residential energy hub (REH).

The increasing transformation of residential loads to REHs can provide powerful capabilities to benefit both customers and the LDC. Therefore, there is a need to assess the flexibility of REHs to provide DR services and evaluate their impact on consumption and distribution grid operation.

Besides home energy management, ESS can also provide flexibility, energy and capacity resource, and other benefits to the LDC such as loss reduction, peak shaving, increased RES integration, islanded operation support. In recent years, several ESS projects with varying sizes and locations have been commissioned by the Independent Electricity System Operator (IESO) in Ontario, Canada, to provide services such as load leveling, emergency reserve, and frequency regulation. For example, IESO York Region Non-Wires Alternatives Demonstration Project investigates the potential of high penetration of distributed energy resources (DERs) as an alternative for traditional infrastructure to meet local demand and electricity market needs without introducing any negative impact on system reliability [9]. In USA, the FERC Order 2222 [10] has been recently put in place that creates an opportunity for ESSs and REHs to indirectly participate in electricity markets through local aggregators and hence promote competition.

The diversity of ESS technologies can provide different capabilities which add value to their contributions in power system applications. There are many ESS projects under development or in the operational stage. In 2014, the IESO of Ontario, Canada, initiated a competitive procurement framework for 50 MW energy storage to provide capacity and ancillary services to the grid. Two consecutive phases were considered for the energy storage deployed; the first phase started in mid of 2014 by selecting five companies to provide ancillary services to the power grid with 34 MW capacity; the second phase offered 10-year contracts to five companies with 16.75 MW capacity in six separate energy storage projects.

By Spring 2018, seven energy storage facility projects have been commissioned and became operational. Two out of the seven are assigned to provide reactive power support and voltage control service, while the others are responsible for regulation services. As of December 2020, three out of the six energy storage projects from the second phase have started commercial operation, while the rest are underway. Table 1.1 shows examples of energy storage projects in Ontario, Canada, at the distribution and transmission grid

level [11].

Table 1.1: Some Energy Storage Projects in Ontario, Canada [11]

Proponent	Location	Technology	Capacity	Objective
Baseload Power Corp.	Milton, Ontario at distribution grid	Flow Battery	4 hours, 2 MW	Grid support and arbitrage
Ameresco Canada Inc.	Newmarket, Ontario at distribution grid	Solid Battery	4 hours, 2 MW Two facilities	Peak shaving and on-going grid relability and stability with increase in RES
SunEdison Canada Origination LP.	IESO grid	Flow Battery (VRB)	3 projects with total 4 hours, 20 MW	N/A
NextEra Canada Development and Acquisitions, Inc.	Distribution grid	Solid Battery (Li-ion)	4 hours, 2 MW	Peak shaving
NRStor Inc.	IESO grid	Compressed Air Energy Storage	7 MWh	N/A

One of the fastest growing ESSs is lithium-ion (Li-ion) batteries, which are a commercial and mature technology used for small-scale and large-scale grid applications. Li-ion batteries represent around 10% of the total installed ESS capacity in Canada [12], and their penetration is expected to increase with the decline in its capital cost [13]. Consequently, there is a need to properly size and site ESSs in an operational-planning framework in order to minimize the total cost of investment for their owner and increase the benefit from their flexible operation. However, it should be noted that the lifetime of Li-ion batteries are highly impacted by their cyclic operation and calendar aging. Although the short-term charging / discharging decisions would accrue financial benefits to the ESS owner, these would negatively impact the asset lifetime [14]. Neglecting the degradation of Li-ion batteries can lead to over-estimation of its available capacity and the expected financial benefit from the asset. In order to capture the inter-temporal changes in the state-of-health (SoH) of battery energy storage system (BESS), there is a need to model the degradation of Li-ion batteries as a function of its charging / discharging actions and its calendar aging, which can be incorporated within power system operation and planning problems.

The ownership of BESS can highly impact its operation, limiting the owners' financial benefit. BESSs are well-known for their prominent role in power systems such as energy arbitrage, peak demand reduction, and ancillary services. To unlock the ultimate benefits of BESS, the investors can transfer the right of BESS control to another entity, such as

an aggregator or the LDC, which requires access to more flexible resources. The LDC, for example, may need high flexibility in operation due to its exposure to volatility in demand, electricity prices, or intermittent generation. Also, the LDC does not have to own the BESS facilities in order to increase its flexible resources. The development of financial benefit allocation frameworks would encourage investors to participate in flexibility provisions and maximize the overall payoff. Therefore, there is a need to evaluate the contribution of individual BESSs each seeking to maximize the overall system benefit, which can hence be modeled as a cooperative game.

1.2 Literature Review

This section reviews the relevant literature pertaining to the topics and issues discussed in this thesis including operation, planning, and incentive design for ESSs and flexibility of residential loads for DR provisions in smart grid.

1.2.1 Flexibility of Residential Loads for Demand Response Provisions

In recent years, several researchers have reported their works on the mathematical modeling of an HEMS that optimizes the operation of household appliances [15–22].

In particular, a mixed integer linear programming (MILP) model was proposed in [22], optimizing the household appliance schedule, for incorporating into automated residential energy controllers. The mathematical model included most of the household appliances in addition to ESS and photovoltaic (PV) panels. The model parameters were determined from practical tests, and the model was implemented on households in Ontario, Canada; the results showed a significant reduction in both energy cost and peak demand while maintaining the customer preferences. The paper [22] forms the basis for the research on flexibility of residential loads presented in this thesis.

Some studies have dwelled upon coordinating the residential loads to provide an aggregated DR service to the utility while maximizing the aggregator's benefit.

In [23], an incentive-based energy consumption scheduling problem was formulated, while considering the interaction amongst households and the LDC, to minimize the total energy cost and the peak-to-average ratio of residential loads. Since the work considered only shiftable loads (i.e. dishwasher, washer, and dryer), minimization of energy consumption of the household appliances was not considered.

In [24], a decentralized HEMS was formulated as a multi-stage stochastic optimization problem to minimize the aggregator's cost by balancing the residential demand with available generation in real-time; four deferrable loads with fixed load profiles were considered. However, neither [23] or [24] considered the modeling of controllable loads with flexible thermal or electrical capacity such as heating, ventilation and air-conditioning (HVAC) and ESS, where energy consumption minimization can be achieved by operating the device within the customer's comfort zone.

In [25], a cooperative energy management system (EMS) was proposed to coordinate the operation of DERs of a neighborhood comprising residential prosumers operating in isolated mode. RESs and ESSs were considered, where the aim of the EMS was to reduce the mismatch between supply and demand. However, the paper considered the residential loads as fixed, without taking into account the inherent flexible operation capabilities of the household appliances.

In [26], a centralized coordination approach was proposed to achieve a pre-defined load profile by applying a day-ahead load shifting technique on residential, commercial, and industrial loads. The results indicated that the proposed load shifting approach reduced the system peak load and operation cost. Nevertheless, the paper did not investigate the impact of demand management on grid operations, such as bus voltage levels and system losses.

Distributed heat pumps, which represented a number of households' controllable loads, and BESS were coordinated in [27] to provide power smoothing services to mitigate the impact of power fluctuations of the integrated RESs on the connection line between a microgrid and main grid.

In [28], a decentralized stochastic optimization model was proposed for controlling the energy consumption of several houses including flexible and non-flexible loads, ESS, and

RES to minimize the total energy cost of the neighborhood using a real-time scheduling algorithm. The paper considered a case study, where a neighborhood with a few houses was coordinated to minimize the total cost. The paper assumed that the RES generation surplus would be curtailed without considering a more economic option of selling the surplus to the LDC. In addition, the work did not address the impact of the decentralized approach on distribution grid operation with multiple neighborhoods.

In [29], a decentralized coordination of multiple prosumers was proposed which aimed to maximize the aggregator's benefit while minimizing the reverse flow of energy at the service point, using a DR program. Other works [30, 31] proposed heuristic approaches to coordinate the DR of residential loads to minimize the cost of each customer, flatten the system load profile, and address the issue of possible peak rebound that might result from uncoordinated DR. The DR of residential loads was achieved by controlling a small set of household appliances- dishwasher, washer, dryer, and plug-in electric vehicles (PEVs). Furthermore, the paper investigated the impact of coordinated DR on distribution operation, and an improvement in the voltage profiles and reduction in system losses was noted. However, the work did not consider some of the basic flexible household appliances such as HVAC and stove.

Coordination of a small number of residential HEMSs, which comprised controllable appliances in addition to PEVs, ESSs, and distributed generation, to minimize the total neighborhood energy procurement cost while mitigating any unfair use of the distribution transformer, was proposed in [32]. In [33], a two-stage nodal pricing scheme was proposed to motivate the residential customers to participate in DR programs considering distribution system operational aspects; however, power system losses were not considered, and several household appliances were not taken into account in the HEMS as possible flexible loads.

In recent times, flexibility provisions have become a very important topic in power systems as a result of the increasing penetration of RESs into the power system, which calls for increased number of flexible resources such as controllable loads and ESSs. Therefore, these flexible resources need to be managed wisely to achieve customer-level and grid-level benefits. For example, flexible loads can provide DR services to the LDC. According to [34], uncoordinated DR might affect the distribution grid operation negatively, whereas proper control of DR can eliminate the adverse impact of such modifications in the demand-side

behavior. Another study stated that strategic operation of ESSs in electricity markets can limit the potential flexibility benefits of such a system [35]. The work [36] proposed a decomposition approach to estimate the controllable and non-controllable residential loads within a total forecasted load of a distribution system, which can be used in DR applications.

In [37], A multi-objective mixed integer non-linear programming (MINLP) based HEMS was proposed considering the customer's energy savings and comfort level, wherein each residential customer was equipped with controllable appliances and ESSs in a residential microgrid.

Table 1.2: Summary of Literature Review on Flexibility of Residential Loads

Paper	REH Model												Grid Operation and Constraints
	Water Heater	Fridge	Stove	HVAC	Lighting	Dishwasher	Washer	Dryer	Pool	ESS	RES	PEV	
[21]	C	F	F	C	NC	C	C	C	NC	C	NC	NC	NC
[23]	F	F	F	F	F	C	C	C	NC	NC	NC	C	Linear feeder model
[24]	NC	NC	NC	NC	NC	C	C	C	NC	NC	NC	C	NC
[25]	F	F	F	F	F	F	F	F	NC	C	C	NC	NC
[26]	NC	NC	C	NC	NC	C	C	C	NC	NC	NC	NC	C
[27]	NC	NC	NC	C	NC	NC	NC	NC	NC	C	C	NC	Tie-line between microgrid and main grid
[28]	Residential loads represented as shiftable and non-shiftable loads									C	C	NC	NC
[29]	Interruptible, uninterruptible, and thremostat-controlled load										C	C	NC
[30, 31]	NC	NC	NC	NC	NC	C	C	C	NC	NC	NC	C	C
[32]	F	F	F	F	F	C	C	C	NC	C	C	C	NC
[33]	C	F	F	C	F	C	C	C	NC	C	NC	C	Linear feeder model
[34]	C	C	C	C	C	C	C	C	NC	NC	NC	NC	C
[38]	C	NC	NC	C	NC	NC	NC	NC	NC	NC	NC	NC	NC
Proposed work	C	C	C	C	C	C	C	C	C	C	C	C	30-bus system

Considered as an optimization variable (C), Fixed Load (F), Not considered (NC)

In [38], an electric storage space heater of a residential customer was modeled to optimize its operation considering the flexibility of heating loads while minimizing the total operation cost; on the other hand, the retailer maximized its profit by optimally determining the electricity prices while minimizing the supply-demand imbalance in the

system. This was achieved by encouraging the flexible residential customers to alter their consumption behavior in response to the announced prices by the retailer. The study investigated the impact of different pricing schemes on both customers and retailer costs. It was noted that the TOU scheme was the best option for the residential loads. However, the retailer model did not consider the distribution grid constraints or the associated power losses, which affects the total cost of the retailer.

Table 1.2 presents an overview of the literature review pertaining to flexibility of residential loads and their ability to provide DR services. Many researchers have simply considered dishwasher, washer and dryer as flexible loads, while the other households appliances were considered fixed loads [23, 24, 30]. Other works have mainly investigated the DR provisions from residential thermal loads [33, 38]. Moreover, to the best of the author's knowledge, very few commercial HEMS solutions exist in the market today that integrate home automation, local generation, and energy storage with the external power system.

The integration of PEVs, ESSs, and/or RESs were considered by a few researchers, which noted the significant changes in the residential load profiles and customers' monthly bills. Very little research has been carried out to explore the impact of residential loads' flexibility and DR provisions on distribution system operations [26,34]. Hence, the inherent benefits of managing flexible resources to facilitate the integration of RESs and ESSs calls for in-depth research on this subject.

1.2.2 Planning for Energy Storage Systems in a Distribution Grid

There is a growing body of literature addressing the issue of integrating ESSs into the distribution grid to assist the LDC in managing grid operations.

The technical and economic advantages include, increasing the operating margins to facilitate RESs and electric vehicles (EVs) penetration [39] and deferring upgrades to the distribution grid. The authors in [40] proposed a multi-objective optimization approach to optimally site distributed generators (DGs), ESSs and RESs. An optimal planning

approach was proposed in [41] and [42] to determine the location, rated energy and power capacity of BESSs to mitigate the impact of uncertainties associated with renewables-based DGs. In [43], a genetic algorithm based planning framework was proposed to optimally size and site ESSs in a distribution system grid in order to minimize system losses, defer system upgrades, and maximize the profit from energy arbitrage. Another work [44] proposed a stochastic approach to coordinate the planning of ESSs and RESs while considering DR. In [45], a chance-constrained approach was proposed for ESSs planning in a distribution grid. However, none of the above works have considered the lifetime of the ESSs nor the impact of degradation on the asset's operation.

Several researchers have considered degradation of ESSs [46–51], but for different studies. In [46], an operational planning scheme was proposed to coordinate wind farms with ESSs to mitigate the impact of wind forecast errors and extend the lifetime of BESSs by reducing frequent charge / discharge operations.

A multi-stage approach was proposed in [47] to optimally plan for transmission expansion and ESS deployments considering a linear degradation rate of BESSs. In [49], a decomposition approach was proposed to optimally determine the size and year of installation of ESSs in a microgrid while assuming an annual degradation factor of the batteries.

A BESS sizing model was proposed in [49] to optimally determine the size and the number of units required to minimize the microgrid operation cost and unserved energy cost. In [50], a planning model for isolated microgrids was proposed considering re-purposed EV batteries, assuming a linear change in the ESS's SoH due to calendar and cycle aging. In [51], the participation of ESSs in frequency regulation in the PJM market was assessed considering the impact of different depth of discharge (DoD) levels on the SoH of various types of Li-ion batteries.

It is noted that researchers have examined several simple approaches to consider the SoH of BESSs in their optimization problems. However, none of the above works have captured the change in BESSs' SoH due to calendar and cycle aging, and the issue of under- or over-estimating BESS capacity resulting in over- or under-capacity planning in the distribution system, being left un-addressed [47, 48, 50].

Some of the works in the literature have reported the development of approaches to estimate the lifetime of Li-ion based BESS. The proposed methods can be classified as: model-based, data-driven, and fusion-based methods [52]. In [53], an SoH estimation approach based on the equivalent internal resistance of Li-ion BESS was proposed to observe the change in the battery SoH in real-time. Another work [54] proposed to estimate the SoH of Li-ion batteries using the data obtained from the battery EMS such as current, voltage and temperature. In [51], a semi-empirical Li-ion battery degradation model was proposed to overcome the issue of limited observation data availability, from operating the ESS for specific applications.

Researchers have proposed a battery life assessment approach that can be integrated in different stationary BESS applications in power system problems. In [51], an off-line battery lifetime assessment was proposed, based on the Rainflow Counting Algorithm (RCA), which requires the history of BESS operations. Such an approach requires the history of operating BESS as an input. However, since distribution system planning problems with BESSs must simultaneously compute the battery State of Charge (SOC) profiles based on BESS operational decisions and the optimal BESS plan, RCA-based degradation models [51] cannot be implemented directly within these models because they require historical data of BESS operations. Therefore, there is a need to develop an estimation approach of BESS's SoH in order to tackle the issue of under- or over-estimating their degraded capacity.

1.2.3 Service Provisions from Energy Storage Systems and Sharing of the Benefits

This subsection discusses different incentive schemes for DR and flexibility provisions procured from ESSs in the smart grid.

Dynamic pricing approach is proposed in [55] to indirectly alter the consumption of residential customers and the operation of their ESS units. In [56], a non-cooperative game is proposed to capture the competitive behavior between residential loads and ESSs to minimizing their electricity cost individually. After that, a non-cooperative

Stackelberg game is proposed to model the interactions between the LDC, who determines the electricity prices, and the residential customers, who respond to the signal by changing demand, to minimize the peak-to-average power ratio.

A Stackelberg game approach is proposed in [57], which possesses individual rationality and incentive compatibility, to model an auction market environment for joint ESS ownership sharing between several facility managers and residential communities. The work aims to exploit the full potential benefits of ESSs owned jointly by different entities and provide various services to a third party. In [58], a Stackelberg game is introduced to maximize the revenue of the shared ESS owner while the electricity retailer aims to minimize the total cost of residential customers. A bargaining based incentive approach is proposed in [59] to encourage joint energy trading between microgrids, each equipped with ESS, and hence to maximize the total obtained benefit.

Another work in [60] proposes a cooperative game theory-based approach to manage the operation of several ESSs and hence minimize the coalition energy cost. The proposed method shows an improvement in the LDC operation by flattening the load profile and reducing the reverse power flow. A coalition game theory-based energy management problem is proposed in [61] to maximize the benefit of a coalition of local energy communities equipped with flexible loads, ESSs, and RESs. The grand coalition effectively increases the total payoffs and improves the overall load profile.

It is noted from the above discussions that most of the works proposed monetary benefits to encourage ESSs to participate in system operations and efficient use of available resources. However, none of the works examined the participation of ESSs based on their marginal contribution to a coalition considering their physical characteristics such as the rate of change in SOC, which significantly impacts the ESS lifetime.

1.3 Research Objectives

The main objectives of the research presented in this thesis include evaluating the flexibility provisions from residential customers through REHs and ESSs and provide a flexibility service to the grid operator. The research objectives are listed below:

- Augment the mathematical model of the residential customer's HEMS reported in [22] to represent it as an REH considering detailed characteristics of ESSs and PV units. The developed model will take into account the detailed interactions, data and information exchanges between different entities within the REH as well as between the REH and the LDC.

- Propose a novel concept of REH flexibility index to quantify the flexibility resource available from a household. Thereafter, develop a coordination scheme that can take into account distinctly individual objectives of each REH as well as that of the LDC, seeking to enhance grid operational efficiency, and hence create an aggregated DR service for the system. This will involve a novel LDC operations model, which will determine the optimal peak reduction requests from the individual REHs.

- Propose a novel neural network (NN) based degradation model to estimate the SoH of Li-ion batteries of an ESS in a distribution system. The data to be used for NN training shall comprise SOC profiles of ESS obtained considering different LDC load mix including a set of simulated REH operations extended over the plan period.

- The developed NN-based SoH model of the ESS will be incorporated into a planning model to determine the optimal energy capacity, power rating, location and year of installation or replacement of ESSs in the distribution system while internalizing the ESS battery capacity degradation due to cycling and aging effects.

- Propose a novel BESS flexibility provision framework based on their capability of providing different charge rate (C-Rate) levels. This framework will allow individual investors to participate in flexibility provisions as a service to the LDC. A cooperative game theory-based approach will be applied to maximize the total system payoff and hence distribute it fairly among all the BESS participants based on their marginal contributions to the total system saving using the Shapley value criterion.

1.4 Outline of the Thesis

The rest of the thesis is organized as follows: Chapter-2 presents background on HEMS and its mathematical model, and the concept of energy hubs, followed by a discussion on ESS and their applications in smart grids. In Chapter-3, the proposed residential loads' flexibility evaluation and a novel coordination framework for DR provisions is presented, along with results of different case studies. In Chapter-4, a novel NN based SoH estimator for a Li-ion battery-based ESS is proposed, which is then incorporated within the LDC's planning model to determine optimal ESS plans. Chapter-5 proposes a cooperative game theory-based approach to distribute the total savings, accrued by the LDC, among BESS owners for their participation in flexibility provisions in a distribution grid. Finally, in Chapter-6 the conclusions and contributions of this thesis are presented, and the scope for future research are outlined.

Chapter 2

Background Review

This chapter presents a brief review of the topics and tools relevant to the research presented in this thesis. A detailed discussion of the HEMS and the REH, and the associated mathematical models are presented. Thereafter, BESS characteristics and their applications in smart grids are briefly discussed, followed by a brief review of the RCA, and the basic features of a NN model.

2.1 Nomenclature

Indices and Sets

h_j	Index for household, $h_j \in \mathcal{H}$
i	Index for household appliances, $i \in \mathcal{A}$
	$i = \{$fridge (fr), water heater (WH), stove (STV), dishwasher (DW), washer (W), dryer (Dry), lighting (LI), pool ($Pool$), energy storage system (ESS), PV panel battery (BPV)$\}$
j,k	Index for bus, $\{j, k\} \in \mathcal{N}$
t	Index for time, $t \in \mathcal{T}$

Parameters

AL_t	Activity level inside a house
$\triangle_{W,DRY}$	Maximum allowed time gap between operation of washer and dryer
E_i^{min}, E_i^{max}	Minimum and maximum energy level of $i \in \{ESS,\ BPV\}$, kWh
EOT_i, LOT_i	Early / late operation time of appliance $i \in \{DW,W,DRY,PMP,STV\}$
$G_{j,k}$	Conductance of feeder between bus j and k
g_i	Heat rate of device $i \in \{HT,WH\}$
HWU_t	Hot water usage at time t
K_t	Price elasticity associated with the illumination inside a house
L_t^{out}, L_t^{min}	Natural / minimum illumination at time t
MUT_i, MDT_i	Minimum uptime / downtime of appliance, $i \in \{AC,HT,DW,W,DRY,PMP,STV\}$
MST_i	Maximum successive operation time of appliance, $i \in \{DW,W,DRY,PMP,STV\}$
$P_{C_i}^{max}$, $P_{D_i}^{max}$	Maximum charging/discharging power of $i \in \{B,ESS\}$, kW
P_{D_0}	Connected load at time t, kW
$P_{h_j,t}^{max}$	House h_j maximum demand at time t, kW
$\widehat{P}_{h_j,t}^{max}$	Updated house h_j maximum demand at time t, kW
P_i	Rated power of appliance i, kW
P_{LI}	Rated power of the lighting system LI, kW
$P_{PV,h_j,t}$	PV generation at time t, kW
ROT_i	Required operation time of appliance $i \in \{DW,W,DRY,PMP,STV\}$, min
$Y_{j,k}$	Magnitude of admittance matrix element, $p.u$

α_i, β_i	Cooling/Warming effect associated with ON / OFF state of device, $i \in \{AC,HT,FR,WH\}$, C°/min
η_1, η_2	Charging/discharging efficiency of ESS, %
ρ^{GAS}	Gas price, $\$/m^3$
ρ_t^{TOU}	Time of use price, $\$/kWh$
ρ^{SEL}	Residential customers electricity selling price to the LDC, $\$/kWh$
ρ_i	Effect of the difference between inside and outside temperature on the inside temperature of device $i \in \{AC,HT,FR,WH\}$
γ_i	Cooling/Warming effect associated with OFF state of device $i \in \{FR,WH\}$
τ	Length of the time interval, minutes
$\Theta_{in}^{min}, \Theta_{in}^{max}$	Minimum and maximum allowable temperature inside a house, C°
Θ_i^{set}	Preferred temperature setting of $i \in \{AC,HT,FR,WH\}$, C°
$\Theta_{out,t}$	Ambient temperature, C°

Variables

$E_{i,t}$	Energy level of $i \in \{ESS,\ BPV\}$ at time t, kWh
L_t	Illumination level at time t, kW
$P_{C_{BPV},t},\ P_{D_{BPV},t}$	Total charging / discharging power from BPV at time t
$P_{i,t}^H,\ P_{i,t}^{LDC}$	Discharging power from device $i \in \{ESS,\ BPV\}$ to house / LDC at time t, kW
$P_{LDC,t}^i$	Charging power drawn by device $i \in \{ESS,\ BPV\}$ from LDC at time t, kW
$P_{LDC,t}^H$	Delivered power by LDC to meet the house demand at time t, kW
$P_{LDC,t}^{BPV}$	Total charging power drawn by BPV at time t, kW
$P_{PV,t}^{BPV}$	Generated power by PV solar panel used to charge the PV battery (BPV) at time, kW

$P^{H}_{PV,t}$	Generated power by PV solar panel consumed by household appliances at time t, kW
$P^{LDC}_{PV,t}$	Generated power by PV solar panel sold to LDC at time t, kW
$S_{C_i,t}$	Binary charging status of $i \in \{ESS,\ BPV\}$ at time t, ON/OFF
$S_{D_i,t}$	Binary discharging status of $i \in \{ESS,\ BPV\}$ at time t, ON/OFF
$S_{i,t}$	Binary status of device i at time t, ON/OFF
$U_{i,t}$	Binary status denoting start up of device i at time t, ON/OFF
$D_{i,t}$	Binary status denoting shut down of device i at time t, ON/OFF
$V_{j,t}$	Voltage at bus j at time t, $p.u$
$\delta_{j,t}$	Voltage angle at bus j at time t, radians
$\Theta_{in,t}$	Temperature inside a house

2.2 REH and Mathematical Model of HEMSs

The REH is a residential building with different energy activities that take place in order to produce, consume, and / or store electricity. To optimize various activities of an REH, HEMSs are in place; these are residential controllers that carry out scheduling of the REH including all house appliances, the ESS, PV panel battery, and the power interchanges with the external grid, considering the customer's preferences and objectives. The objective of the HEMS is to minimize the energy consumption, energy cost, or maximize the comfort level of the REH customer. In doing so, the HEMS helps the household to better evaluate, visualize, and manage its energy consumption by providing updated information on its energy use and the current energy price. According to [62], a study by Hydro One shows that "*Providing real-time displays to customers on Regulated Price Plan (RPP) and Time-of-Use (TOU) rates increased the load shifting impacts on typical days from 3.7% to 5.5% and on hot days (over 30°C) to 8.5%. In addition, real-time feedback to the HEMS can decrease the overall energy consumption up to 13%*".

The HEMS requires the REH customer to update its preferences, such as the minimum and maximum allowable temperature setting inside the house, in order to autonomously control the appliances. Two-way communication infrastructure is required to facilitate such autonomous control of the appliances / devices by the HEMS; HomePlug, ZigBee, and Wi-Fi are the three common open communication protocols [63].

Several mathematical models have been proposed to optimize the household appliances' and devices' operations; the HEMS mathematical model formulated in [64,65] extends the work reported in [22]. A brief description of the HEMS model is presented next.

2.2.1 HEMS Objective Functions

The objective functions of the HEMS, for a given REH, that have been considered, are:

Minimize Cost:

$$J1 = \sum_{t\in\mathcal{T}} \Bigg[\rho_t^{TOU} \Big\{ \sum_{\substack{i\in\mathcal{A} \\ i\notin\{LI,ESS,BPV\}}} P_i S_{i,t} + P_{LI} L_t + \sum_{i\in\{BPV,ESS\}} P^i_{LDC_t} + P_{D0} \Big\} + \sum_{i\in\{HT,WH\}} \rho^{GAS} g_i S_{i,t} - \rho^{SEL} \Big\{ \sum_{i\in\{BPV,ESS\}} P^{LDC}_{D_{i,t}} + P^{LDC}_{PV,t} \Big\} \Bigg] \quad (2.1)$$

In (2.1), the terms within the first curly brackets denotes the total power drawn from the grid to supply the following: household appliances, lighting system, the charging power drawn by the ESS and the PV panel battery, and the uncontrollable load. The total gas consumption is represented by the term associated with ρ^{GAS}, where the price of gas is assumed to be a fixed rate, equivalent to 2.9 cents/kWh [22]. The terms associated with ρ^{SEL} represents the total income from selling power to the LDC.

Minimize Energy Consumption:

$$J2 = \sum_{t\in\mathcal{T}} \Bigg[\sum_{\substack{i\in\mathcal{A} \\ i\notin\{LI,ESS,BPV\}}} P_i S_{i,t} + P_{LI} L_t + \sum_{i\in\{BPV,ESS\}} P^i_{LDC_t} + \sum_{i\in\{HT,WH\}} g_i S_{i,t} \Bigg] \quad (2.2)$$

In (2.2), the customer seeks to minimize the energy consumption from household appliances, lighting system, charging power of ESS and PV panel battery, and gas consumption.

Maximize Comfort Level:

$$J3 = \sum_{t\in\mathcal{T}} \Bigg[\sum_{i\in\{AC,HT,WH,FR\}} \left| \Theta^{in}_{i,t} - \Theta^{set}_i \right| \Bigg] \quad (2.3)$$

The temperature deviations of certain appliances from their preferred set points represents the customer comfort level. Therefore, maximizing the customer's comfort level can be attained by minimizing the temperature deviations from the pre-defined set points.

2.2.2 Operational Constraints of the Household Appliances

In this section, the constraints of the HEMS mathematical model are presented. The typical household appliances / devices comprises: HVAC, dishwasher, fridge, lighting system, pool pump, stove, washer and dryer, and water heater, in addition to an ESS and a PV panel.

Home Power Balance and Peak Load Constraints:

$$\sum_{i \in \mathcal{A}} P_i S_{i,t} = P^H_{LDC,t} + \sum_{i \in \{B,ESS\}} P^H_{D_{i,t}} + P^H_{PV,t}, \quad \forall t \in \mathcal{T} \tag{2.4}$$

$$\sum_{i \in \mathcal{A}} P_i S_{i,t} + \sum_{i \in \{B,ESS\}} P^{LDC}_{i,t} - \sum_{i \in \{B,ESS\}} P^H_{D_{i,t}} - P^H_{PV,t} \leq \widehat{P}^{max}_t \tag{2.5}$$

Constraint (2.4) ensures that the total power demand of the REH appliances is met by the power drawn from the grid, discharged to the house from the ESS and PV panel battery, and that generated by the PV system. It should be noted that while the PV panel batteries represent stationary storage, the ESSs denote the mobile storage devices in the house, such as PEVs. In (2.5), the peak load constraint ensures that the total load of the REH is within a limit specified by LDC, $\widehat{P}^{max}_t$.

Heating, Ventilation, and Air Conditioning System operation

The following constraints are used to represent the HVAC operation, considering the household preferences such as minimum and maximum temperature inside the house.

$$\Theta^{min}_{in,t} \leq \Theta_{in,t} \leq \Theta^{max}_{in,t}, \quad \forall t \in \mathcal{T} \tag{2.6}$$

$$S_{i,t} = \begin{cases} 0 \quad \text{or} \quad 1 & \text{if t}\in \mathcal{T}, i \in \{AC,HT\} \\ 0 & \text{if t}\notin \mathcal{T}, i \in \{AC,HT\} \end{cases} \tag{2.7}$$

$$S_i\Big|_{t=1} = \begin{cases} 1 & \text{if } \Theta_{in}\Big|_{t=0} \Theta^{max}_{in,t}, i = AC \\ 0 & \text{if } \Theta_{in}\Big|_{t=0} \Theta^{min}_{in,t}, i = AC \end{cases} \tag{2.8}$$

$$S_i\Big|_{t=1} = \begin{cases} 1 & \text{if } \Theta_{in}\Big|_{t=0} \Theta_{in,t}^{min}, i = HT \\ 0 & \text{if } \Theta_{in}\Big|_{t=0} \Theta_{in,t}^{max}, i = HT \end{cases} \tag{2.9}$$

$$S_{AC,t} + S_{HT,t} \leq 1, \quad \forall t \in \mathcal{T} \tag{2.10}$$

In (2.6), the AC and HT operations are based on a pre-set minimum (Θ_{in}^{min}) and maximum (Θ_{in}^{max}) temperature inside the REH. Constraint (2.7) is used to allow the operation of the HVAC at certain set of time intervals only. As a result, the AC system operates when the inside temperature is above Θ_{in}^{max}; while, the HT system operates when the inside temperature is less than Θ_{in}^{min}, as shown in (2.8) and (2.9), respectively. Constraint (2.10) prevents simultaneous operation of the AC and HT.

The indoor temperature depends on many factors such as the activity level of the customer and the ambient temperature, as given below:

$$\Theta_{in,t} = \Theta_{in,t-1} + \tau\Big[\beta_{AC} AL_t - \alpha_{AC} S_{i,t} + \rho_{AC}(\Theta_{out,t} - \Theta_{in,t})\Big], \quad \forall i = AC, t \in \mathcal{T} \tag{2.11}$$

$$\Theta_{in,t} = \Theta_{in,t-1} + \tau\Big[\beta_{HT} AL_t + \alpha_{HT} S_{i,t} - \rho_{HT}(\Theta_{out,t} - \Theta_{in,t})\Big], \quad \forall i = HT, t \in \mathcal{T} \tag{2.12}$$

$$U_{i,t} - D_{i,t} = S_{i,t} - S_{i,t-1}, \quad \forall i \in \{AC,HT\}, t \in \mathcal{T} \tag{2.13}$$

$$U_{i,t} + D_{i,t} \leq 1, \quad \forall i \in \{AC,HT\}, t \in \mathcal{T} \tag{2.14}$$

$$\sum_{k=t}^{t+MUT_i} S_{i,k} \geq MUT_i - M(1 - U_{i,t}), \quad \forall i \in \{AC,HT\}, t \in \mathcal{T} \tag{2.15}$$

$$\sum_{k=t}^{t+MDT_i-1} S_{i,k} \leq M(1 - D_{i,t}), \quad \forall i \in \{AC,HT\}, t \in \mathcal{T} \tag{2.16}$$

Equations (2.11) and (2.12) models the change in the indoor temperature of the REH as a result of HVAC operation, the changes in the activity level of the customer, or the changes in the ambient temperature. Equations (2.13) and (2.14) are the coordinating constraints for the start-up and shut-down decisions of the AC and HT. In addition, minimum up-time (MUT_i) and minimum down-time (MDT_i) of the AC and HT are considered in (2.15) and (2.16).

Dishwasher

The dishwasher mathematical model is presented below:

$$S_{i,t} = \begin{cases} 0 \quad \text{or} \quad 1 & \text{if t}\in \mathcal{T}, i \in \{DW\} \\ 0 & \text{if t}\notin \mathcal{T}, i \in \{DW\} \end{cases} \tag{2.17}$$

$$U_{i,t} - D_{i,t} = S_{i,t} - S_{i,t-1}, \quad \forall i = DW, t \in \mathcal{T} \tag{2.18}$$

$$U_{i,t} + D_{i,t} \leq 1, \quad \forall i = DW, t \in \mathcal{T} \tag{2.19}$$

$$\sum_{t\in\mathcal{T}} S_{i,t} = ROT_i, \quad \forall i = DW, t \in \mathcal{T} \tag{2.20}$$

$$\sum_{k=t}^{t+MST_i} S_{i,k} \leq MST_i + M(1 - U_{i,t}), \quad \forall i = DW, t \in \mathcal{T} \tag{2.21}$$

$$\sum_{k=t-MUT_i+1}^{t} U_{i,k} \leq S_{i,t}, \quad \forall i = DW, t \in \{EOT_i + MUT_i + 1, LOT_i\} \tag{2.22}$$

$$\sum_{k=t-MDT_i+1}^{t} D_{i,k} \leq 1 - S_{i,t}, \quad \forall i = DW, t \in \{EOT_i + MDT_i + 1, LOT_i\} \tag{2.23}$$

The dishwasher operates within the pre-determined time intervals preferred by the customer as modeled in (2.17). Minimum up-time, minimum down-time, and required operation time in addition to the maximum successive operation time constraints are expressed mathematically in (2.20) to (2.23).

Fridge

The following mathematical model pertaining to fridge operation is formulated considering the technical aspects of the fridge as well as the customer preferences.

$$S_{i=FR,t} = \begin{cases} 0 \quad \text{or} \quad 1 & \text{if t}\in \mathcal{T} \\ 0 & \text{if t}\notin \mathcal{T} \end{cases} \tag{2.24}$$

$$S_{i=FR}\Big|_{t=1} = \begin{cases} 1 & \text{if } \Theta_i\Big|_{t=0} = \Theta_{i,t}^{max} \\ 0 & \text{if } \Theta_i\Big|_{t=0} = \Theta_{i,t}^{min} \end{cases} \tag{2.25}$$

$$\Theta_i^{min} \leq \Theta_{i,t} \leq \Theta_i^{max}, \quad \forall i{=}FR, t \in \mathcal{T} \tag{2.26}$$

$$\Theta_{i,t} = \Theta_{i,t-1} + \tau\Big[\beta_i A L_{i,t} - \alpha_i S_{i,t} + \gamma_i\Big], \quad \forall i{=}FR, t \in \mathcal{T} \tag{2.27}$$

The time intervals where the fridge can be in operation are modeled in (2.24). The constraint (2.25) ensures that if the initial temperature of the fridge is above the predetermined maximum temperature, then it should be in operation; or else it should be in a standby mode. The REH's preferred minimum (Θ_{FR}^{min}) and maximum (Θ_{FR}^{max}) temperature inside the fridge is specified in (2.26). The effect of the activity level, ON and OFF states, on the fridge operation are represented by β_{FR}, α_{FR}, and γ_{FR} respectively and presented in (2.27).

Lighting System

The model of the lighting system is affected by two factors: daylighting (L_t^{out}) and the minimum illumination required at time t (L_t^{min}).

$$L_t + L_t^{out} \geq (1 + K_t) L_t^{min}, \quad \forall t \in \mathcal{T} \tag{2.28}$$

The constraint (2.28) ensures that the illumination level at time t is greater than the minimum required illumination. In addition, the lighting system load of the REH is price elastic, which is modeled using K_t, which is equal to zero during the peak prices and unity during the off-peak prices.

Pool Pump

The installation of pool pump along with the swimming pool is required to allow the REH to keep the water quality relatively high by treating the swimming pool water for a certain

period of time during the day. The mathematical model of its operational constraints are as follows:

$$S_{i=PMP,t} = \begin{cases} 0 \quad \text{or} \quad 1 & \text{if t}\in \mathcal{T}, \\ 0 & \text{if t}\notin \mathcal{T} \end{cases} \tag{2.29}$$

$$\sum_{t\in\mathcal{T}} S_{i,t} = ROT_i, \quad \forall i = PMP, t \in \mathcal{T} \tag{2.30}$$

$$U_{i,t} \geq S_{i,t} - S_{i,t-1}, \quad \forall i = PMP, t \in \mathcal{T} \tag{2.31}$$

$$\sum_{k=t-MUT_i+1}^{t} U_{i,t} \leq S_{i,t}, \quad \forall i = PMP, t \in \{EOT_i + MUT_i + 1, LOT_i\} \tag{2.32}$$

$$\sum_{k=t-MDT_i+1}^{t} U_{i,t} \leq 1 - S_{i,t-MDT_i}, \quad \forall i = PMP, t \in \{EOT_i + MDT_i + 1, LOT_i\} \tag{2.33}$$

$$\sum_{k=t}^{t+MST_i} S_{i,k} \leq MST_i + M(1 - U_{i,t}), \quad \forall i = PMP, t \in \mathcal{T} \tag{2.34}$$

The above set of constraints ensure that the operation of pool pump is within the customer's preferred pool operation time.

Stove

The mathematical model of the stove is presented to help determine the optimal operation time, based on the REH customer's objective, within their preferred operation time period. The mathematical optimization model of the stove is shown below.

$$S_{i,t} = \begin{cases} 0 \quad \text{or} \quad 1 & \text{if t}\in \mathcal{T}, i = STV \\ 0 & \text{if t}\notin \mathcal{T}, i = STV \end{cases} \tag{2.35}$$

$$U_{i,t} \geq S_{i,t} - S_{i,t-1}, \quad \forall i = STV, t \in \mathcal{T} \tag{2.36}$$

$$\sum_{t\in\mathcal{T}} S_{i,t} = ROT_i, \quad \forall i = STV, t \in \mathcal{T} \tag{2.37}$$

$$\sum_{k=t-MUT_i+1}^{t} U_{i,k} \leq S_{i,t}, \quad \forall i = STV, t \in \{EOT_i + MUT_i + 1, LOT_i\} \tag{2.38}$$

$$\sum_{k=t}^{t+MST_i} S_{i,k} \leq MST_i + M(1 - U_{i,t}), \quad \forall i = STV, t \in \mathcal{T} \tag{2.39}$$

Washer and Dryer

The mathematical model of the washer and dryer is presented below:

$$S_{i,t} = \begin{cases} 0 \quad \text{or} \quad 1 & \text{if t}\in \mathcal{T}, i = \{W, Dry\} \\ 0 & \text{if t}\notin \mathcal{T}, i = \{W, Dry\} \end{cases} \tag{2.40}$$

$$U_{i,t} - D_{i,t} = S_{i,t} - S_{i,t-1}, \quad \forall i = \{W, Dry\}, t \in \mathcal{T} \tag{2.41}$$

$$U_{i,t} + D_{i,t} \leq 1, \quad \forall i = \{W, Dry\}, t \in \mathcal{T} \tag{2.42}$$

$$\sum_{t\in\mathcal{T}} S_{i,t} = ROT_i, \quad \forall i = \{W, Dry\}, t \in \mathcal{T} \tag{2.43}$$

$$\sum_{k=t}^{t+MST_i} S_{i,k} \leq MST_i + M(1 - U_{i,t}), \quad \forall i = \{W, Dry\}, t \in \mathcal{T} \tag{2.44}$$

$$\sum_{k=t-MUT_i+1}^{t} U_{i,t} \leq S_{i,t}, \quad \forall i = \{W, Dry\}, t \in \{EOT_i + MUT_i + 1, LOT_i\} \tag{2.45}$$

$$\sum_{k=t-MDT_i+1}^{t} D_{i,k} \leq 1 - S_{i,t}, \quad \forall i = \{W, Dry\}, t \in \{EOT_i + MDT_i + 1, LOT_i\} \tag{2.46}$$

The constraints (2.40) to (2.46) are modeled to provide the REH customer with the optimal operation schedule for both the washer and dryer based on the customer preferences. The washer and dryer are required to operate in a chronological sequence, where the operation of the dryer should follow the operation of the washer. The following constraints are

included to coordinate the sequential operation of the washer and dryer.

$$U_{DRY,t} \leq \sum_{k=t-\triangle_{W,DRY}}^{t-MUT_W} U_{W,t-k}$$

$$\forall i = \{W, Dry\}, \quad t \in \{EOT_i + \triangle_{W,DRY}, LOT_i - MUT_W\} \tag{2.47}$$

$$S_{DRY,t} + S_{W,t} \leq 1, \quad \forall t \in \mathcal{T} \tag{2.48}$$

$$\sum_{t \in \mathcal{T}_{DRY}} U_{DRY,t} = \sum_{t \in \mathcal{T}_W} U_{W,t} \tag{2.49}$$

Water Heater

Similar to the mathematical model of the fridge, the water heater model is presented below:

$$S_{i,t} = \begin{cases} 0 \quad \text{or} \quad 1 & \text{if t} \in \mathcal{T}, i = WH \\ 0 & \text{if t} \notin \mathcal{T}, i = WH \end{cases} \tag{2.50}$$

$$S_{i,t=1} = \begin{cases} 1 & \text{if } \Theta_{i,t=0} = \Theta_{i,t}^{min}, i = WH \\ 0 & \text{if } \Theta_{i,t=0} = \Theta_{i,t}^{max}, i = WH \end{cases} \tag{2.51}$$

$$\Theta_{i,t}^{min} \leq \Theta_{i,t} \leq \Theta_{i,t}^{max}, \quad \forall i = WH, t \in \mathcal{T} \tag{2.52}$$

$$\Theta_{i,t} = \Theta_{i,t-1} + \tau \Big[\alpha_i S_{i,t} - \beta_i HWU_t - \gamma_i \Big], \quad \forall i = WH, t \in \mathcal{T} \tag{2.53}$$

Constraints (2.50) to (2.53) represent the mathematical model of the water heater. The allowable operating time is restricted by (2.50), while the initial operational decision is determined based on constraint (2.51). The allowable water temperature within the appliances is constrained by (2.52), and dynamically modeled as in (2.53).

Photovoltaic Panel with a Battery

REHs with PV panels are assumed to be equipped with a 3.6 kW PV panel; the modified model with more detailed and realistic architecture is discussed below:

Solar Panel:

$$P_{PV,t} = P^{LDC}_{PV,t} + P^{BPV}_{PV,t} + P^{H}_{PV,t}, \quad \forall t \in \mathcal{T} \tag{2.54}$$

As shown in (2.54), the PV panel generates power, and the HEMS optimizes its usage by distributing it to the battery, household, and grid,

Battery:

$$E_{BPV,t} = E_{BPV,t-1} + \tau\Big[\Big\{P^{BPV}_{LDC,t} + P^{BPV}_{PV,t}\Big\}\eta_1 - \Big\{P^{LDC}_{BPV,t} + P^{H}_{BPV,t}\Big\}/\eta_2], \ \forall t \in \mathcal{T} \tag{2.55}$$

$$E^{min}_{BPV} \leq E_{BPV,t} \leq E^{max}_{BPV}, \quad \forall t \in \mathcal{T} \tag{2.56}$$

Equation (2.55) presents the inter-temporal changes of energy level of the battery and (2.56) defines the limits on its energy level. The charging and discharging relationships are formulated as follows:

$$P_{C_{BPV},t} = P^{BPV}_{LDC,t} + P^{BPV}_{PV,t}, \quad \forall t \in \mathcal{T} \tag{2.57}$$

$$P_{D_{BPV},t} = P^{LDC}_{BPV,t} + P^{H}_{BPV,t}, \quad \forall t \in \mathcal{T} \tag{2.58}$$

In (2.57), the battery can be charged from the PV panel power, or grid power; (2.58) denotes that the battery can discharge power to the house, or sell to the grid.

$$P_{C_{BPV},t} \leq S_{C_{BPV},t} P^{max}_{C_{BPV}}, \quad \forall t \in \mathcal{T} \tag{2.59}$$

$$P_{D_{BPV},t} \leq S_{D_{BPV},t} P^{max}_{D_{BPV}}, \quad \forall t \in \mathcal{T} \tag{2.60}$$

Constraints (2.59) and (2.60) represent the maximum charging and discharging power of the battery; the charging and discharging processes do not occur simultaneously, as ensured by the following:

$$S_{C_{BPV},t} + S_{D_{BPV},t} \leq 1, \quad \forall t \in \mathcal{T} \tag{2.61}$$

Energy Storage System

$$E_{ESS,t} = E_{ESS,t-1} + \tau[P^{ESS}_{LDC,t}\eta_1 - (P^{LDC}_{ESS,t} + P^{H}_{ESS,t})/\eta_2], \quad \forall t \in \mathcal{T} \tag{2.62}$$

$$E^{min}_{ESS} \leq E_{ESS,t} \leq E^{max}_{ESS}, \quad \forall t \in \mathcal{T} \tag{2.63}$$

$$P^{ESS}_{LDC,t} \leq S_{C_{ESS},t} P^{max}_{C_{ESS}}, \quad \forall t \in \mathcal{T} \tag{2.64}$$

$$P^{LDC}_{ESS,t} + P^{H}_{ESS,t} \leq S_{D_{ESS},t} P^{max}_{D_{ESS}}, \quad \forall t \in \mathcal{T} \tag{2.65}$$

$$S_{C_{ESS},t} + S_{D_{ESS},t} \leq 1, \quad \forall t \in \mathcal{T} \tag{2.66}$$

Equation (2.62) relates the change in energy level of the ESS as affected by the power drawn, and discharged by the ESSs to the grid, and to the house. Note that the self-discharge phenomenon of BESS is neglected in this thesis and hence not included in the mathematical models of the ESS. Constraint (2.63) ensures that the ESS energy level is within the minimum and maximum limits; and limits on charging and discharging power of the ESS are given by (2.64) and (2.65), respectively. Constraint (2.66) ensures that the charging and discharging process does not occur simultaneously.

Table 2.1 shows the typical parameters and preferences for the REH.

2.3 Energy Storage Systems

2.3.1 Energy Storage System Characteristics

The main characteristics and terms associated with ESSs are discussed here pertain to their integration with the power grid [67].

1. Storage capacity: it quantifies the available energy in the ESS after a full charging process, and is defined by the total energy stored (kWh). The amount of available energy that can be used, is governed by the Depth of Discharge (DoD). Furthermore, fast charging and discharging processes cause the ESS's efficiency to deteriorate, which decreases the obtained energy from the storage capacity.

Table 2.1: Parameters of the HEMS Model of a Typical REH [66]

Device	Parameter	Setting Value	Parameter	Setting Value	Parameter	Setting Value
Fridge (FR)	Θ_{fr_0}	3	α_{fr}	2.75	P_{fr}	0.6
	Θ_{fr}^{min}	0	β_{fr}	0.605		
	Θ_{fr}^{max}	10	γ_{fr}	0.14		
Water Heater (WH)	Θ_{wh_0}	50	α_{wh}	4.4	P_{wh}	0.6
	Θ_{wh}^{min}	48	β_{wh}	0.068	HR_{wh}	0.297
	Θ_{wh}^{max}	58	γ_{wh}	0.05	CG	0.029
Stove (STV)	EOT	65	ROT	12	P_{stv}	1.5
	LOT	88	MUT	4	$MSOT$	12
Dishwasher (DW)	EOT	65	MUT	8	P_{DW}	0.7
	LOT	92	MDT	4	$MSOT$	8
Washer (W)	EOT	64	MUT	8	P_{w}	0.45
	LOT	92	MDT	4	MSOT	8
Dryer (DRY)	EOT	64	MUT	8	P_{dry}	1.1
	LOT	92	MDT	4	$Gap_{W,Dry}$	8
Lighting	EOT	1	LOT	96	P_{li}	0.15
Pool (PMP)	EOT	29	MUT	1	P_{pmp}	0.75
	LOT	96	MDT	1	ROT	40
Energy Storage System (ESS)	E_{min}	1	$P_{C_{ESS}}^{max}$	0.45	EOT	1
	E_{max}	3.6	P_{ESS}^{max}	0.45	LOT	96
PV Panel Battery (BPV)	E_{min}	1	$P_{C_B}^{max}$	0.45	EOT	1
	E_{max}	3.6	$P_{D_B}^{max}$	0.45	LOT	96

2. SOC: it indicates the charging level of an ESS with respect to the maximum amount of energy that can be stored (considering its degraded state), typically expressed in percent.

3. Ramp rate: the rate of change of the ESS output power. It is usually expressed in terms of kW/s.

4. Round-trip efficiency: the ESS efficiency can be evaluated based on the energy loss during charging and discharging processes. The round-trip efficiency represents the relationship between the fraction of energy stored in the ESS to that can be retrieved.

5. Cycle and cycle life: a cycle of ESS can be defined as a discharging process followed by a complete recharging process. The number of charge-discharge cycles that can

be performed by an ESS until it reaches the stage when it is no longer suitable for a given application is called Cycle Life.

6. C-Rate: under ideal conditions, C-Rate = 1 means the total energy of the ESS is depleted in one hour, C-Rate = 2 means the energy depletion rate is doubled, i.e., depletes in 30 minutes, and so on.

7. Derating factor: it is a multiplier applied to the ESS energy capacity or rated power in order to take into account the SoH and degradation of the ESS.

The above characteristics vary in their values from one ESS technology to another. Different ESS technologies are available to provide specified services to the power grid. This thesis assumes BESS as the sole form of ESS which is present in a distribution system. BESS can be classified as solid-state and flow batteries. The first includes Li-ion, lead-acid (PbO_2), nickel-cadmium, and sodium sulphur technologies (NaS), while the latter includes vanadium redox (VRB), polysulphide bromide, and zinc-bromine. BESS operational life and cycle life depends upon the number of charge-discharge cycles. In addition, two factors play an essential role in determining the amount of energy that can be delivered and the degradation of the BESS, namely, the SOC and the DoD.

BESSs are one of the most mature energy storage technologies. These are able to deliver electrical energy using the chemical energy generated by electrochemical reactions [68]. The capacity of BESS varies from less than 10 kWh to several MWh with efficiency range between $60 - 90\%$ depending in two factors: operational cycle and electrochemistry type. Li-ion batteries have found several applications in power systems, their main advantages include high efficiency, fast response time, and significantly high life cycle [69].

2.4 Cycle Counting Using RCA

The RCA is a well-known methodology applied in material fatigue analysis, which can be used for fatigue life prediction [70]. it captures and extracts the irregular cycles from a loading history of an object.

The RCA has recently been used [71] to count the number of operational cycles of a BESS which is subject to degradation in its life due to charging and discharging stress. The stress on the BESS is represented in the form of DoD. In other words, a high DoD reduces the lifetime of the BESS, as shown in Figure 2.1 [72]. In addition, the operation of the BESS usually has irregular cycles, which can be counted using the RCA and used to study their impact on the asset life.

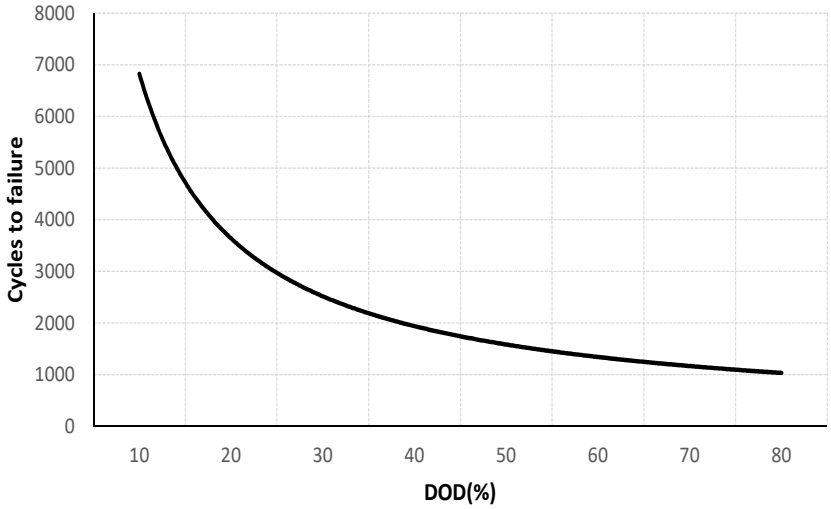

Figure 2.1: Typical cycles to failure vs. DoD curve of Li-ion batteries [72].

The RCA counting method includes four main steps: hysteresis filtering, peak-valley filtering, discretization, and a counting method (e.g. Four Point Method or Pagoda roof method). Hysteresis filtering aims to eliminate the short cycles which do not significantly contribute to the total damage of BESS. Peak-valley filtering comes after to identify the peaks and the valleys reversal in the operation profile of ESS. A peak is formed in the SOC profile when the change in SOC is negative, while a valley is formed when a change in the SOC is positive. Figure 2.2 and 2.3 presents an example SOC profile, where the alphabetical enumeration shows peak and valley points over time. Also, the green and red lines demonstrate the charging and discharging reversals, respectively, where each reversal represents a half cycle with a particular amplitude. In Pagoda roof method, the green and red lines represent flow of water from a number of Pagoda roofs. A half cycle can be counted at the end of a green or red line, which shows the termination of a water flow.

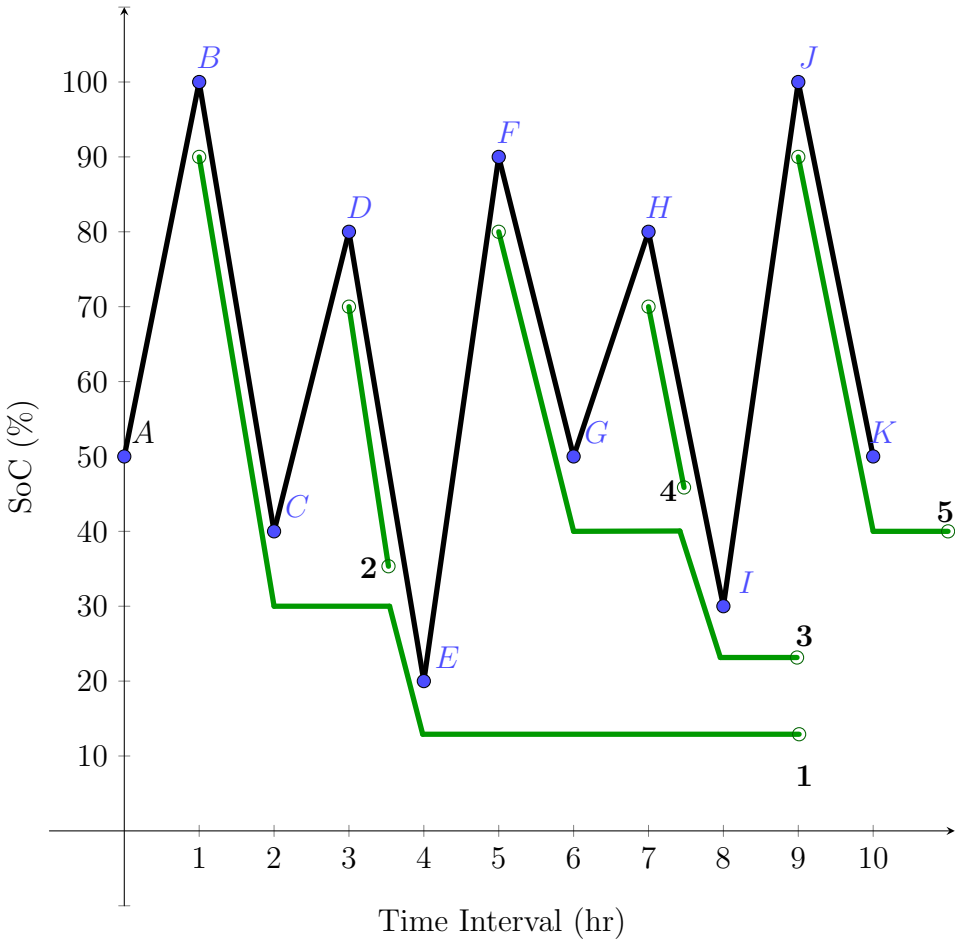

Figure 2.2: Peak filtering of an ESS operation profile.

The following cases show the possible termination scenarios of the water flow:

- The end of the flow can happen when a higher peak is reached, in peak filtering, or lower valley, in valley filtering. In Figure 2.3, water flow 1 encounters a lower valley C as compared to its starting valley A, and this counted as a half-cycle.
- A water flow merges with another water flow which started at an earlier peak or valley. As in Figure 2.2, the flow-2 merges with flow-1.
- A water flow arrives at the end of the time horizon, as shown in Figure 2.3, flow-3.

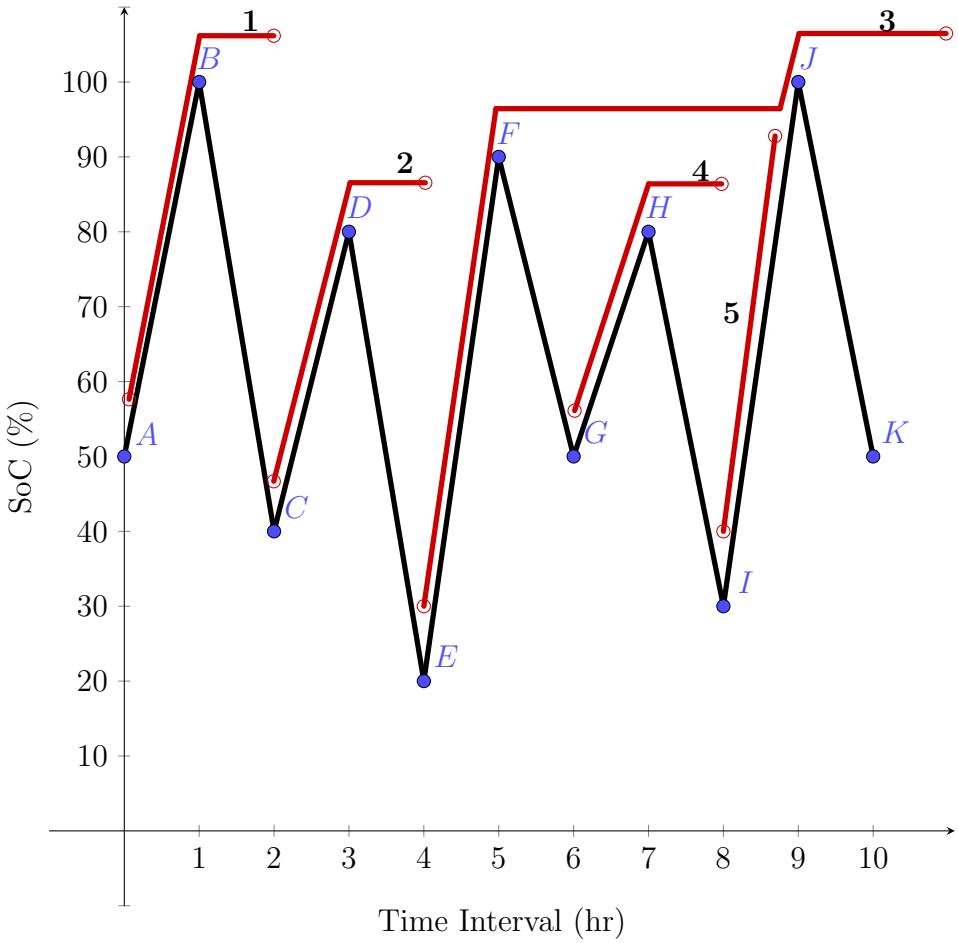

Figure 2.3: Valley filtering of an ESS operation profile.

Table 2.2 shows the range of each reversal and the cycle count. The obtain table from RCA then reduces by combining the cycles with the same range. Finally, the counted cycle can be used to estimate the cumulative damage on an asset such as BESSs.

2.5 Artificial Neural Network

The NN can be defined as [73], "*A neural network is an interconnected assembly of simple processing elements, units or nodes, whose functionality is loosely based on the*

Table 2.2: Rainflow Counting Algorithm Result

From	To	Absolute Range	Cycle Count
A	B	50	0.5
B	C	60	0.5
C	D	40	0.5
D	E	60	0.5
E	F	70	0.5
F	G	40	0.5
G	H	30	0.5
H	I	50	0.5
I	J	70	0.5
J	K	50	0.5

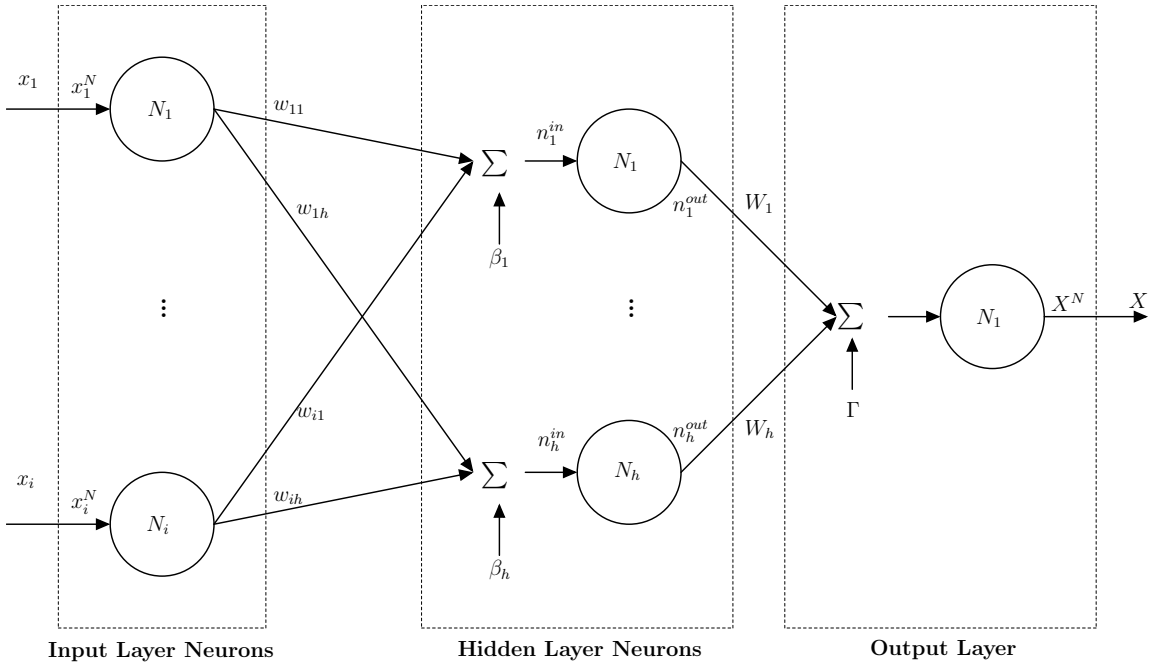

Figure 2.4: NN structure with a single hidden layer and output.

animal neuron. The processing ability of the network is stored in the inter-unit connection strengths, or weights, obtained by a process of adaptation to, or learning from, a set of training patterns". An NN consists of different layers, namely, input layer, hidden layers, and output layer, as in Figure 2.4. Each layer consists of a number of basic units called neurons. The input of the NN goes through different mathematical transformations, as follows:

Pre-processing input and post-processing output

Before training a NN, data preparation is required to normalize and standardize the input and output variables to re-scale the data into an acceptable range for the NN, hence improve its performance [74]. Different scaling techniques can be applied in pre-processing the inputs such as Min-Max normalization, mean normalization, and Z-score normalization. Min-Max normalization, for example, maps the range of features as follows:

$$x_i^N = \frac{2\ (x_i - \underline{x})}{(\overline{x} - \underline{x})} - 1 \tag{2.67}$$

Where, x_i^N is the normalized vector of x_i. The equation maps the feature x_i, given that its minimum and maximum values $\underline{x}$ and $\overline{x}$, respectively, falls between [-1,1].

Training

The input neurons pass the pre-processed data to the neurons of the subsequent layers. A neuron $i \in I$ of the input layer is linked with all neurons of the hidden layer $h \in H$ by weights w as shown below:

$$[w] = \begin{pmatrix} w_{11} & w_{12} & \cdots & w_{1h} \\ w_{21} & w_{22} & \cdots & w_{2h} \\ \vdots & \vdots & \ddots & \vdots \\ w_{i1} & w_{i2} & \ldots & w_{ih} \end{pmatrix} \tag{2.68}$$

The input to a hidden layer neuron can be represented as follows:

$$n_h^{in} = \sum_{i=1}^{I} w_{ih}\, x_i^N + \beta_h, \quad \forall h \tag{2.69}$$

The first component of (2.69) represents the weighted sum of the NN inputs, while the second component is the bias (β_h) of the hidden layer neuron h. The input to a hidden layer neuron, then, is processed using an activation function to calculate the hidden layer neuron's output. There are several types of activation functions such as Sigmoid function, Hyperbolic Tangent Function, and Softmax Function. Using the commonly used Sigmoid activation function, the hidden layer neuron output is:

$$n_h^{out} = \frac{2}{1 + \exp\left(-2\, n_h^{in}\right)} - 1 \tag{2.70}$$

The calculated output n_h^{out} of the hidden layer neuron using (2.70) is passed through the activation function of the output layer neuron, which can be a linear transfer function, as follows:

$$X^N = \sum_{h}^{N_H} n_h^{out}\, W_h + \Gamma \tag{2.71}$$

Finally, the normalized output (X^N) of the output layer neuron represents the normalized predicted output value, which can be post-processed to obtain the required output value, as presented below:

$$X = \frac{(X^N - \underline{X}^N)(\overline{X} - \underline{X})}{2} + \underline{X} \tag{2.72}$$

2.6 Cooperative Game Theory

Game theory can be defined as the field of mathematical modeling of the interaction between a number of rational players [75], where each player's decision making process is impacted by other players. Such competitive behavior is classified into two categories: non-

cooperative and cooperative games. The first presents the strategic behavior of individual players without an external entity that forces rules, so as to maximize their own benefits. On the other hand, the second is governed by a set of rules to maximize the benefit of a coalition of players. In this thesis, a coalitional game is considered, where a group of BESSs acts together to maximize their payoffs and provides different services to the LDC. The redistribution of the total system saving between BESS's owners are achieved using the Shapley value criterion.

The Shapley value criterion associates a unique payoff for every individual within a coalition. The payoffs should satisfy the following axioms [76]:

- *Additivity: A sum of the cost saving, which a player receives as a member of every coalition formed with other players, represents the cost saving allocated to that player.*
- *Dummy player: If the total value of different possible coalitions remains the same when a player joins the coalition, it is called a dummy player.*
- *Efficiency: The sum of the players' payoffs represents the value of the grand coalition. In other words, the payments given to the players in a coalition represents the total payoffs that can be achieved from their cooperation.*
- *Symmetry: If two players are identical to each other with no change in the coalition's value, those players are symmetrical.*

Therefore, the Shapley value criterion represents the marginal contribution of a player to a coalition, which is mathematically given as follows [77]:

$$v(h) = v(S) - v(S - h) \tag{2.73}$$

The marginal contribution of a player h to a coalition S is given by the change in the utility value of the coalition after h's joining the coalition. The sum of a player h's marginal contributions is divided by $c(q)$, the number of all formed coalitions of size q that contains the player h, and n is the total number of players. The Shapley value can be calculated as

follows:

$$\phi_h = \frac{1}{n} \sum_{q=1}^{n} \frac{1}{c(S)} \sum_{h \in S} \Big[v(S) - v(S-h) \Big] \tag{2.74}$$

where,

$$c(q) = \frac{(n-1)!}{(n-q)!(q-1)!} \tag{2.75}$$

2.7 Summary

In this chapter, some essential background topics required for this research were introduced. The concepts of REH and HEMS with their mathematical model were discussed. A brief discussion of the RCA and NN were presented. Finally, cooperative game theory definition and the Shapley value were discussed.

Chapter 3

Flexibility of Residential Loads for Demand Response Provisions in Smart Grid[1]

This chapter proposes a two-stage optimization framework wherein multiple HEMSs simultaneously optimize their respective energy consumption patterns and determine their flexibility provisions, which is communicated to the LDC. The LDC aggregates the controllable demand profile and the flexibilities of each HEMS to optimize its operational performance and hence the peak reduction signals which are sent to the HEMSs. Studies are carried out considering a 33-bus distribution system coordinating with 1,295 houses, each with varying customer preferences and objectives, to demonstrate the applicability of the proposed scheme.

The mathematical model of the HEMS was discussed in Chapter 2; the LDC's operational model and the proposed coordination between the REHs and the LDC is discussed here.

[1]This chapter has been published as:
O. Alrumayh and K. Bhattacharya, "Flexibility of Residential Loads for Demand Response Provisions in Smart Grid," in *IEEE Transactions on Smart Grid*, vol. 10, no. 6, pp. 6284-6297, Nov. 2019.

3.1 Nomenclature

Indices and Sets

h_j	Index for household located at bus j
i	Index for household appliances, $i \in \mathcal{A}$
j,k	Index for bus ($j = s$, substation), $(j,k) \in \mathcal{N}$
q	Index for Energy Storage Device (ESS) and Battery (B)
t	Index for time, $t \in \mathcal{T}$
$\mathcal{H}$	Set of households

Parameters

γ^{FLEX}	Objective function weight assigned by LDC on scheduled flexibility
$E^{min}_{q,h_j,t}$, $E^{max}_{q,h_j,t}$	Minimum and maximum energy level, kWh
$E^{Initial}_{B}$, E^{Final}_{B}	Initial and final energy level of battery, kWh
$E^{AR}_{q,h_j,t}$	Energy level at arrival, kWh
$G_{j,k}$	Conductance of feeder between buses, $p.u$
g_{i,h_j}	Gas consumption rate, m^3/hr
$P^{max}_{C_{q,h_j}}$, $P^{max}_{D_{q,h_j}}$	Maximum charging/discharging power, kW
$P_{D0_{h_j}}$	Connected load in house, kW
$P^{min}_{g_j}$, $P^{max}_{g_j}$	Minimum and maximum generation level, $p.u$
$P_{LI_{h_j}}$	Rated power of the lighting system, kW
P_{i,h_j}	Rated power of appliance, kW
$P^{d}_{j,t}$	Active power drawn by residential loads, $p.u$
$P^{Imp}_{j,t}$	Total power purchased by LDC from residential loads, $p.u$
$P^{CAP}_{j,t}$	Peak load of the feeder, $p.u$

$P_{h_j,t}^{\overline{FLEX}}$	Customer flexibility available, kW
$P_{j,t}^{\overline{FLEX}}$	Aggregated bus-wise flexibility, kW
$P_{PV_{h_j},t}$	PV panel generation in house, kW
$Q_{j,t}^{d}$	Reactive power drawn by residential loads, $p.u$
$t_{h_j}^{AR}$, $t_{h_j}^{DEP}$	Electric vehicle arrival/departure from/to house h_j , min
V_j^{min}, V_j^{max}	Minimum and maximum voltage level, $p.u$
$Y_{j,k}$	Magnitude of admittance matrix element
β	Peak load factor
η_1, η_2	Charging/discharging efficiency, %
ω_{h_j}	Charging level factor at departure of household h_j
ρ_t^{TOU},ρ^{SEL}, ρ^{GAS}	Time of use price $\$/kWh$, selling price to the LDC $\$/kWh$, and Gas price $\$/m^3$
τ	Length of the time interval
$\theta_{j,k}$	Angle of complex Y-bus matrix element, $p.u$
Θ_{i,h_j}^{set}	Preferred temperature setting of appliance, $^\circ C$

Variables

$E_{q,h_j,t}$	Energy level, kWh
$L_{h_j,t}$	Illumination level
$P_{C_{B,h_j},t}$	Total charging power drawn by Battery, kW
$P_{C_{B,h_j},t}^{PV}$	Generated power by PV solar panel used to charge the battery, kW
$P_{C_{q,h_j},t}^{LDC}$	Charging power drawn by device, kW
$P_{D_{B,h_j},t}$	Total discharged power from Battery, kW
$P_{D_{q,h_j},t}^{H}$	Discharging power from device to house, kW
$P_{D_{q,h_j},t}^{LDC}$	Discharging power from device to LDC, kW

$P^{g}_{j,t}$	Active power drawn from substation at bus, $p.u$
$P^{FLEX}_{j,t}$	Active power flexibility scheduled, $p.u$
$P^{H}_{LDC_{h_j,t}}$	Delivered power by LDC to meet house demand, kW
$P^{i}_{LDC_{h_j,t}}$	Delivered power by LDC to meet appliance i demand, kW
$P^{H}_{PV,h_j,t}$	PV generated power consumed by household appliances, kW
$P^{LDC}_{PV,h_j,t}$	Generated power by PV solar panel sold to LDC in house, kW
$P^{max}_{h_j,t}$	House h_j maximum demand, kW
$\widehat{P}^{max}_{h_j,t}$	Updated house maximum demand, kW
$Q^{g}_{j,t}$	Reactive power drawn from substation at bus, $p.u$
$Q^{FLEX}_{j,t}$	Reactive power flexibility, $p.u$
$S_{C_{q,h_j,t}}$	Binary charging status of device, ON/OFF
$S_{D_{q,h_j,t}}$	Binary discharging status of device, ON/OFF
$S_{i,h_j,t}$	Binary status of device, ON/OFF
$V_{j,t}$	Voltage at bus, $p.u$
$\delta_{j,t}$	Voltage angle at bus, $p.u$
$\Theta^{in}_{i,h_j,t}$	Temperature level of appliance,$^{\circ}C$
$\alpha_{h_j,t}$	flexibility index of customer

3.2 Proposed Coordination Framework and Mathematical Models

In [22] and [65], a comprehensive representation of a generic REH was presented, and which was equipped with an HEMS. The REH was equipped with the following appliances: fridge, water heater, lighting system, air-conditioning, dishwasher, washer, dryer, stove, and pool, an ESS and a rooftop PV panel (see Fig.3.1). The charging and discharging operations of the ESS are controlled by the HEMS; the ESS is charged by the power drawn from the grid, while at peak demand hours, it can discharge power to the grid and earn revenue. The PV panel battery can be charged either by the power drawn from the grid or from the PV panel directly. The stored energy in the PV panel battery can be used to supply the REH or sold to the grid. The HEMS controls the PV panel operation also, i.e., how much is allocated to meet the house load, to charge the PV panel battery, or sell to the grid. Indeed, the ESS and the PV panel battery creates an additional power demand of the REH when in charging mode. The PV generation depends on the weather conditions and PV panel features. Note that while the PV panel batteries represent stationary storage, the ESSs essentially account for the mobile storage devices present in the house, such as PEV.

In this work, a two-stage framework is proposed to aggregate and coordinate the contributions of a large number of HEMS within REHs to provide a flexibility service to the LDC. The HEMS mathematical model is formulated by significantly improving upon the model in [22], which optimizes the operations of typical home appliances and ESSs to determine the optimal interactions with the LDC such as the power to be sold to or purchased from the LDC, while considering different objectives of the REH. Thereafter, a residential feeder is considered, where, at each bus, several such REHs, equipped with HEMS are assumed being served by the LDC; each home receives a control signal from the LDC pertaining to a cap on its hourly load, based on which each HEMS re-optimizes their loads to meet the prescribed cap. This creates an aggregated flexibility capacity at each bus, through load shifting, HEMS optimization, and LDC imposed load cap at the feeder bus. This proposed decentralized approach maintains privacy of the individual customers, not requiring them to provide their electricity usage profiles to the LDC; each

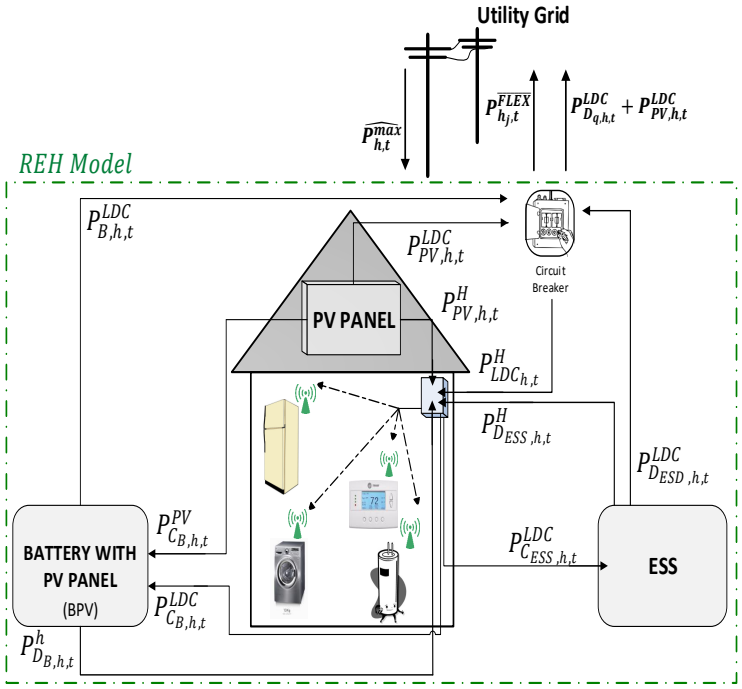

Figure 3.1: Schematic of a Residential Energy Hub.

HEMS achieves its own objective, while the overall framework converges to an equilibrium, to the satisfaction of all parties. Such coordination between the HEMS and the LDC can improve grid operations by flattening the system load profile, improving bus voltages, reducing losses, and LDC's operating costs. Indeed, the work considers a realistic scenario where multiple REHs with different behaviors, preferences, and locations, are coordinated to provide flexibility to the LDC taking advantage of their inherent elasticity.

Figure 3.2 shows a detailed layout of the proposed coordination scheme. This layout has three levels, namely, REH level, LDC level, and coordination level.

3.2.1 Residential Energy Hub and HEMS (Stage: Ia, Ib, Ic)

The following three stages are required to present different REH customer consumption behaviors, to formulate the HEMS mathematical model, and to evaluate the REH

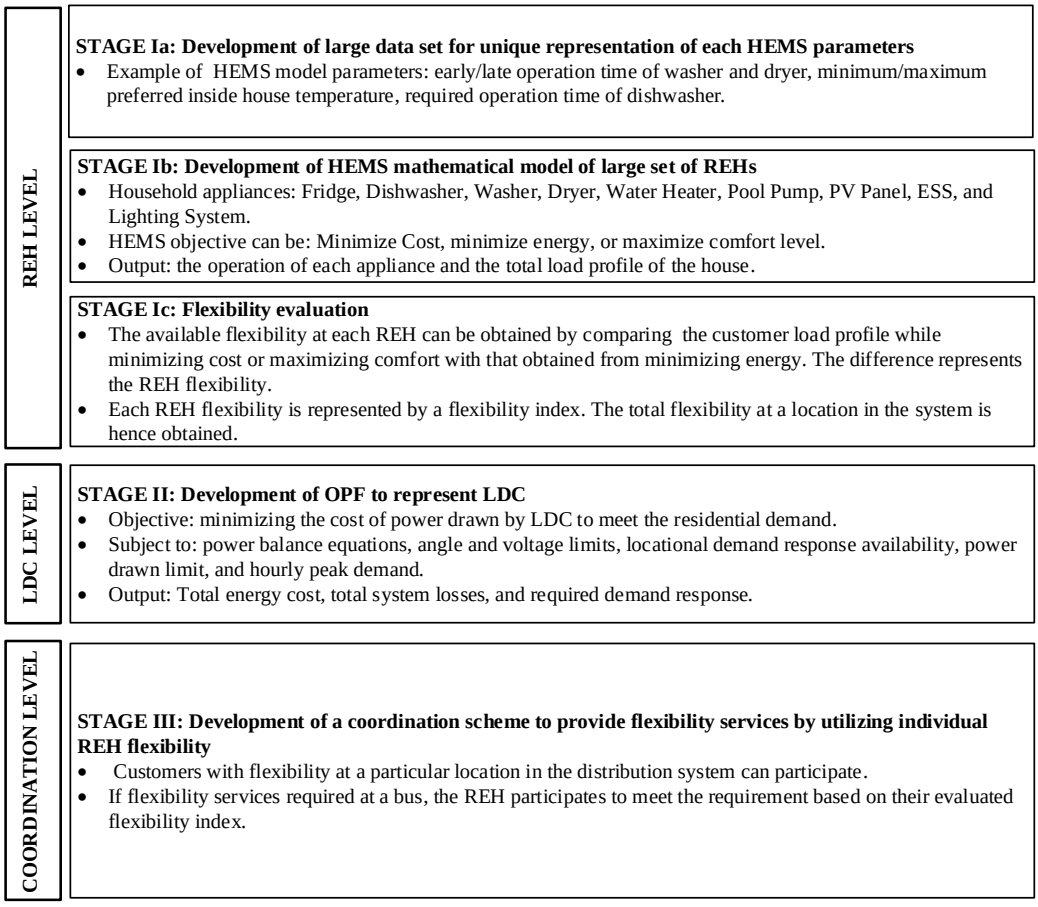

Figure 3.2: Required levels and stages of the proposed coordination scheme.

flexibility.

Stage-Ia: In order to represent each HEMS individually, unique objective functions, activity levels, and customer preferences (e.g. the required operation time and minimum up/down time of washer, dryer, stove) are generated randomly.

Stage-Ib: The HEMS mathematical model is formulated and solved considering the mathematical model (2.4)-(2.66) discussed in Chapter-2 with some modifications to present the two-way communication between residential loads and the LDC, discussed later.

Objective Functions

Three different objectives are used for the multiple HEMSs considered in this work, as given below:

Minimize Cost: the objective of REH h_j located at bus j is to minimize its total cost of energy, net of revenue earned.

$$J1_{h_j} = \sum_{t\in\mathcal{T}} \Bigg[\rho_t^{TOU} \Big\{ \sum_{\substack{i\in\mathcal{A} \\ i\notin\{LI,ESS,BPV\}}} P_{i,h_j} S_{i,h_j,t} + \sum_{z\in LI} P_{LI_{h_j}} L_{h_j,t} + \sum_{i\in\{BPV,ESS\}} P^i_{LDC_{h_j,t}} + P_{D0_{h_j}} \Big\} + \sum_{i\in\{HT,WH\}} \rho^{GAS} g_{i,h_j} S_{i,h_j,t} - \rho^{SEL} \Big\{ \sum_{i\in\{BPV,ESS\}} P^{LDC}_{D_{i,h_j,t}} + P^{LDC}_{PV,h_j,t} \Big\} \Bigg], \ \forall\, h_j \in \mathcal{H} \quad (3.1)$$

In (3.1), the terms within the first curly brackets represents the power drawn by household appliances, the lighting system, the charging power drawn by the ESS and PV panel battery, and the uncontrolled load; which all together, denote the total power drawn from the grid. The term associated with ρ^{GAS} presents the total cost of gas consumption. The discharged power from ESS and PV panel battery accounts for the power sold to the grid.

Minimize Energy Consumption: the REH minimizes its total energy consumption over the day.

$$J2_{h_j} = \sum_{t\in\mathcal{T}} \Bigg[\sum_{\substack{i\in\mathcal{A} \\ i\notin\{LI,ESS,BPV\}}} P_{i,h_j} S_{i,h_j,t} + \sum_{z\in LI} P_{LI_{h_j}} L_{h_j,t} + \sum_{i\in\{BPV,ESS\}} P^i_{LDC_{h_j,t}} + P_{D0_{h_j}} + \sum_{i\in\{HT,WH\}} g_{i,h_j} S_{i,h_j,t} \Bigg], \forall h_j \in \mathcal{H} \quad (3.2)$$

Maximize Comfort Level: the REH maximizes its comfort level by minimizing the

temperature deviations of certain appliances from their preferred set points.

$$J3_{h_j} = \sum_{t \in \mathcal{T}} \left[\sum_{i \in \{AC,HT,WH,FR\}} \left(\Theta^{in}_{i,h_j,t} - \Theta^{set}_{i,h_j} \right)^2 \right], \quad \forall h_j \in \mathcal{H} \tag{3.3}$$

Note that (3.3) is linearized using the method reported in [78] to arrive at an MILP model.

Appliance Constraints: the REH h_j appliances operational model was discussed in detail in Chapter-2 and it included the equations (2.4) to (2.66). In the present work, the REH model is further improved by incorporating the following constraints:

Peak Load Constraint: Ensures that the total load of REH h_j is within a limit specified by the LDC, $\widehat{P}^{max}_{h_j,t}$.

$$\sum_{i \in \mathcal{A}} P_{i,h_j} S_{i,h_j,t} + \sum_{i \in \{BPV,ESS\}} P^{LDC}_{i,h_j,t} - \sum_{i \in \{BPV,ESS\}} P^{H}_{D_{i,h_j,t}} - P^{H}_{PV,h_j,t} \leq \widehat{P}^{max}_{h_j,t}, \forall h_j \in \mathcal{H} \tag{3.4}$$

In (3.4), the REH load includes the appliances' consumption; charging power of ESS and PV panel battery, net of the power discharged from the ESS; the PV panel battery; and that generated by the PV panel to supply some of the REH loads.

$$\widehat{P}^{max}_{h_j,t} = P^{max}_{h_j,t} - \alpha_{h_j,t} P^{FLEX}_{j,t}, \quad \forall t \in \mathcal{T}; \forall h_j \in \mathcal{H}; \forall j \in \mathcal{N} \tag{3.5}$$

Constraint (3.5) represents the two-way communication between the LDC and the HEMS- the updated maximum demand of REH h_j, $\widehat{P}^{max}_{h_j,t}$, is based on the previous maximum allowable demand, $P^{max}_{h_j,t}$, and a portion of the flexibility requested by the LDC at bus j; $\alpha_{h_j,t}$ represents the REH's flexibility index, which is explained in Stage-III.

REH Power Balance: Ensures that the total power demand of the household appliances is met by the power drawn from the grid and power discharged to the REH from the ESS and PV panel battery, and that generated by the PV system, as given below:

$$\sum_{i \in \mathcal{A}} P_{i,h_j} S_{i,h_j,t} = P^{H}_{LDC,h_j,t} + \sum_{i \in \{B,ESS\}} P^{H}_{D_{i,h_j,t}} + P^{H}_{PV,h_j,t}, \quad \forall t \in \mathcal{T}; \ \forall h_j \in \mathcal{H} \tag{3.6}$$

The optimal decisions of the HEMS includes the operating decisions of appliances, the energy sold or purchased to/from the utility grid, the charging/discharging decisions of the ESS and the PV panel battery, and the resulting aggregated load profile of the REH.

Stage-Ic: In this last stage of the house level, flexibility provisions of the REH is determined as follows:

$$\triangle P_{h_j,t} = \left[\sum_{i\in\mathcal{A}} P_{i,h_j} S_{i,h_j,t}\right]_{J1_{h_j}\, or\, J3_{h_j}} - \left[\sum_{i\in\mathcal{A}} P_{i,h_j} S_{i,h_j,t}\right]_{J2_{h_j}}, \forall t \in \mathcal{T};\ \forall h_j \in \mathcal{H} \tag{3.7}$$

$$\alpha_{h_j,t} = \frac{\triangle P_{h_j,t}}{\sum\limits_{h\in\mathcal{H}} \triangle P_{h_j,t}}, \quad \forall t \in \mathcal{T}; \forall h_j \in \mathcal{H} \tag{3.8}$$

The flexibility of the REH, given by (3.7), is obtained from the difference between its scheduled load at an hour using the energy cost minimizing model with that obtained from the energy consumption minimizing model. For some REHs seeking to maximize comfort, the flexibility is the difference between its scheduled load at an hour using the maximizing comfort level model with that obtained from the energy consumption minimizing model. The total flexibility at a bus is the sum of the flexibility from all REHs connected at the bus, given by, $\sum\limits_{h\in\mathcal{H}} \triangle P_{h_j,t}$. The REH flexibility index $\alpha_{h_j,t}$ in (3.8), is obtained by normalizing an REH's flexibility by the total flexibility at that bus. The optimal flexibility is proportionally allocated to each REH based on the value of $\alpha_{h_j,t}$.

3.2.2 LDC Operations Model (Stage-II)

The objective of the LDC is to minimize total system losses and a weighted component of the total flexibility, as given below:

$$J = \sum_{t\in\mathcal{T}} \Big[\frac{1}{2}\sum_{j=1}^{N}\sum_{k=1}^{N} G_{j,k}\Big(V_{j,t}^2 + V_{k,t}^2 - 2V_{j,t}V_{k,t}\cos(\delta_{j,t} - \delta_{k,t})\Big) + \sum_{j=1}^{N} \gamma^{FLEX} P_{j,t}^{FLEX}\Big] \tag{3.9}$$

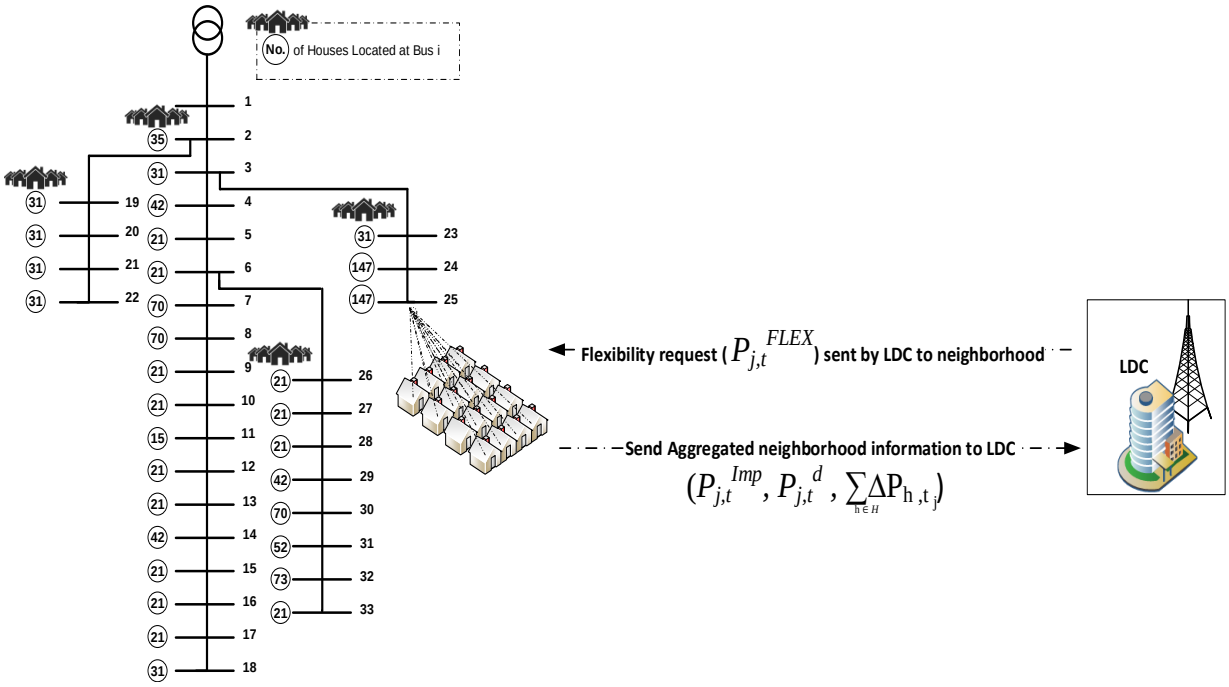

Figure 3.3: Schematic of coordination between HEMS and LDC.

and subjected to the following power flow equations,

$$P_{j,t}^{g} + P_{j,t}^{Imp} + P_{j,t}^{FLEX} - P_{j,t}^{d} = \sum_{k=1}^{N} V_{j,t} V_{k,t} Y_{j,k} \cos\left(\theta_{j,k,t} + \delta_{k,t} - \delta_{j,t}\right), \quad \forall t \in \mathcal{T};\ \forall (j,k) \in \mathcal{N} \quad (3.10)$$

$$Q_{j,t}^{g} + Q_{j,t}^{FLEX} - Q_{j,t}^{d} = -\sum_{k=1}^{N} V_{j,t} V_{k,t} Y_{j,k} \sin\left(\theta_{j,k,t} + \delta_{k,t} - \delta_{j,t}\right), \quad \forall t \in \mathcal{T};\ \forall (j,k) \in \mathcal{N} \quad (3.11)$$

Where,

$$P_{j,t}^{Imp} = \sum_{h}^{\mathcal{H}} \Big(\sum_{i \in \{B, ESS\}} P_{D_{i,h_j,t}}^{LDC} + P_{PV,h_j,t}^{LDC} \Big), \quad \forall t \in \mathcal{T}; \forall j \in \mathcal{N} \quad (3.12)$$

In (3.11), $Q^{d}_{j,t}$ and $Q^{FLEX}_{j,t}$ are obtained from $P^{d}_{j,t}$ and $P^{FLEX}_{j,t}$ a using constant load power factor of 0.9, $P^{Imp}_{j,t}$ is the aggregate power import by the LDC from all REHs located at bus j, as given in (3.12). And, given that,

$$P^{d}_{j,t} = \sum_{h}^{\mathcal{H}} \Big(\sum_{\substack{i \in \mathcal{A} \\ i \notin \{LI, ESS, BPV\}}} P_{i,h_j} S_{i,h_j,t} + \sum_{z \in LI} P_{LI_{h_j}} L_{h_j,t} + \sum_{i \in \{BPV, ESS\}} P^{i}_{LDC_{h_j,t}} + P_{D0_{h_j}} \Big), \quad \forall t \in \mathcal{T};\ \forall j \in \mathcal{N} \tag{3.13}$$

In (3.13), $P^{d}_{j,t}$ represents the aggregated load at bus j and time t from multiple REHs. The LDC operations model also includes constraints on bus voltages and power drawn from the substation, as given below:

$$V^{min}_{j} \leq V_{j,t} \leq V^{max}_{j}, \quad \forall t \in \mathcal{T};\ \forall j \in \mathcal{N} \tag{3.14}$$

$$P^{min}_{g_j} \leq P^{g}_{j,t} \leq P^{max}_{g_j}, \quad \forall t \in \mathcal{T};\ \forall j = s \tag{3.15}$$

3.2.3 Coordination of Multiple HEMS and LDC (Stage-III)

A novel coordination scheme between the multipleREHs and the LDC is presented herein.

- It is assumed that all REH are equipped with HEMS which receive input updates such as customer preferences and weather forecast, as shown in Fig.3.4 under "Data collection and analysis".
- The REHs are clustered in three groups based on their objective function and their possession of ESS and PV panel. The HEMSs then optimizes the operations, using the optimization models OPT.1, OPT.3, and OPT.5, of their respective household appliances considering one of: cost minimization or comfort maximization objective, and appliance operational constraints, see Fig.3.4. Furthermore, the last process at the house level is to evaluate the available household flexibility.

- The resulting optimal load profile and other optimal decisions, such as how much power the house can sell to the distribution grid, and the available flexibility are communicated to the LDC, one day ahead, $P_{j,t}^{Imp}$, $P_{j,t}^{d}$, and $P_{j,t}^{\overline{FLEX}}$ (see Fig.3.3 and 3.4).

- The LDC develops a bus-wise load profile by aggregating the customers' optimized load profiles, executes the LDC operations model, and hence evaluates its system operating conditions considering its objective and constraints (3.9)-(3.15). In addition to the mentioned constraints, the LDC can take advantage of the inherent flexibility of the customers by imposing a peak demand cap. Such decision is limited by the customers' evaluated flexibility, see constraint (3.16). This cap changes the operation schedules of the participating customers and benefits the LDC. The peak load of the feeder at bus j, hour t, is $P_{j,t}^{cap}$; when the LDC has to request for flexibility from customers, it sends a request signal $P_{j,t}^{FLEX}$, as shown in Fig.3.3; with an appropriate choice of β, where $P_{j,t}^{FLEX}$ is limited by the aggregated customers' flexibility, at bus j, as given below:

$$\begin{aligned} \beta P_{j,t}^{cap} \leq P_{j,t}^{FLEX} \leq P_{j,t}^{\overline{FLEX}} \quad if \quad P_{j,t}^{\overline{FLEX}} \geq 0, \ \ \forall\, j \in \mathcal{N} \\ -\beta P_{j,t}^{cap} \geq P_{j,t}^{FLEX} \geq P_{j,t}^{\overline{FLEX}}\, if \quad P_{j,t}^{\overline{FLEX}} \leq 0, \quad \forall\, j \in \mathcal{N} \end{aligned} \tag{3.16}$$

  In (3.16), $P_{j,t}^{\overline{FLEX}}$ positive denotes that the customers are willing to reduce their consumption at bus j and time t, from their optimal schedule to the minimum energy consumption operation. While, $P_{j,t}^{\overline{FLEX}}$ negative indicates the customer is willing to increase its consumption.

- From this analysis, the hour-wise optimal flexibility use required by the LDC is determined considering the bus-wise flexibility obtained from (3.7)-(3.8).

- This bus-wise, hourly, optimal flexibility is then proportionally allocated to each house based on the flexibility index $\alpha_{h_j,t}$ of the customer, and communicated to individual HEMS. The respective HEMS in turn incorporates these signals as a 'peak demand cap' (3.5), and re-optimizes their respective appliance schedules.

- Note that, a household will only submit to the LDC its aggregate load profile, how much it would sell/buy to/from the grid, and how much flexibility provision is available next day. There will be no exchange of private information of the customer or its activity schedules.
- The HEMS and the LDC optimization models are interlinked by external signals, as shown in Fig.3.3, wherein the LDC receives the $P_{j,t}^{Imp}$, $P_{j,t}^{d}$, and $P_{j,t}^{\overline{FLEX}}$ signals from HEMS while the HEMS receives $P_{j,t}^{FLEX}$ signal from the LDC, based on which the optimal decisions of each, are determined. This is a two-stage sequential process involving information exchange and effective communication between the houses and the LDC.

The proposed coordination scheme enables each REH to carry out its desired operation based on its own objective while preserving information privacy and security while at the same time providing a flexibility service to the LDC to improve grid operations and reliability.

3.3 Results and Discussions

3.3.1 Case Study

In this work, the LDC is responsible for managing a 33-bus distribution system and meeting the demand of 1,295 houses connected at its various buses. The number of houses at each bus is shown in Fig.3.3 (within the circles), which is obtained assuming that the connected load at a house is 7 kW. In order to represent each HEMS individually, unique objective functions, activity levels, and customer preferences (i.e, the required operation time and minimum up/down time of washer, dryer, stove, etc.) are randomly generated. Furthermore, the TOU rates applicable in Ontario, Canada, are used in this study [79]. The list of parameters and their values, associated with a single typical HEMS model is provided in the Appendix.

Three customer clusters are considered to evaluate the flexibility of residential customers in providing DR services to the LDC: Cluster-1: 80% of the customers own

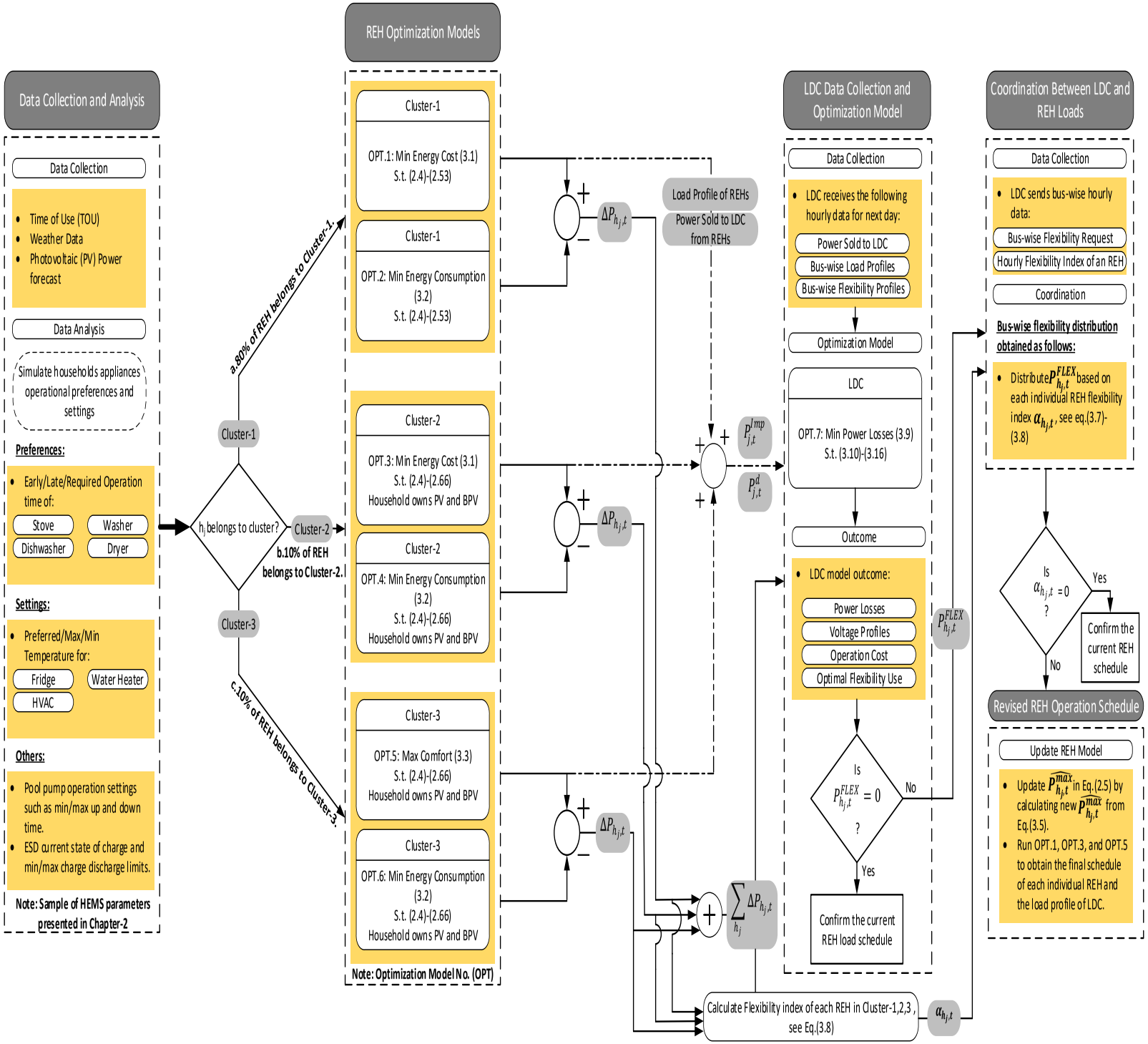

Figure 3.4: Coordination of multiple HEMS and LDC.

typical household appliances and seek to minimize their energy cost; Cluster-2: 10% customers own typical household appliances, ESS, and PV panel, and seek to minimize their energy cost; and Cluster-3: 10% customers own typical household appliances, ESS, and PV panel, and seek to maximize their comfort level. Each cluster of customers are distributed at all buses uniformly. It is important to mention that many households do not change their initial consumption level either because of their limited flexibility in consumption patterns or their limited affect on the LDC system operation. The customers from Cluster-2 and -3 do not impact the system peak load since they own RESs which reduce their energy consumption during peak hours. Consequently, the results of Cluster-1 customers are only discussed in this paper. Different peak reduction requests (PRR) values have been considered to evaluate the customers flexibility, as follows:

- Case-1: Base case, no PRR requested by LDC, $\beta = 1$
- Case-2: PRR request by LDC is 5%, *i.e.*, $\beta = 0.95$;
- Case-3: PRR request by LDC is 10%, *i.e.*, $\beta = 0.9$;
- Case-4: PRR request by LDC is 20%, *i.e.*, $\beta = 0.8$;

3.3.2 HEMS Level Outcomes

At the house level, Table-3.1 presents one typical household's appliance-wise consumption on a summer day (house #400 located at bus-14). Figure 3.5 (A) and (B) shows a residential customer's load profile while minimizing energy and energy cost, respectively. In addition, it presents the customer flexibility in Fig.3.5 (C), and this information is communicated to the LDC.

It can be noted that the energy cost rate of the household increases from Case-I (Base Case) to the cases with flexibility provisions, as a result of the PRR imposed by the LDC, which limits the power that can be drawn from the grid at low price hours. Fig.3.6 shows the ON/OFF operation of the dishwasher in house #400, which depends on the required

Table 3.1: Energy Consumption and Cost of REH #400 per Day, for Different $P_{j,t}^{FLEX}$

Device		CASE 1 (Base)		CASE 2 (5% PRR)		CASE 3 (10% PRR)		CASE 4 (20% PRR)	
		(kWh)	($)	(kWh)	($)	(kWh)	($)	(kWh)	($)
fridge		1.425	0.501	1.463	0.520	1.425	0.522	1.425	0.517
water heater	Elec.	0.225	0.078	0.225	0.078	0.225	0.078	0.225	0.078
	Gas	0.111	0.013	0.111	0.013	0.111	0.013	0.111	0.013
lighting		1.245	0.453	1.245	0.453	1.245	0.453	1.245	0.453
AC		5.225	1.855	5.363	2.038	5.363	2.001	5.225	1.982
Dishwasher		0.350	0.091	0.350	0.131	0.350	0.161	0.350	0.142
Washer		0.225	0.059	0.225	0.074	0.225	0.100	0.225	0.089
Dryer		0.555	0.144	0.555	0.181	0.555	0.262	0.555	0.225
Stove		1.125	0.293	1.125	0.393	1.125	0.483	1.125	0.497
Pool		1.875	0.538	1.875	0.641	1.875	0.627	1.875	0.614
Total		12.361	4.024	12.536	4.522	12.499	4.700	12.361	4.608
Cost of Energy ($/$kWh$)		0.3255		0.361		0.376		0.373	

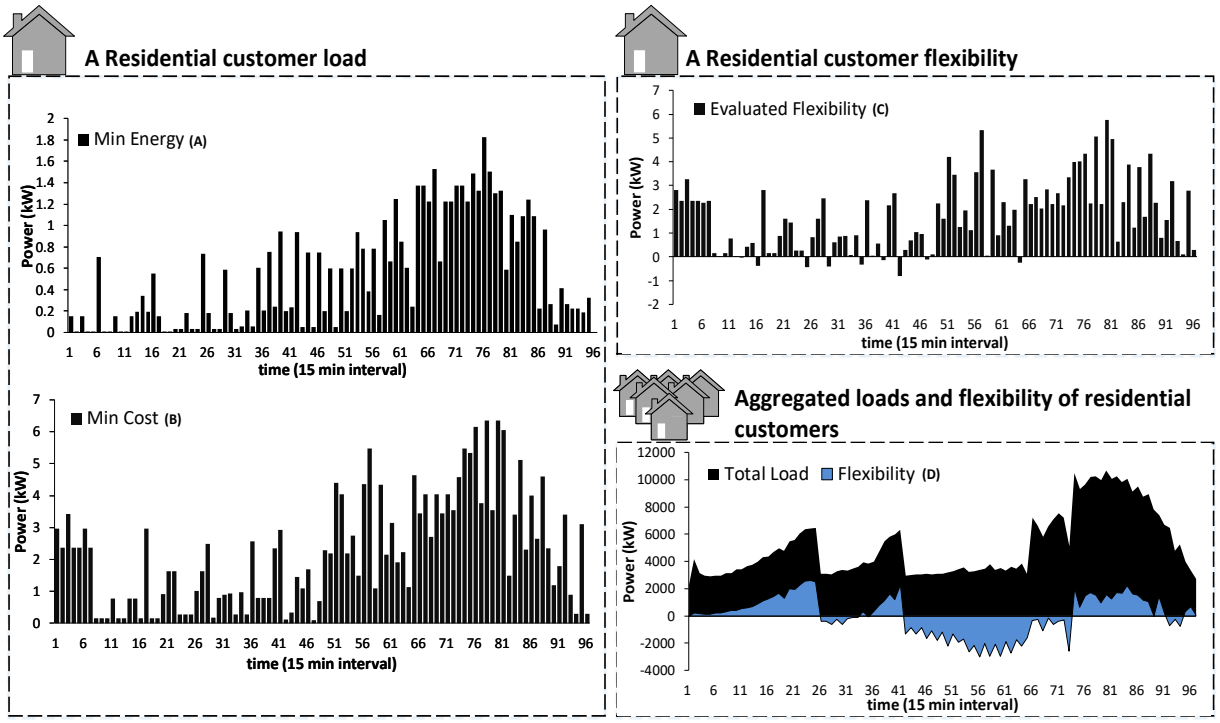

Figure 3.5: Load and flexibility profiles at residential and grid levels.

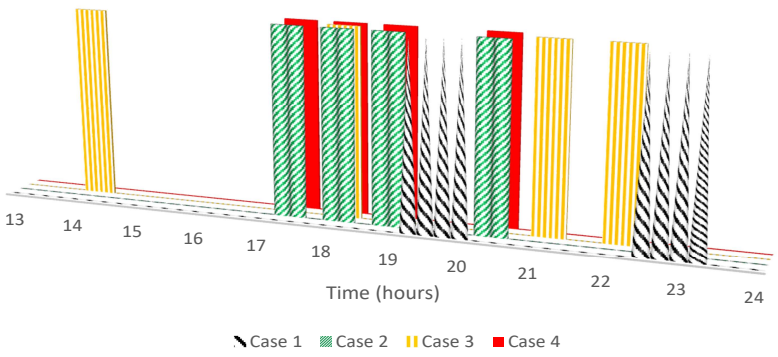

Figure 3.6: Optimal operation of selected appliance (dishwasher) at house #400.

operation time (i.e., eight time intervals), operation interval (i.e., from 2 PM to midnight), and the minimum time gap between two consecutive operations (minimum of two time intervals). In Case-1 (Base Case), the operation of the dishwasher is scheduled at two periods, each of four time intervals. It can be noted that the optimal schedule changes with different peak caps signals (β values) imposed by the LDC.

Fig.3.7 shows the temperature deviation inside house #400, refrigerator and the operation of the water heater for different values of β (different peak caps) imposed by the LDC. Note that the range specified by the customer for the minimum and maximum temperature, governs the degree of customer flexibility that would be available.

Fig.3.8 illustrates the variation in the total household consumption between Case-1 and Case-2; and Case-1 and Case-3, respectively. It is noted that the peak hours of power usage of the house is shifted as a result of peak signals sent by the LDC.

3.3.3 LDC Level Outcomes

At the LDC side, Fig.3.9 presents the total load profile of the distribution system. It can be noted from the figure that TOU tariffs, which are applicable in the present work, causes peak rebound effects at hours 19-21, which means that a peak demand is created when

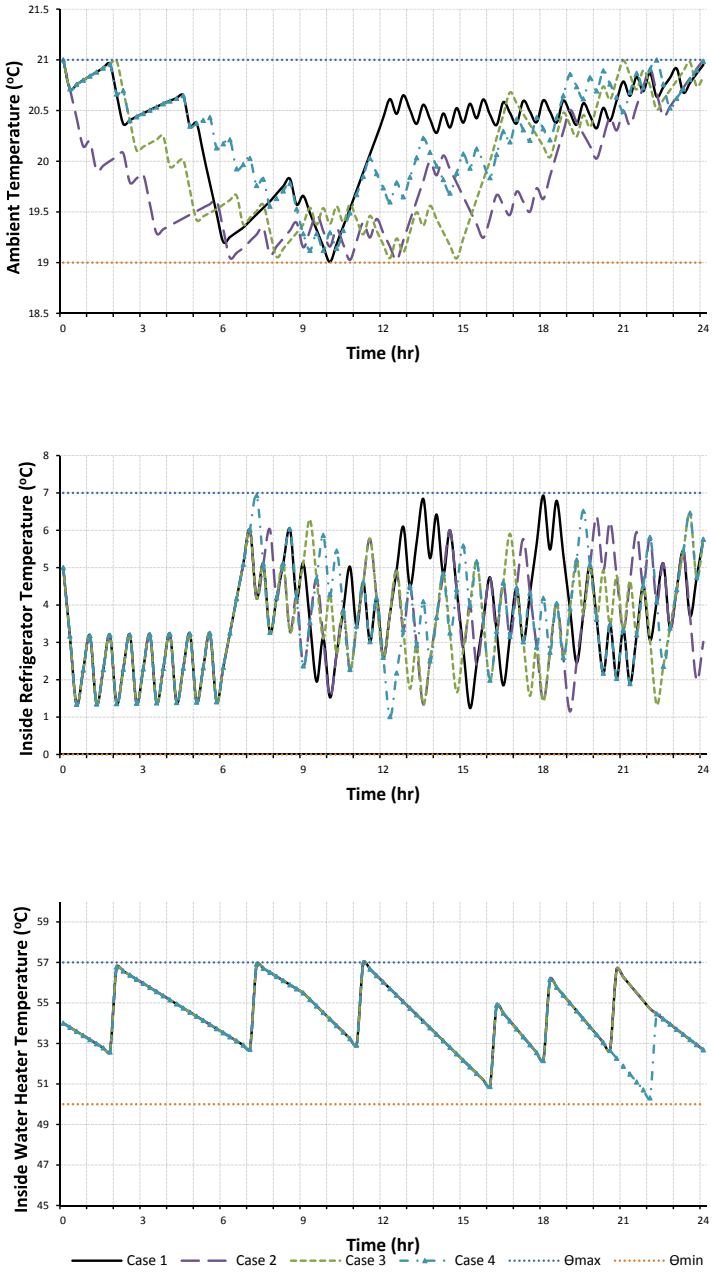

Figure 3.7: Temperature profile inside house #400, refrigerator, and water heater.

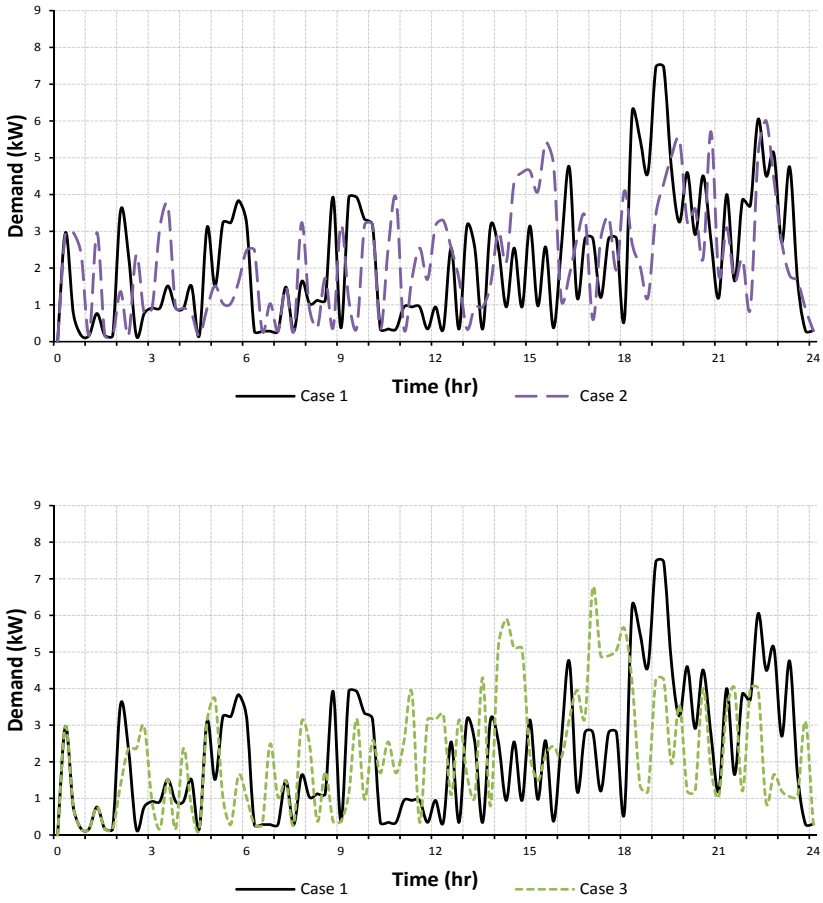

Figure 3.8: Optimal load profile for House h_j at different PRR requests.

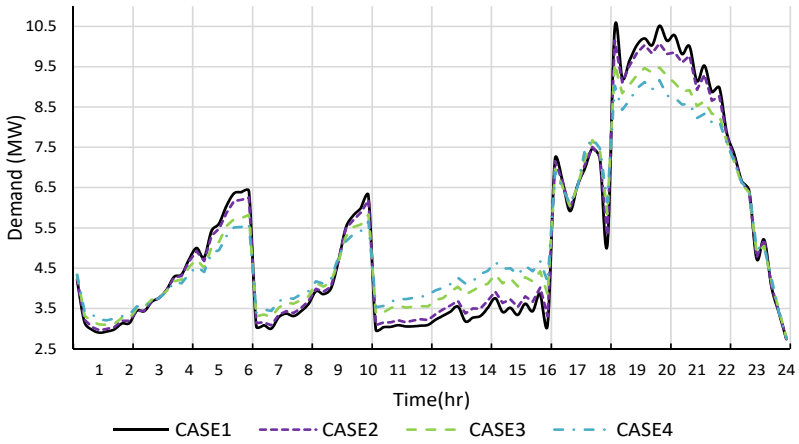

Figure 3.9: Total load profile of LDC.

the TOU price reduces to the off-peak price levels at hour 19. In order to circumvent this situation, the LDC utilizes the available flexibility, inherent in the customers' consumption patterns (i.e, as shown in Fig.3.5), to improve the total load shape and reduce the peak demand at those hours.

Table 3.2: LDC Load Profile Characteristic and Power Losses

Case	Minimum Load (kW)	Peak Load (kW)	Average Load (kW)	Power Losses (Rate of Change%)
Case 1 (0% PRR)	2722.1	10515.78	5175.45	—
Case 2 (5% PRR)	2735.5 (0.49%)	10150.97 (-3.47%)	5178.01 (0.05%)	-1.341%
Case 3 (10% PRR)	2754.7 (1.2%)	9580.18 (-8.9%)	5187.2 (0.23%)	-6.124%
Case 4 (20% PRR)	2765.7 (1.6%)	9164.81 (-12.85%)	5198.2 (0.44%)	-17.830%

Table 3.2 illustrates the improvements in the total load profile of the LDC and system losses, for the different cases considered. It is important to note that the proposed coordination scheme not only shifts the peak load, but it also reduces it, and increases both the minimum and the average load of the distribution system, thus flattening the load profile. It is assumed that the LDC requested for a reduction in the peak load between 6 to 10 PM. As noted from Table 3.2, there is a significant reduction in the peak load while the shifted controllable loads increase the total average load of the system.

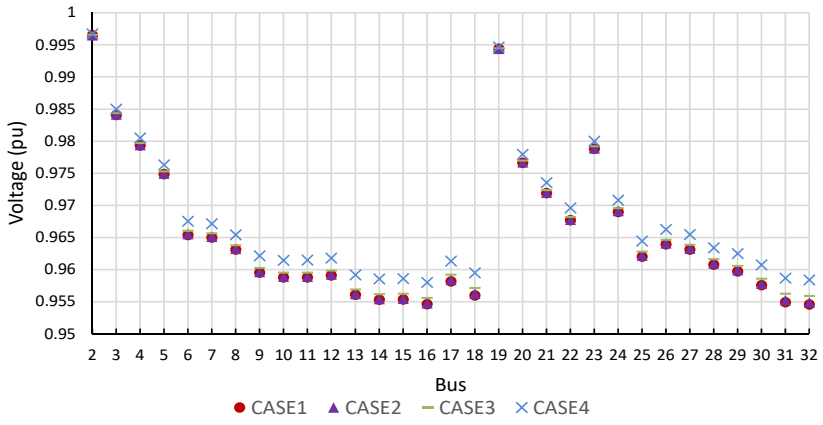

Figure 3.10: Average voltage at each bus at different PRR requests.

Moreover, the inherent flexibility of the customers reduces the system losses as well. Fig.3.10 shows an improvement in the average voltage profile at each bus over the day, when the proposed DR scheme is applied, and justifies the usefulness of the proposed coordination scheme toward efficient grid operations.

Table 3.3: Model Statistics

	House Level					**Grid Level**
	OPT.1	OPT.3	OPT.5	OPT.2	OPT.4-6	OPT.7
Model Type	MILP					NLP
Solver Type	CPLEX					SNOPT
Single Variables	2,223	3,857	2,223	2,223	3,857	19,203
Single Equations	2,403	3,638	2,400	2,442	3,553	9,527
Discrete Variables	962	1,328	952	992	1,344	
Resource Usage, s	0.2	0.254	0.134	0.188	0.232	8.6
Absolute Gap	7	3	7.5	6	9	
Relative Gap	0.09	0.05	0.09	0.07	0.09	

*Optimization Model (OPT)

3.3.4 Computational Aspects

The proposed REH model is an MILP problem which is solved using CPLEX solver; the LDC operations model is a nonlinear programming (NLP) problem, solved using SNOPT solver, in both cases on the GAMS platform [80]. The optimization models are executed on a Dell PowerEdge R810 server, Windows 10 Education 64-bit operating system, with 4 Intel(R) core(TM) i7 processors and 16 GB of RAM. The individual HEMS optimization programs are executed in parallel by individual customers, and each require less than 30 seconds to solve. Different optimization models are assigned for each individual HEMS, see Fig.3.4. Table 3.3 presents an overview of the model statistics of the HEMS and LDC model.

The proposed coordination scheme can be implemented in real-time or day ahead, without any difficulty. It is important to note that the maximum amount of PRR that can be requested by the LDC, can vary based on the customers' willingness to change their consumption patterns. In fact, some customers do not influence the grid operation, so the LDC does not impose such a peak cap to limit the flexibility of their energy consumption.

3.4 Summary

This chapter proposed a novel, two-stage coordination scheme between multiple HEMS and the LDC in order to enhance the grid operational efficiency, reduce peak demand, minimize power losses; and reduce customers' energy cost. At the residential customer level, each individual HEMS optimizes the household appliances schedule based on pre-defined requirements and goals by the household. In addition, each customer's inherent flexibility is evaluated using the proposed approach, which is aggregated with other neighborhood households to provide flexibility services to the LDC. Bus-wise aggregated loads, power sold to the LDC, and total available flexibility from households, are communicated to the LDC system operator, who evaluates its system operation and determines the bus-wise PRR. Each customer is sent a peak cap signal by the LDC.

The proposed two-stage coordination scheme captures the procurement of flexibility provisions by the LDC in real-time. An advantage of this two-stage coordination scheme

is the disaggregation and distribution of the computational burden amongst each entity, as compared to that in a centralized optimization model which would need to optimize thousands of REHs as well as the LDC's operations simultaneously.

Chapter 4

Inclusion of Battery SoH Estimation in Smart Distribution Planning with Energy Storage Systems[1]

Chapter 3 proposed the coordination of a large number of HEMSs to evaluate their inherent flexibility, and hence provide a DR service to the LDC. This chapter, on the other hand, examines the impact of multiple self-optimized HEMSs operating in an uncoordinated manner, on the distribution grid. Thereafter, a novel NN based SoH estimator for a Li-ion battery based BESS is proposed, which is incorporated within a framework and mathematical model for planning and integrating BESS in the distribution grid.

[1]This chapter has been accepted for publication in:
O. Alrumayh, S. Wong, and K. Bhattacharya, "Inclusion of Battery SoH Estimation in Smart Distribution Planning with Energy Storage Systems," *IEEE Transactions on Power Systems*, (available in IEEE Xplore Early Access).

4.1 Nomenclature

LDC Operations and Planning Model with ESS

Indices and Sets

h_j	Index of houses, $h_j \in \mathcal{H}$
j, k	Index of buses in distribution system, $(j,k) \in \mathcal{N}$
n, y	Index of year, $(n,y) \in Y$
t	Index of time, $t \in \mathcal{T}$

Parameters

C_P^{F}	Fixed installation cost of ESS, \$
$C_P^{\mathrm{V}}, C_E^{\mathrm{V}}$	Variable installation cost of ESS associated with power (\$/kW) and energy (\$/kWh), respectively
$C^{\mathrm{OM_F}}$	Fixed operation and maintenance cost of ESS, \$/kW-year
$C^{\mathrm{OM_V}}$	Variable operation and maintenance cost of ESS, \$/kWh
C^{REP}	Replacement cost of ESS, \$/kW
DOD_j	Depth of discharge limit of ESS j, $p.u$
DY	Number of seasonal representative days
$\underline{EPR}, \overline{EPR}$	Limits of energy to power ratio
HY	Number of hours per year, h
$P_{j,y,t}^{d}$	Residential load demand, $p.u$
$P^{\min}, P^{\max}$	Power limits of distribution substation, $p.u$
$P^{\mathrm{STD}}, E^{\mathrm{STD}}$	Standard power/energy capacity of ESS available in market
R	Discount rate, %
$V^{\min}, V^{\max}$	Voltage limits, $p.u$

α_{DOD}	Maximum allowable change in SOC
η^{CH}/η^{DCH}	Charging and discharging efficiency of ESS, %
$\Upsilon_{y,t}$	Electricity price, \$/kWh

Variables

$E_{j,y,t}$	Actual energy capacity of ESS, $p.u$
J_1, J_2, J_3	ESS installation, operation, and replacement cost, respectively, \$.
NU^P, NU^E	Integer multiplier of standard size of ESS
$OT_{j,y,t}, OY_{j,y}$	Number of hours/years ESS in service, respectively
$P^{SS}_{j,y,t}, Q^{SS}_{j,y,t}$	Active/reactive power drawn from substation, $p.u$
$P^{d}_{j,y,t}, Q^{d}_{j,y,t}$	Active/reactive power demand from residential loads, $p.u$
$P^{INST}_{j,y}, E^{INST}_{j,y}$	Installed power/energy capacity of ESS, $p.u$
$P^{Rate}_{j,y}, E^{Rate}_{j,y}$	Rated power/energy capacity of ESS, $p.u$
$P^{CH}_{j,y,t}, P^{DCH}_{j,y,t}$	Active power to be charged/discharged to/from ESS, $p.u$
$SoC_{j,y,t}$	State of charge of ESS, $p.u$
$\widehat{SoH}_{j,y,t}$	Estimated SoH of ESS, %
$V_{j,y,t}$	Voltage at bus, $p.u$
$Z^{INST}_{j,y}, Z^{REP}_{j,y}$	Binary installation and replacement decisions of ESS, respectively.
$Z^{PI}_{j,y}, Z^{PR}_{j,y}$	Binary presence indicator of ESS after installation / replacement.
$\overline{\Delta SoC}_{j,y,t}$	Maximum allowable change in $SoC_{j,y,t}$, $p.u$
$\delta_{j,y,t}$	Voltage angle at bus, $p.u$

Degradation Model

Indices and Sets

$\mathtt{K}$	Index of cycle, $\mathtt{K} \in \mathcal{K}$

Parameters

$\delta_{\mathtt{K}}$	Depth of discharge of $\mathtt{K}^{th}$ cycle
$\sigma_{\mathtt{K}}$	State of charge of $\mathtt{K}^{th}$ cycle
$T_{\mathtt{K}}$	Ambient temperature during $\mathtt{K}^{th}$ cycle
$\beta_{sei}, \alpha_{sei}$	Parameters of the early degradation model

Variables

f_t, f_c	Calendar and cycle aging, respectively
f_{sei}	Degradation function of ESS during early cycles
f_d	Degradation function of ESS
$SoH_{j,y,t}$	Reference SoH of ESS, %
$a_{\mathtt{K}}$	Cycle indicator, $[0.5, 1]$

Neural Network Model

Indices and Sets

i	Index of input, $i \in I$
o	Index of hidden layer neuron, $o \in O$

Parameters

β_o, Γ	Hidden/output layer neuron bias
$n^{in}_{o,j,y,t}, n^{out}_{o,j,y,t}$	Input and output of a hidden layer neuron
$w_{i,o}, W_o$	Input weight and layer weight, respectively
$x^{i}_{j,y,t}, x^{i,N}_{j,y,t}$	Actual and normalized input i
$X_{j,y,t}, X^{N}_{j,y,t}$	Actual and normalized output of NN

4.2 Proposed Planning Framework and Mathematical Models

The proposed ESS planning framework considering the inclusion of a Li-ion battery SoH estimation model is presented in Fig. 4.1. The framework comprises the following steps:

- The REH Operations Model (discussed in Section II.A) and based on [81] is executed to develop bus-wise load profiles. These load profiles are used to simulate an LDC Operations Model (discussed in Section II.B) to obtain a set of SOC profiles of the ESS.
- Using the RCA (discussed in Section II.C) on these SOC profiles, the Li-ion based ESS cycle parameters are determined, which are input to a degradation model [51] to obtain the reference SoH (discussed in Section II.D).
- The SOC and SoH profiles, so obtained, are used to train a NN, and the function relationship of the SoH is extracted (discussed in Section II.E).
- This functional relationship is included in the LDC planning model to determine the optimal plan decisions. The estimated SoH profiles obtained from the planning model are send back to the NN-based estimator to re-train and improve the SoH estimation function for revising the plan decisions. The framework arrives at the optimal plan when the mismatch in the estimation of SoH with the reference, is minimal.

4.2.1 REH Operations Model

The HEMS are residential controllers that carry out scheduling of the REH including all house appliances and power interchanges with the external grid, considering the customer's preferences and objectives, such as minimizing its daily energy cost. In this work, the REH operations model is taken from [81], and simulated for daily load profiles over a 10 year horizon (i.e. 365 x 10 days).

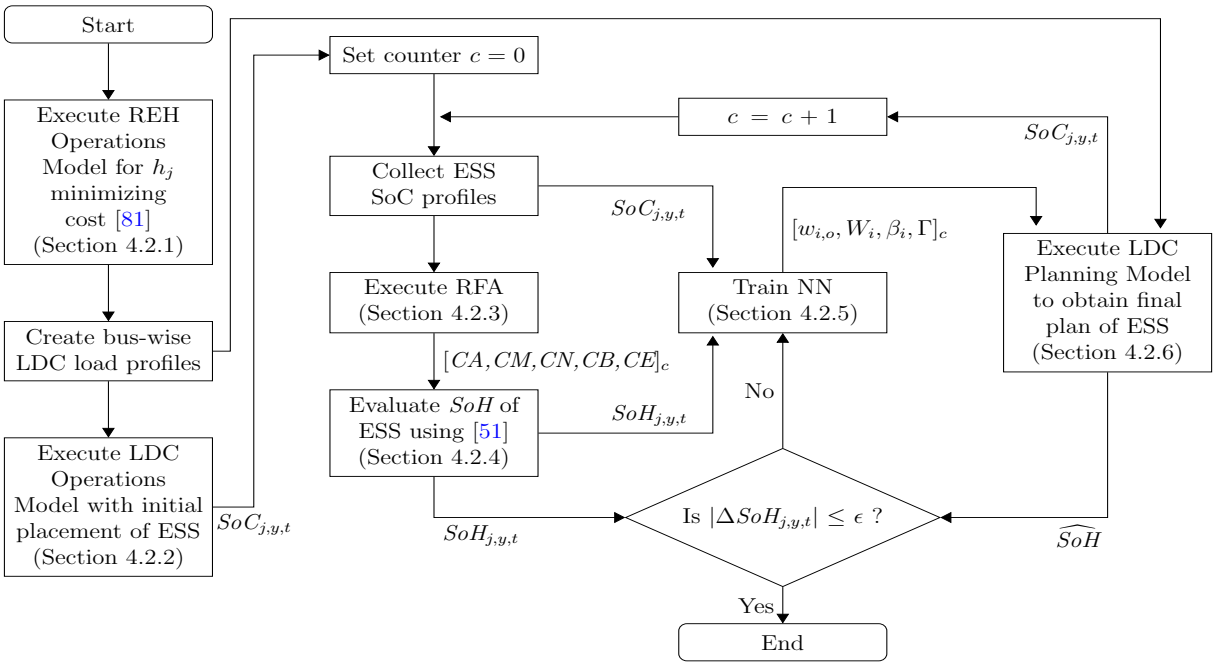

Figure 4.1: Proposed ESS planning framework considering smart REHs and battery SoH.

4.2.2 LDC Operations Model

After completing the simulation of all REHs, bus-wise load profiles are created over a period of ten years. The LDC operations model including ESS is then simulated to analyze the operational decisions of the ESS.

Objective Function

minimize LDC's daily operation cost, comprising the cost of importing power from external grid at electricity price $\Upsilon_{y,t}$ to meet the residential load demand.

$$J = \sum_{y=1}^{Y} \sum_{t=1}^{T} \Upsilon_{y,t} P^{SS}_{j=1,y,t} \tag{4.1}$$

subject to the following constraints:

Load Flow Equations

Linearized power flow equations, as in [82] are used:

$$P^{SS}_{j,y,t} - P^{d}_{j,y,t} + (P^{DCH}_{j,y,t} - P^{CH}_{j,y,t}) = \sum_{k=1,k\neq j}^{\mathcal{J}} \Big(K_{j,k,1}(\delta_{j,y,t} - \delta_{k,y,t}) + K_{j,k,2}(V_{j,y,t} - V_{k,y,t}) \Big) \quad (4.2)$$

$$Q^{\mathrm{SS}}_{y,t} - Q^{d}_{j,y,t} = \sum_{k=1,k\neq j}^{N} K_{j,k,2}(\delta_{j,y,t} - \delta_{k,y,t}) + K_{j,k,1}(V_{j,y,t} - V_{k,y,t}) \quad (4.3)$$

where,

$$K_{j,k,1} = \frac{\frac{x^2_{j,k}}{r^2_{j,k}+x^2_{j,k}}}{x_{j,k}}, K_{j,k,2} = \frac{\frac{r_{j,k}x_{j,k}}{r^2_{j,k}+x^2_{j,k}}}{x_{j,k}}, \ \forall (j,k) \in \mathcal{J} \quad (4.4)$$

These are subject to bus voltage constraints and limits on power drawn from the substation, as given below:

$$V^{\min}_{j} \leq V_{j,y,t} \leq V^{\max}_{j} \quad (4.5)$$

$$P^{\min} \leq P^{SS}_{j=1,y,t} \leq P^{\max} \quad (4.6)$$

The following equations present the operational constraints of the ESS:

$$SoC_{j,y,t+1} = SoC_{j,y,t} + \eta^{CH} P^{CH}_{j,y,t} - \frac{P^{DCH}_{j,y,t}}{\eta^{DCH}} \quad (4.7)$$

$$-\overline{\Delta SoC}_{j,y,t} \leq SoC_{j,y,t} - SoC_{j,y,t-1} \leq \overline{\Delta SoC}_{j,y,t} \quad (4.8)$$

where,

$$\overline{\Delta SoC}_{j,y,t} = \alpha_{DOD}\, E_{j,y,t} \quad (4.9)$$

The inter-temporal change in the SOC level is defined by (4.7), and the same is limited by minimum and maximum allowable changes, given by (4.8). Equation (4.9) states that the value of the maximum allowable change in SOC is a fraction, α_{DOD}, of $E_{j,y,t}$.

$$(1 - \overline{DoD})\, E_{j,y,t} \leq SoC_{j,y,t} \leq E_{j,y,t} \quad (4.10)$$

$$SoC_{j,y,t=1} = SoC_{j,y,t=24} = 0.5\ E_{j,y,t} \tag{4.11}$$

$$P^{CH}_{j,y,t} \leq P^{Rate}_{j,y} \tag{4.12}$$

$$P^{DCH}_{j,y,t} \leq P^{Rate}_{j,y} \tag{4.13}$$

In (4.10), the physical capacity of the ESS limits its SOC considering the maximum allowable DoD. It is assumed that the SOC of the ESS at the beginning and end of the daily operation are equal, equation (4.11), to prevent the optimization model from choosing the maximum SOC at the beginning of the day and fully discharge at the end of the day. Moreover, the rated power of the ESS constraints the power charging/discharging capability from/to the ESS in (4.12) and (4.13).

4.2.3 RainFlow Counting Algorithm

The RCA is a well known approach in the analysis of fatigue data [70]. It has been used in some recent works [83] and [84] for analysis of ESS operation, wherein the RCA counts the number of irregular cycles within a given operation period. The algorithm requires the SOC profile of the ESS as an input, as shown in Fig. 4.1, in order to obtain the following:

- Cycle amplitude (CA).
- Cycle mean value (CM).
- Cycle number (CN).
- Cycle begin and end times (CB, CE).

The results obtained from applying the RCA are used to calculate the variables of the degradation model, discussed next.

4.2.4 Degradation Model of ESS

In [51], a mathematical model was proposed to evaluate lithium-ion battery cell life considering calendar and cycle aging. Calendar aging represents the battery's inherent

degradation over time, as a function of the average temperature ($\overline{T}$) and the average SOC of the battery ($\overline{\sigma}$). Cycle aging represents the loss of life due to the charging and discharging of the battery, represented as a function of the DoD, SOC, and temperature. This is given as follows [51]:

$$f_d(t, \delta, \sigma, T) = f_t(t, \overline{\sigma}, \overline{T}) + \sum_{\mathtt{K}}^{\mathcal{K}} a_k f_c(\delta_{\mathtt{K}}, \sigma_{\mathtt{K}}, T_{\mathtt{K}}) \tag{4.14}$$

The first term in (4.14) represents the effect of calendar aging (f_t) while the second term represents the degradation as a result of cycle aging (f_c). In addition, ESS degradation during its operation in the early cycles is given by [51],

$$f_{sei} = \beta_{sei} f_d \tag{4.15}$$

The $SoH_{j,y,t}$ of ESS can be represented as follows:

$$SoH_{j,y,t} = 1 - \alpha_{sei} \cdot e^{-f_{sei}} - (1 - \alpha_{sei}) \cdot e^{-f_d} \tag{4.16}$$

where α_{sei} denotes the portion of the ESS capacity lost during the early operation. The third term in (4.16) represents the degradation due to calendar and cycle aging. In order to apply the degradation model (4.14)-(4.16) to irregular cycle operation of ESS, the outcomes of the RCA are used as inputs to the degradation model, as follows [51]:

- $\delta_{\mathtt{K}} = 2\ CA_{\mathtt{K}}$.
- $\sigma_{\mathtt{K}} = CM_{\mathtt{K}}$.
- $\overline{\sigma}$ = Average value of CM.
- $T_{\mathtt{K}}$ = Mean temperature between start and end time of $\mathtt{K}^{th}$ cycle.
- $\overline{T}$ = Mean value of the temperature profile.

The following subsection presents a novel SoH estimation approach (i.e. $\widehat{SoH}$) for an ESS in a distribution system that does not require RCA.

4.2.5 Proposed NN Based ESS SoH Estimator

This paper adopts the degradation model in [51] to propose a novel approach for estimating the SoH of the ESS. For this purpose, an NN-based mathematical model of the SoH is developed to be embedded within the planning model in order to take into account the impact of calendar and cycle aging in determining the optimal ESS size, location, and operation decisions.

In order to estimate the SoH of ESS ($\widehat{SoH}$), a supervised learning technique is applied to train the NN with outcomes of the LDC operation of model, i.e., SOC profiles of 365 days for 10 years operation, as shown Fig. 4.1. The required output vector of the NN is the target SoH ($SoH_{j,y,t}$), which is determined as follows: (a) Use RCA to find CA, CB, CE, CN, and CM. (b) Calculate the input of the degradation model $\delta_{\mathtt{K}}$, $\sigma_{\mathtt{K}}$, $\overline{\sigma}$, $T_{\mathtt{K}}$, and $\overline{T}$, as discussed in Section 4.2.4 and shown in Fig. 4.1. (c) Evaluate the ESS SoH using the degradation model adopted in Section 4.2.4, the output of which represents the target vector of the NN. As a result, a $[87,600 \times 2]$ order matrix training set and a $[87,600 \times 1]$ target vector are used for the NN training. Accordingly, the $\widehat{SoH}$ of an ESS located at bus (j) at year (y) and time (t) can be expressed as a function of SOC and operation time, as given below:

$$\widehat{SoH}_{j,y,t} = f(SoC_{j,y,t}, OT_{j,y,t}) \tag{4.17}$$

The NN has one hidden layer with two hidden layer neurons, which is obtained by trial-and-error; the NN is trained using Marquardt learning technique in MATLAB [85]. The resulting structure of the NN-based SoH Estimator is shown in Fig. 4.2. The mathematical representation of the NN function is developed as follows:

- Pre-processing input: The inputs of the NN $x^i_{j,y,t} = \{SoC_{j,y,t}, OT_{j,y,t}\}$ are normalized to lie in the interval $[-1, 1]$ using *mapminmax* function in MATLAB, as shown below:

$$x^{i,N}_{j,y,t} = \frac{2(x^i_{j,y,t} - \underline{x^i_{j,y,t}})}{\overline{x^i_{j,y,t}} - \underline{x^i_{j,y,t}}} + \underline{x^{i,N}_{j,y,t}}, \tag{4.18}$$

  The underline and overline notations denote the respective minimum and maximum values of the inputs.

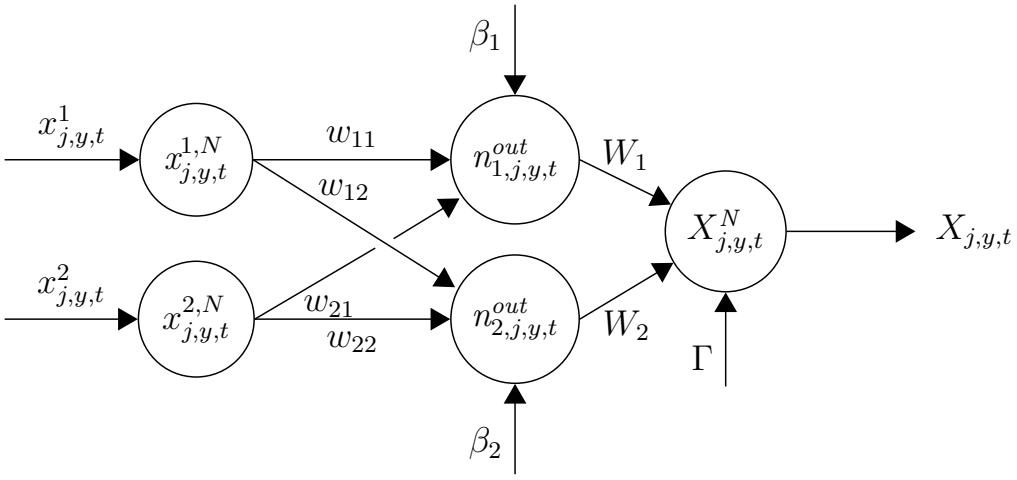

Figure 4.2: Structure of the proposed NN-based SoH estimator.

- Hidden layer activation function: The pre-processed inputs with appropriate weights, $w_{i,o}$ $[\forall i \in 1, ..., H,\ o \in 1, ..., O]$, are summed up at every hidden layer neuron. In addition, each hidden layer neuron has its own bias (β_o). The summed signals present the input to a hidden layer neuron (n^{in}_o), as given below:

$$n^{in}_{o,j,y,t} = \sum_{i=1}^{I} w_{i,o}\ x^{i,N}_{j,y,t} + \beta_o \tag{4.19}$$

  This input value is passed through an activation function (i.e. $tansig$), which transforms $n^{in}_{o,j,y,t}$ into an output signal ($n^{out}_{o,j,y,t}$), as follows:

$$n^{out}_{o,j,y,t} = \frac{2}{1 + \exp\left(-2\ n^{in}_{o,j,y,t}\right)} - 1 \tag{4.20}$$

- Output layer function: The calculated $n^{out}_{o,j,y,t}$ represents the input of the output layer, which is also multiplied by a layer weight (W_o). Ultimately, a linear function is applied in the output layer, which results in the output of the NN, $X^N_{j,y,t}$, as shown below:

$$X^N_{j,y,t} = \sum_{o}^{O} n^{out}_{o,j,y,t}\, W_o + \Gamma \tag{4.21}$$

The obtained output from the NN ($X^N_{j,y,t}$) represents the normalized SoH of the ESS ($SoH^N_{j,y,t}$).

- Post-process output: The obtained output (2.71) is post-processed to obtain the estimated output (i.e. SoH), as follows (refer Fig. 4.2):

$$X_{j,y,t} = \frac{(X^N_{j,y,t} - \underline{X^N_{j,y,t}})(\overline{X_{j,y,t}} - \underline{X_{j,y,t}})}{2} + \underline{X_{j,y,t}} \tag{4.22}$$

The mathematical model (4.22) of the SoH of the ESS at bus j at year y and time t is incorporated in planning model, discussed in the following subsection.

4.2.6 LDC Planning Model

The LDC planning model seeks to optimally allocate, size, and replace a number of ESS at different buses in the distribution grid, considering the following objective function.

Objective Function

$$J = J_1 + J_2 + J_3 \tag{4.23}$$

Equation (4.23) comprises the ESS installation cost (J_1), operation cost (J_2), and ESS replacement cost (J_3), as follows:

ESS Installation Cost: comprises power capacity cost ($\$/kW$), energy capacity cost ($\$/kWh$), and a fixed installation cost ($\$$), as given below:

$$J_1 = \sum_{y=1}^{Y} \sum_{j}^{\mathcal{N}} \left[\frac{1}{(1+R)^y} \left(C^{\mathrm{V}}_P P^{INST}_{j,y} + C^{\mathrm{V}}_E E^{INST}_{j,y} + C^{\mathrm{F}} Z^{INST}_{j,y} \right) \right] \tag{4.24}$$

Operation Cost: comprises fixed and variable operation and maintenance cost (O&M), the cost associated with ESS charging and discharging, and the cost of buying power from the external grid, as given below:

$$J_2 = \sum_{y=1}^{Y} \sum_{j}^{\mathcal{N}} \left[\frac{C^{\mathrm{OM_F}}}{(1+R)^y} \, P_{j,y}^{Rate} + \frac{365}{\mathrm{DY}} \sum_{t}^{T} \frac{1}{(1+R)^y} \left(C^{\mathrm{OM_V}} (P_{j,y,t}^{CH} + P_{j,y,t}^{DCH}) + \Upsilon_{y,t} P_{j=1,y,t}^{SS} \right) \right] \quad (4.25)$$

Replacement Cost: included when the ESS reaches its end of life and has to be replaced, as given below:

$$J_3 = \sum_{y=1}^{Y} \sum_{j}^{\mathcal{N}} \frac{C^{\mathrm{REP}}}{(1+R)^y} E_{j,y}^{INST} Z_{j,y}^{REP} \quad (4.26)$$

The objective function is subject to the following constraints:

Selection Decisions of ESS

The selection of the ESS size should be based on standard unit of power and energy capacity ratings available in the market, modeled as follows:

$$E_{j,y}^{INST} = NU^E \; E^{\mathrm{STD}} \quad (4.27)$$

$$P_{j,y}^{INST} = NU^P \; P^{\mathrm{STD}} \quad (4.28)$$

NU^E and NU^P are integer variables that determine the rated energy and power capacities respectively, based on the available standard sizes in the market, E^{STD} (e.g. 50 kWh) and P^{STD} (e.g. 50 kW). Furthermore, the energy capacity of the ESS for a certain power rating, is determined based on its energy to power ratio, as follows:

$$\underline{EPR}\ P_{j,y}^{INST} \leq E_{j,y}^{INST} \leq P_{j,y}^{INST}\ \overline{EPR} \tag{4.29}$$

The installation year decision ($Z_{j,n}^{INST}$) is activated only once during the planning horizon, as indicated below:

$$\sum_{n=1}^{y} Z_{j,n}^{INST} \leq 1 \tag{4.30}$$

The variable $Z_{j,y}^{PI}$ indicates the presence of ESS after an installation decision. The following constraint coordinates the installation year decision ($Z_{j,n}^{INST}$) in the presence of ESS:

$$Z_{j,y}^{PI} = \sum_{n=1}^{y} Z_{j,n}^{INST} \tag{4.31}$$

The binary decision variable $Z_{j,y}^{PR}$ indicates the presence of ESS after replacement ($Z_{j,y,t}^{REP}$) and is modeled as follows:

$$Z_{j,y}^{PR} = \sum_{n=1}^{y} Z_{j,n}^{REP} \tag{4.32}$$

The two binary indicators $Z_{j,y}^{PI}$ and $Z_{j,y}^{PR}$ are used in counting the number of operation years after installation of a new ESS.

The installed energy/power capacity determines the rated capacity of ESS after the year of installation, as follows:

$$E_{j,y}^{Rate} = \sum_{n=1}^{y} E_{j,n}^{INST}\ ;\ P_{j,y}^{Rate} = \sum_{n=1}^{y} P_{j,n}^{INST} \tag{4.33}$$

It is important to account for ESS energy capacity degradation in order to achieve an optimal plan involving sizing, year, and location of the ESS. Therefore, the de-rated ESS energy capacity can be modeled considering its estimated SoH and rated capacity, as follows:

$$E_{j,y,t} = \widehat{SoH}_{j,y,t} E_{j,y}^{Rate} \tag{4.34}$$

The following constraint models the estimated SoH of the ESS at installation or replacement, as follows:

$$\widehat{SoH}_{j,y,t=1} \geq Z^{INST}_{j,y} + Z^{REP}_{j,y} \tag{4.35}$$

It is assumed that ESS installation or replacement is done at the beginning of the year, at which time the battery SoH is 100%; else, $\widehat{SoH}$ is calculated as per Section 4.2.5.

Inclusion of SoH Estimator

The first step to estimate the SoH of the ESS is the pre-processing of the required inputs (i.e. $SoC_{j,y,t}$ and $OT_{j,y,t}$). The inputs to the extracted NN mathematical model are normalized and scaled to the range of $[-1, 1]$, as below:

$$SoC^{N}_{j,y,t} = \frac{2(SoC_{j,y,t} - \underline{SoC_j} Z^{PI}_{j,y})}{\overline{SoC} - \underline{SoC_j}} - 1 \tag{4.36}$$

In (4.36), $\underline{SoC_j}$ is assumed to be 20% of the ESS installed capacity. $SoC^{N}_{j,y,t} = 1$ when $SoC_{j,y,t} = \overline{\overline{SoC}}$, and $SoC^{N}_{j,y,t} = -1$ when $Z^{PI}_{j,y} = 0$. Similarly, the following equation normalizes the operation time of the ESS.

$$OT^{N}_{j,y,t} = \frac{2\, OT_{j,y,t}}{T} - 1 \tag{4.37}$$

where,

$$OT_{j,y,t} = HY(OY_{j,y} - Z^{PI}_{j,y}) + (t-1)Z^{PI}_{j,y} \tag{4.38}$$

In (4.38), the first term on the RHS denotes the total number of ESS operational hours from installation/replacement until the previous year, while the second term denotes the number of hours of operation in the current year. Furthermore, note that $OY_{j,y}$ is a function of installation and replacement decisions, which represents the total number of years of operation after ESS is installed/replaced, as follows:

$$OY_{j,y} \leq \sum_{n=1}^{y} Z^{PI}_{j,n} + M \sum_{n=1}^{y} Z^{REP}_{j,n} \tag{4.39}$$

$$OY_{j,y} \geq \sum_{n=1}^{y} Z_{j,n}^{PI} - M \sum_{n=1}^{y} Z_{j,n}^{REP} \tag{4.40}$$

$$OY_{j,y} \leq \sum_{n=1}^{y} Z_{j,n}^{PR} + M(1 - \sum_{n=1}^{y} Z_{j,n}^{REP}) \tag{4.41}$$

$$OY_{j,y} \geq \sum_{n=1}^{y} Z_{j,n}^{PR} - M(1 - \sum_{n=1}^{y} Z_{j,n}^{REP}) \tag{4.42}$$

Equations (4.39) and (4.40) coordinate the counting of $OY_{j,y,t}$ for an ESS in service after installation, while (4.41) and (4.42) counts the number of years an ESS is in service after a replacement.

The normalized inputs (i.e. $SoC_{j,y,t}^{N}$ and $OT_{j,y,t}^{N}$) are passed to the hidden layer of the NN, as follows:

$$n_{o,j,y,t}^{out} = \frac{2}{1 + e^{-2\,(w_{1,o}\; SoC_{j,y,t}^{N} + w_{2,o}\; OT_{j,y,t}^{N} + \beta_o)}} - 1 \tag{4.43}$$

Finally, $\widehat{SoH}_{j,y,t}^{N}$, which is the normalized output of the NN, can be expressed as follows:

$$\widehat{SoH}_{j,y,t}^{N} = \sum_{o \in O} n_{o,j,y,t}^{out}\; W_o + \Gamma \tag{4.44}$$

Budget Constraint

The net present value (NPV) of the installation cost should not exceed the NPV of the allocated budget:

$$J_1 \leq Budget \tag{4.45}$$

The constraints of the LDC operations model, discussed in Section 4.2.2 (i.e. (4.2) to (4.13)), are further included in the planning model in addition to the above constraints.

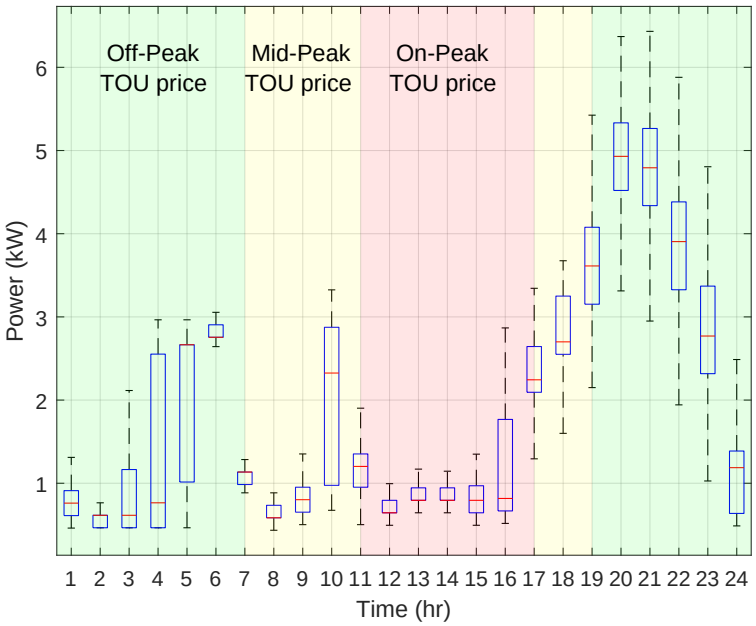

Figure 4.3: Residential load profile.

Table 4.1: Tuned Weights and Biases of the NN

Parameter	Hidden Layer				Output Layer	
Weight	w_{11}	$-0.164E-4$	w_{12}	0.2218	W_1	-0.4328
	w_{21}	$0.447E-6$	w_{22}	-0.0661	W_2	-16.5719
Bias	β_1	$-0.5117E-2$	β_1	$0.3317E-3$	Γ	$0.3260E-2$

4.3 Results and Discussions

In this work, a 33-bus test system is used to determine the optimal ESS size, location and year of installation / replacement considering the impact of its calendar and cycle aging on its SoH. The residential load demand is assumed to increase 3% annually. The planning period is 10 years; each year is represented by one day, and each day's operational aspects, such as load and generation profiles and charge / discharge decisions, are modeled hourly. The representative day is the one which has the highest peak demand of that year. This is a conservative approach, using the worst-case scenario and planning accordingly, so that

Table 4.2: ESS Optimal Plan (Considering Scenario-1 Load Profile).

Case Study	Optimal Plan Decisions*		Operation Cost (NPV-OC)	Installation Cost (NPV-OC)
Case-1 (Proposed Approach)	(2, 9, 400, 1500) (8, 4, 150, 600) (19, 5, 500, 2000) (30, 6, 250, 1000)	(4, 5, 450, 1800) (17, 7, 400, 1600) (23, 10, 500, 2000)	$64,000	$5,988,000
	Total Rated Power/Energy: 2.65 MW/10.5 MWh		Total: $6,052,000	
Case-2 (Without Degradation)	(2, 7, 300, 1200) (8, 5, 500, 2000) (17, 4, 200, 800) (23, 5, 150, 600)	(4, 5, 500, 2000) (15, 9, 250, 1000) (19, 10, 300, 1150) (30, 6, 250, 1000)	$68,000	$5,815,000
	Total Rated Power/Energy: 2.5 MW/9.75 MWh		Total: $5,881,000	
Case-3 (Fixed Degradation Rate)	(2, 5, 500, 2000) (8, 7, 250, 1000) (17, 6, 250, 1000) (23, 4, 400, 1600)	(4, 10, 400, 1600) (15, 9, 400, 1600) (19, 8, 250, 1000) (30, 5, 500, 2000)	$77,000	$6,844,000
	Total Rated Power/Energy: 2.95 MW/11.8 MWh		Total: $6,921,000	

*(Bus number, Year of Installation, Rated Power (kW), Rated Energy (kWh))

the system has sufficient redundancy and margin. The choice of one representative day per year reduces the computational burden of the planning model.

To implement the planning framework proposed in Fig. 4.1, 2,600 individual REH operations models [81] are executed to obtain their daily optimal load profiles, and hence the LDC's load profiles at each bus are created. Figure 4.3 shows the distribution of the REH loads at each hour, indicating the minimum and maximum, 25^{th} and 75^{th} percentiles, and the median consumption of the customers. Note that during the on-peak TOU prices, the variation in customer load is small, which depicts harmonized operation of REHs. The HEMS helps the household in shifting its demand from on-peak TOU price to off-peak price hours.

The LDC operations model is executed for (365 x 10 days) considering the respective REH load profiles to obtain the corresponding optimal SOC profiles of the ESS. This data set is divided into a training set (60%), validation set (20%), and testing set (20%). The *Dividerand* function of the MATLAB NN-Toolbox [85] is applied to divide the data set using random indices. The training stage takes place to build the NN-based SoH estimator. Fig. 4.4 presents the error distribution between $SoH_{j,y,t}$ and $\widehat{SoH}$ with the number of incidences. The main outcomes of the NN, as stated in Fig. 4.1, are the input weights, layer weights, and biases at hidden and output layer neurons. Table 4.1 shows

Table 4.3: ESS Optimal Plan Using the Proposed Approach (case-1) for Different Load Profile Scenarios

	Optimal Plan Decisions*	
Scenario-1 IEEE RTS Load	(2, 9, 400, 1500) (8, 4, 150, 600) (19, 5, 500, 2000) (30, 6, 250, 1000)	(4, 5, 450, 1800) (17, 7, 400, 1600) (23, 10, 500, 2000)
	Total: 2.65 MW/10.5 MWh	
Scenario-2 50% IEEE RTS load 50% REH penetration	(2, 5, 600, 2000) (8, 10, 350, 1400) (23, 9, 250, 1000)	(4, 3, 950, 1550) (19, 7, 150, 600)
	Total: 2.3 MW/6.55 MWh	
Scenario-3 IEEE RTS Load 20% PV penetration (-ve load)	(4, 5, 500, 2000) (15, 5, 450, 1800) (19, 10, 350, 1400)	(8, 4, 150, 600) (17, 8, 500, 2000) (23, 6, 350, 1400)
	Total: 2.3 MW/9.2 MWh	
Scenario-4 50% IEEE RTS load 50% REH penetration 20% PV penetration (-ve load)	(2, 4, 550, 1900) (19, 5, 700, 2000) (30, 7, 300, 1200)	(17, 10, 350, 1400) (23, 3, 250, 300)
	Total: 2.15 MW/6.8 MWh	

*(Bus number, Year of Installation, Rated Power (kW), Rated Energy (kWh))

the resulting parameters of the NN, which are used to construct the SoH functional relation given in (4.44).

Next, the proposed LDC planning model is executed to obtain the optimal ESS plan decisions over the 10 year horizon including ESS energy and power capacity, location, and installation years, considering the following case studies:

- Case-1: Estimated SoH-integrated LDC planning model.
- Case-2: Without degradation of ESS.
- Case-3: Fixed annual degradation rate of 5%.

Furthermore, each case has been studied considering four load profile scenarios:

Table 4.4: NPV of Operation and Installation Costs for Various Cases and Scenarios ($1000)

Case	Scenario-1		Scenario-2		Scenario-3		Scenario-4	
	NPV-OC	NPV-IC	NPV-OC	NPV-IC	NPV-OC	NPV-IC	NPV-OC	NPV-IC
1	64	5,988	65	4,800	62	5,364	69	4,630
2	68	5,815	66	4,106	53	5,264	68	4,038
3	77	6,844	76	4,980	68	6,142	69	4,772

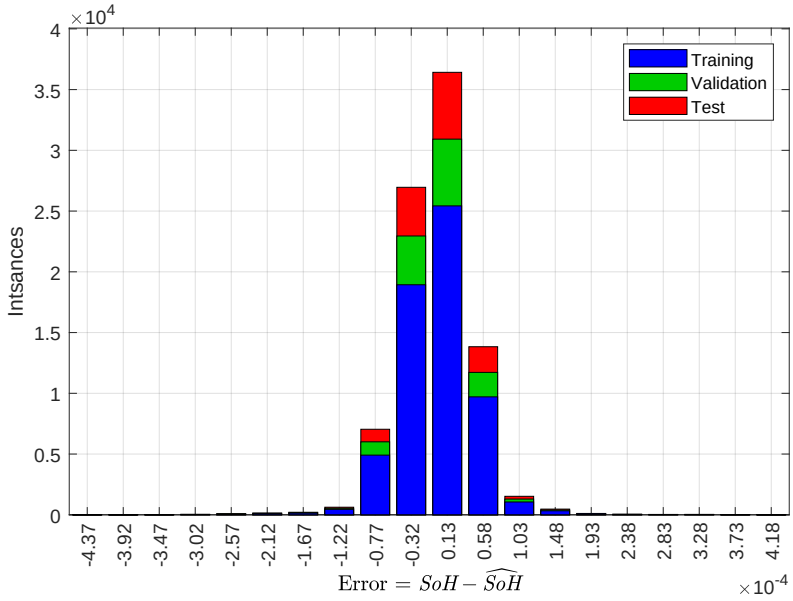

Figure 4.4: Training, validation, testing histogram of NN-based SoH estimator.

- Scenario-1: System demand profile is modeled using the IEEE RTS load.
- Scenario-2: System demand profile is a mix of 50% penetration of REHs and rest modeled using the IEEE RTS load.
- Scenario-3: System demand profile is a mix of 20% penetration of PVs and rest modeled using the IEEE RTS load.
- Scenario-4: System demand profile is a mix of 50% penetration of REHs, 20% penetration of PVs, and rest modeled using the IEEE RTS load.

Two load profiles are used: IEEE RTS load and REHs. Assuming that the connected load of an REH is 3 kW, the number of REHs connected at a bus is determined by dividing the IEEE RTS peak load at a bus by 3 kW. Each REH model is then executed to build a bus-wise load profile [81]. The total demands of Scenario-1 and Scenario-2 are shown in Fig. 4.5. In Scenario-3 and Scenario-4, it is assumed that PV facilities are commissioned at buses 3, 17, and 30 in years 3, 6, and 8, respectively, with their power capacity being 20% of the load at that bus. Note that, in the system load profile, the PVs appear as a negative load.

The case studies, Table 4.2, examine the impact the proposed approach vs less accurate SoH models in LDC planning framework while the (load profile) scenarios, Table 4.3, examine the impact of load mix and PV penetration on ESS sizing, siting, and year of installation / replacement. These tables also show the optimal ESS planning combinations for each scenario and case; and Table 4.4 shows the associated operation and installation cost NPVs.

It is seen from Table 4.2 that in Case-1, the LDC needs to invest in a total ESS capacity of 2.65 MW/10.5 MWh across seven ESS units. The NPV of the ESS installation cost is M$5.99. In Case-2, eight ESS units are invested in by the LDC although the total ESS capacity is 2.5 MW, 9.75 MWh for a total cost that is 2.8% lower than Case-1. This is because the SoH of the ESS units are considered to remain unchanged in Case-2. On the other hand, Case-3 requires 2.95 MW, 11.8 MWh of ESS capacity when using a fixed-rate degradation.

Table 4.3 shows the LDC optimal plan for the four scenarios. In the first scenario, the total capacity of ESS units is higher in than Scenario-2 as a consequence of the former's longer duration of peak demand (Fig. 4.5). In Scenario-3, the integration of PV results in an approx. 10% reduction in installed ESS capacity compared to Scenario-1. However, the integration of PV units does not significantly influence the decisions of ESS in the presence of REHs, as seen comparing Scenario-2 with Scenario-4, because the maximum PV power output occurs during the mid-day and does not coincide with the peak demand of the uncoordinated REHs which appear at the onset of off-peak TOU prices.

Scenario-1 has total LDC NPV costs around M$6.05, M$5.88, and M$6.92 for Case-1,

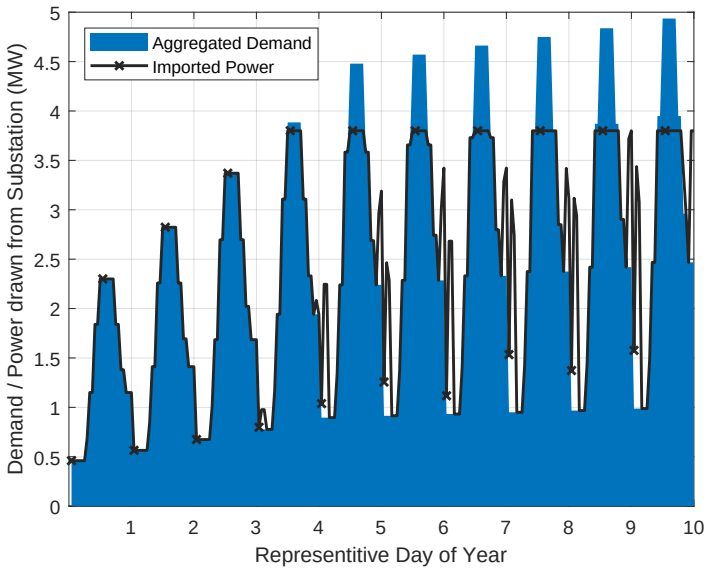

(a) Scenario-1

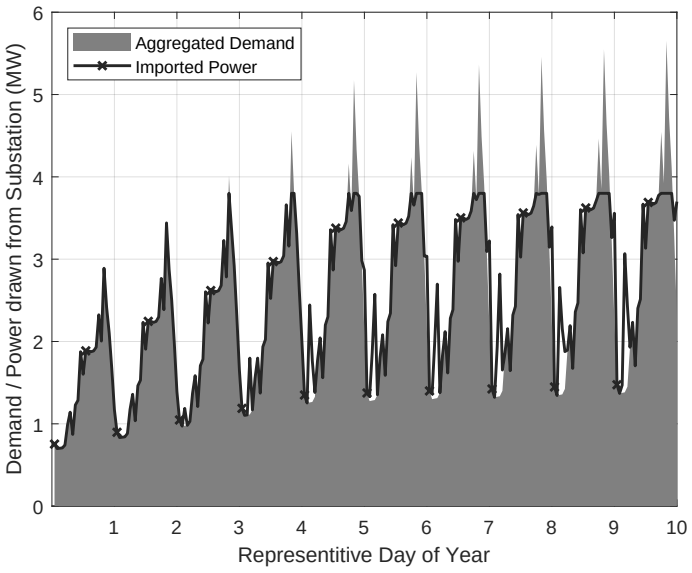

(b) Scenario-2

Figure 4.5: Total distribution system demand and power drawn from substation for Case-1 (Proposed Approach) over the planning period.

Case-2, and Case-3, respectively (Table 4.4). On average, LDC cost in Case-2 is around 8% lower than in Case-1 since, for the former, ESS SoH is fixed at 100%, which results in over-estimation of the available energy capacity of the Li-ion batteries. On the other hand, in Case-3 the average LDC cost is around 10% higher than Case-1 because of the under-estimation of ESS SoH when using the fixed-rate degradation, leading to higher operation and installation costs.

Figure 4.6 shows the SoH and $\widehat{SoH}$ profiles of the ESS located at bus-8 over a 24-hour operation considering the proposed degradation model of Case-1. It is noted that the proposed NN-based mathematical model captures the hourly SoH profile ($\widehat{SoH}$) due to calendar and cycle aging with a relatively small error, as compared to SoH.

Figure 4.7 shows the reference SoH, $SoH_{j,y,t}$, the estimated SoH from Case-1, $\widehat{SoH}$, and the SoH profile considering a fixed deterioration of 5%, as in Case-3, over the plan period. $SoH_{j,y,t}$ is obtained using the off-line degradation model proposed in [51] and discussed in Section 4.2.4. In contrast, the $\widehat{SoH}$ profile is calculated using the proposed NN-based SoH estimator model, which is shown precise compared to $SoH_{j,y,t}$.

$SoH_{j,y,t}$ obtained from the different load mix scenarios are shown in Fig. 4.8; Scenario-1 has consistently the lowest SoH. It is noted that the load mix has some influence on the battery degradation: the penetration of PV units and the presence of REHs improve the overall SoH of Li-ion batteries by around 1% every year, as a consequence of the adoption of RES or REH, which results in a reduction in the peak duration of the system load and requires steep discharge from ESS.

Figure 4.5 shows the LDC's aggregated system demand and the power it imports over the substation in Scenarios-1 and -2 for the representative day in each planning year. The ESS units supply the net difference between demand and imports. Figure 4.9 shows the total demand and power imported from external grid over a day in the last year of the planning period for Scenario-1 and -2. The SOC of ESS located at bus 23 is also included, which shows high / low SOC during low / high RTS and REH demand, respectively.

Figure 4.10 shows the bus voltage profiles during peak demand hours: hour-18 in Scenario-1 and hour-20 in Scenario-2 of the terminal year. Note that the voltages are always within pre-specified limits (i.e. 0.9 to 1.0 $p.u.$). Scenario-2 shows a higher deviation

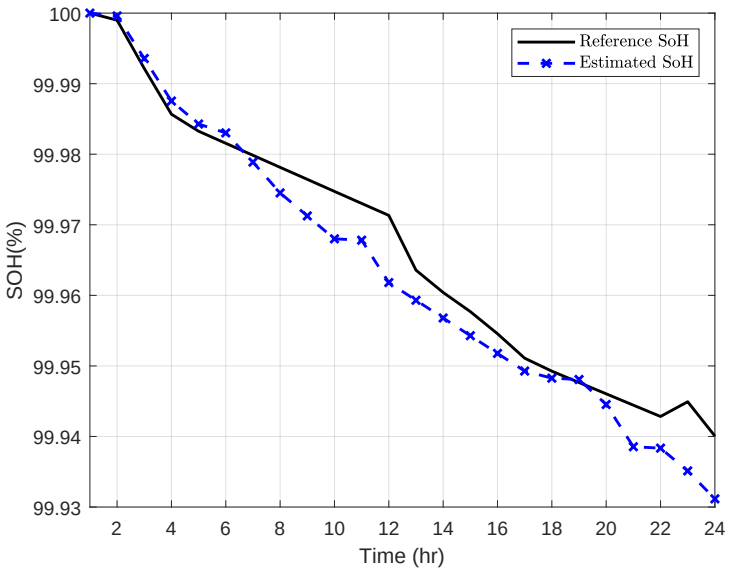

Figure 4.6: Comparison of SoH profiles of ESS located at Bus-8 over a day.

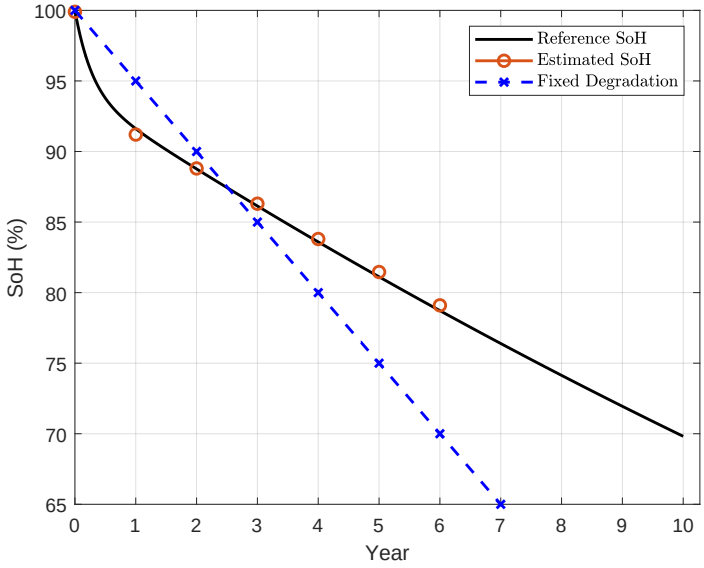

Figure 4.7: Comparison of SoH profiles of ESS located at Bus-8 over the plan period.

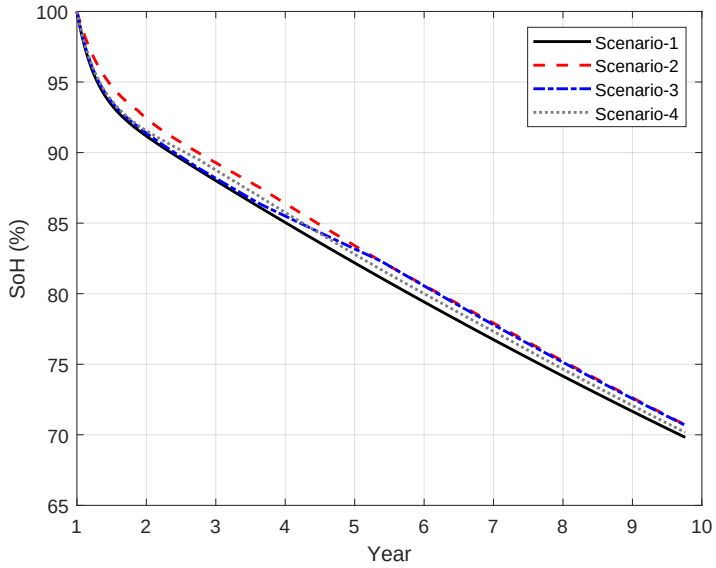

Figure 4.8: Estimated SoH profiles of optimal ESS at Bus-23 for various scenarios.

in voltage from the nominal value of 1.0 *p.u.* as compared to Scenario-1 as a consequence of the higher demand from mixed loads in the former. The voltage profile in Case-1 is also lower in Scenarios-1 and -2 than the voltage profiles in Case-2 and -3.

4.4 Summary

A novel NN-based SoH estimator was developed using a large cluster of smart loads, simulated to represent the total load of the distribution grid; and a large data set of ESS operations, simulated to mimic the LDC's behavior in controlling the ESSs. The hence extracted functional relationship of SoH was integrated within a planning model, which included a large penetration of smart REHs. The NN model was re-trained using the updated outcomes of the planning model to improve the plan decisions. The results showed a relatively small error between the estimated and the reference SoH of ESS. The case studies demonstrated the impact of neglecting calendar and cycle aging and under- / over-estimation of the ESS capacity on the plan decisions of the LDC.

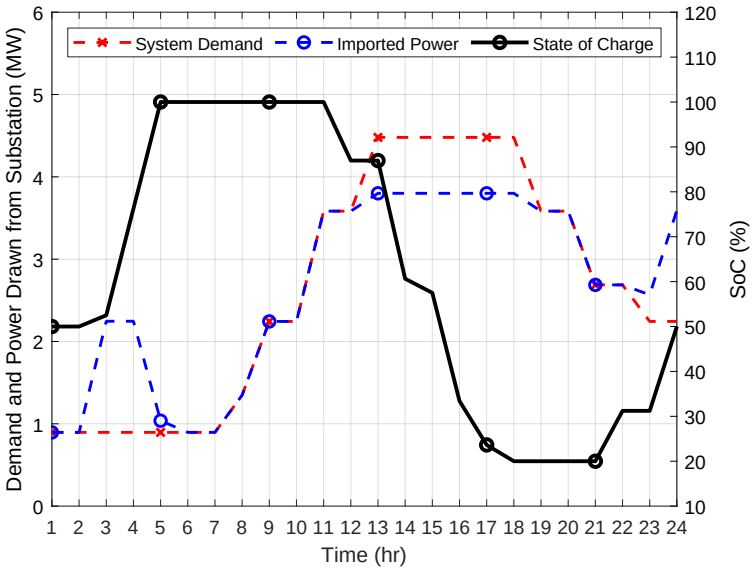

(a) Scenario-1

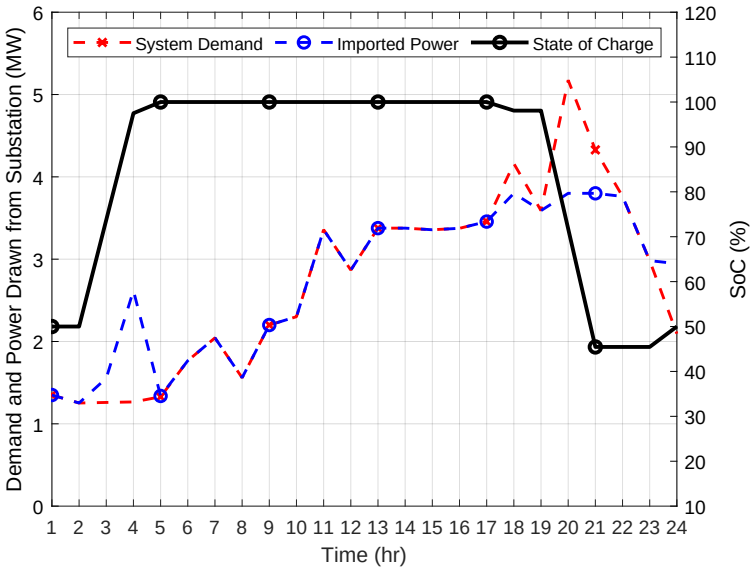

(b) Scenario-2

Figure 4.9: Total demand, power imported from external grid, and ESS operation over one-day of year-10.

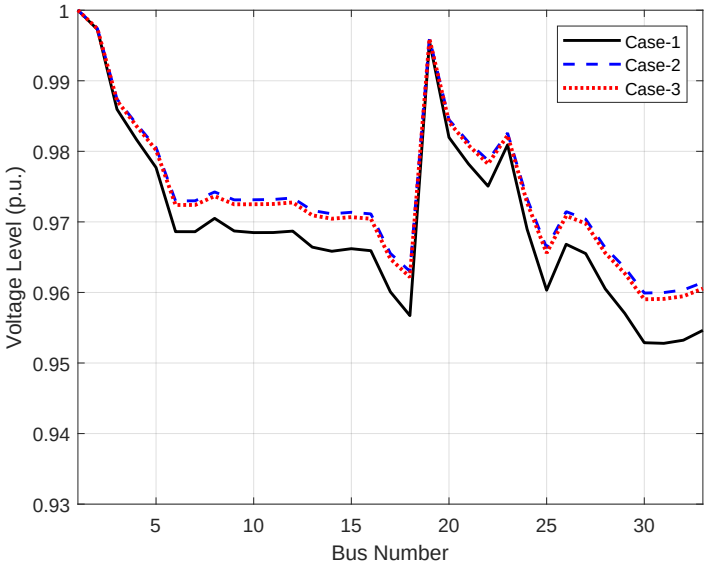

(a) Scenario-1

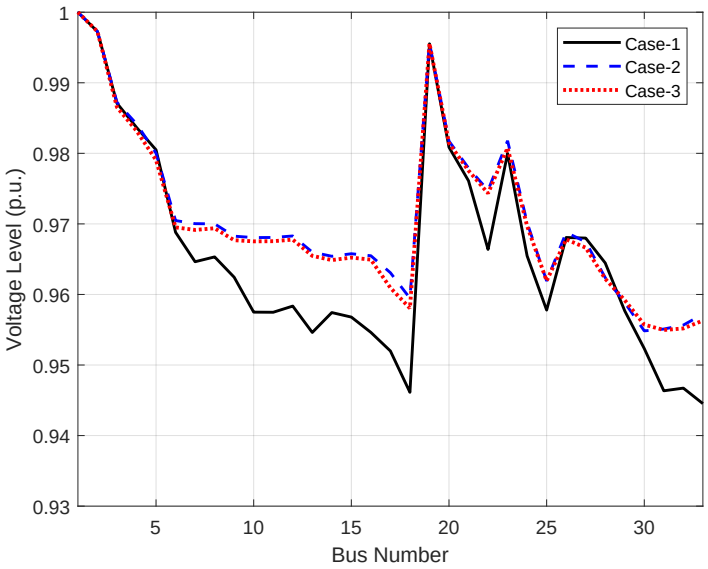

(b) Scenario-2

Figure 4.10: System voltage profiles for different case studies, for Scenario-1 and -2, during peak demand in the terminal year.

Chapter 5

Cooperative Operation of Battery Energy Storage Systems Participating in Flexibility Services Provisions[1]

In the previous chapter, LDC-owned BESSs are optimally sized and sited in the distribution grid to help meet distribution grid constraints and minimize total system costs. On the other hand, this chapter investigates the investor-owned BESSs capability in providing the LDC with flexibility services. It proposes a cooperative game theory-based approach to optimally distribute the total system saving between several BESSs participating in flexibility service provision in the distribution grid. This work assumes that the participants in flexibility service provision are all Li-ion battery-based ESSs and, furthermore, that the specific flexibility service attained from these batteries are based on the C-Rate under

[1] An earlier version of this work has been published in:
O. Alrumayh, S. Wong, H. Alharbi and K. Bhattacharya, "Incentives for Demand Response and Flexibility Services Procured from Energy Storage Systems," Proc. IEEE Power & Energy Society General Meeting 2020.

[1] The present work to be submitted for publication in:
O. Alrumayh, S. Wong and K. Bhattacharya, "Cooperative Operation of Battery Energy Storage Systems Participating in Flexibility Services Provisions," in *IEEE Transactions on Power System*.

which it must operate to offer such service. The proposed approach ensures the maximum benefit of LDC from the cooperative behavior and the flexibility of BESSs; furthermore, it ensures fairness in distributing savings between the ESSs by taking into account the marginal contribution of the participant to the coalition.

5.1 Nomenclature

Indices and Sets

j, k	Index of buses in distribution system, $(j,k) \in \mathcal{J}$.
j, h	Index of a participant location in distribution grid, $(j,h) \in \mathcal{J}$.
s	Index of services provided by BESS, $s \in \mathcal{S}$.
t	Index of time, $t \in \mathcal{T}$.

Parameters

$a_s,\ b_s, c_s$	Linearized BESS degradation cost function.
C^B	Total cost of BESS, \$.
CR_s	Maximum change rate in SOC.
C-Rate_s	Change rate in SOC.
$\overline{E_j}, \underline{E_j}$	Minimum and maximum of ESS, $p.u.$
n	Total number of BESS investors.
q	Size of a BESS coalition.
$\underline{SoC},\ \overline{SoC}$	Minimum and maximum of SOC, %.
$\sigma_t^{\mathrm{HEP}},\ \sigma^{Peak}$	Hourly electricity price and peak price, $\$/kWh$.
σ_t^{TOU}	Time-of-use price, $\$/kWh$.
$P_{j,t}^d$	Hourly distribution grid demand, $p.u.$

η^{CH}, η^{DCH}	Charging and discharging efficiency of ESS, %.
γ_s, ω_s	Coefficients of fitting degradation function.
τ	Time interval, 15 min.

LDC Operation Model:

Variables

$P_{j,t}^{SS}$	Active power drawn from substation, *p.u.*
P^{Peak}	Peak power drawn from substation, *p.u.*
$Q_{j,t}^{SS}$	Reactive power drawn from substation, *p.u.*
$V_{j,t}$	Voltage level, *p.u.*
$\delta_{j,t}$	Voltage angle, *p.u.*

BESS Operation Model:

Variables

DoD	Depth of discharge of BESS, *p.u.*
$DGC_{t,s}$	Degradation cost, $.
$E_{j,t}$	Energy stored in BESS, *p.u.*
L_s	Number of cycles of BESS, *p.u.*
$P_{j,t}^{CH}, P_{j,t}^{DCH}$	Active Power to be charged/discharged to/from ESS at time of use price, *p.u.*
$SoC_{j,t}$	SOC of BESS, *p.u.*
$SoC_{j,t}^{L}$	Linearization of the product term of SOC and binary variable, *p.u.*
$\Delta SoC_{j,t,s}$	Change in SOC of BESS, *p.u.*
$\Delta SoC_{j,t,s}^{+}$	Positive change in SOC of BESS, *p.u.*
$\Delta SoC_{j,t,s}^{-}$	Negative change in SOC of BESS, *p.u.*
$Z_{j,t,s}, Z_{j,t,s}^{-/+}$	Binary variable.

5.2 Proposed Flexibility Services Framework

5.2.1 Flexibility Services: Definitions

The lifetime of Li-ion batteries is impacted by many factors such as DoD, C-Rate and ambient temperature as well as operational decisions. Various operational states of a Li-ion battery are modeled in this work based on its ability to provide different ranges of flexibility services which are defined in terms of the SOC limits of the BESS. These are low flexibility (LF) denoted by $s_1^{-/+}$, moderate flexibility (MF) denoted by $s_2^{-/+}$ and high flexibility (HF) denoted by $s_3^{-/+}$; their respective ranges of operation are given in Table 5.1. The change in SOC of a service s is dependent on one of the main characteristics of BESSs, which is C-Rate. As shown in Table 5.1, LF, MF, and HF have C-Rate values of 1, 2 and 4 respectively. The maximum rate of change (CR_s) of a service, limits the change in SOC, which can be calculated as follows:

$$\text{CR}_s = \frac{\text{C-Rate}_s}{\tau}(\overline{SoC} - \underline{SoC}), \quad \forall s \in S \tag{5.1}$$

In (5.1), $\underline{SoC}$ and $\overline{SoC}$ denote the minimum (i.e. 20%) and maximum SOC (i.e. 100%) of BESS, τ is the number of time intervals per hour; $\tau = 4$ is selected, denoting time intervals of 15 minutes. Therefore, it can be easily seen from (5.1) that $\text{CR}_{LF} = 20\%$, providing low flexibility, while $\text{CR}_{HF} = 80\%$, which provides high flexibility.

Table 5.1: Flexibility Service Definition

Service	Notation	$\lvert\Delta SoC\rvert$ (%)	C-Rate
Low Flexible (LF)	$s_1^{-/+}$	0 - 20	1
Moderate Flexible (MF)	$s_2^{-/+}$	20 - 40	2
High Flexible (HF)	$s_3^{-/+}$	40 - 80	4

Referring to Figure 5.1, say at time $t-2$, the BESS SoC_{t-2} is at minimum level of 20% (point-A). The battery can be charged over the ranges of s_1^+, s_2^+, or s_3^+ which corresponds to changes in SOC from 0% - 20%, 20% - 40%, or 40% - 80%, respectively. The selected

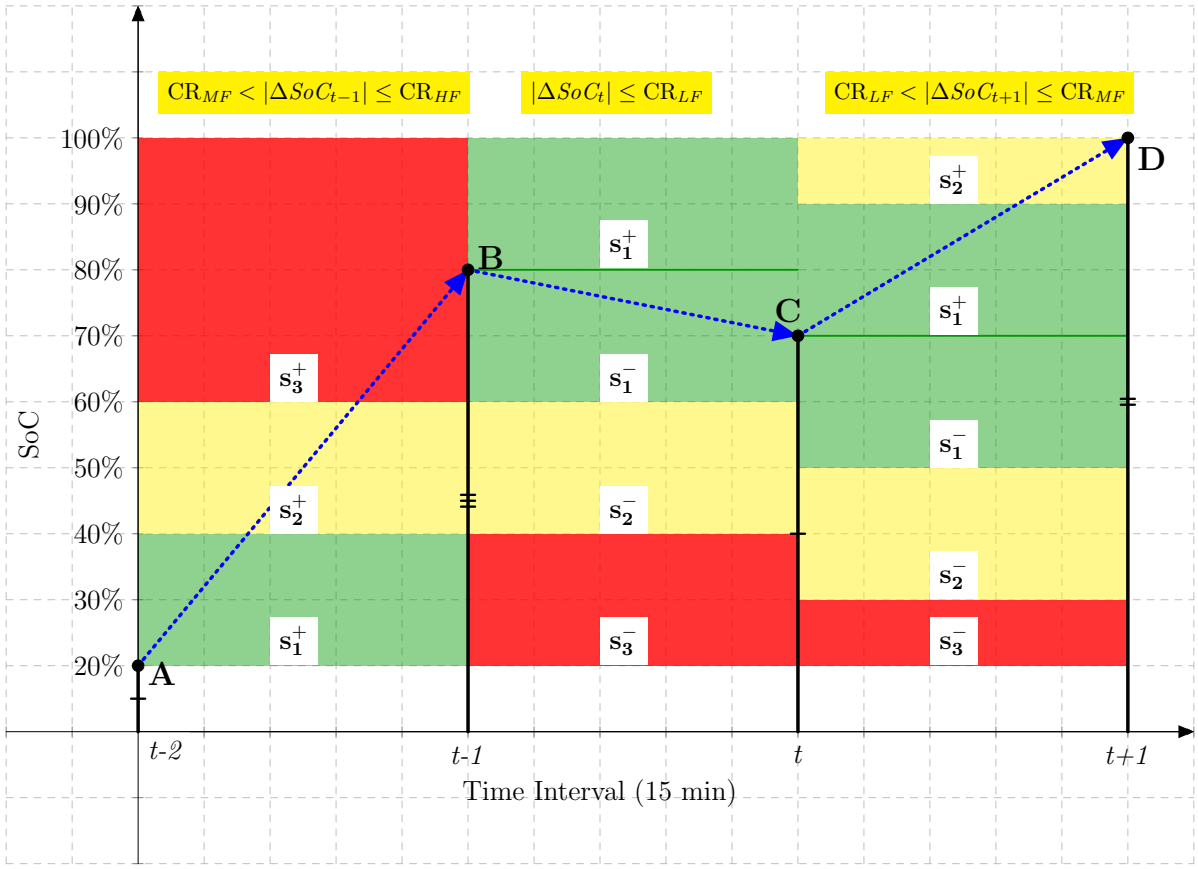

Figure 5.1: The proposed flexibility services classifications based on change in SoC.

service at time $t-1$ is shown to be s_3^+ for $\Delta SoC_{t-1} = 60\%$, which takes the SOC to 80% (point-B) and meets the following constraint:

$$\mathrm{CR}_{MF} < |\Delta SoC_{t-1}| \leq \mathrm{CR}_{HF}, \quad \forall t \in T \tag{5.2}$$

Equation (5.2) shows that the absolute change in SOC is limited by CR_{MF} and CR_{HF}, which are 40% and 80%, respectively. From point B, the BESS can opt for services s_1^+, s_1^-, s_2^- and s_3^- based on their corresponding ranges. As an example, s_1^- is selected for $\Delta SoC_t = 10\%$ and the SOC profile at time t reaches point-C, where the change in SOC belongs to LF service as shown below:

$$0 \leq |\Delta SoC_t| \leq \mathrm{CR}_{LF}, \quad \forall t \in T \tag{5.3}$$

Equation (5.3) defines the limits of LF service, where CR_{LF} equals 20%. Finally, from point-C, the services s_2^+, s_1^+, s_1^-, s_2^- and s_3^- are available based on their corresponding ranges of SOC. The service s_2^+ is selected for $\Delta SoC_{t+1} = 30\%$ and the SOC profile reaching point D at time $t+1$. The mathematical representation of the range of MF service is shown below:

$$\mathrm{CR}_{LF} < |\Delta SoC_{t+1}| \leq \mathrm{CR}_{MF}, \quad \forall t \in T \tag{5.4}$$

It should be noted that the selection of a service will impact the number of cycles of the BESS. Also note that out of the six services defined in this proposed framework, namely, s_1^+, s_1^-, s_2^+, s_2^-, s_3^+ and s_3^-, each time interval will have a subset of available services which will depend on the SOC of the preceding interval.

5.2.2 BESS Degradation Cost Function

Figure 5.2 demonstrates the relationship between the number of cycles of BESS and the DoD at different C-Rates. It shows an exponential drop in number of cycles with the increase of DoD. For C-Rate = 1, the experimental data is represented by its curve fit equation, given as follows [86]:

$$L_s = \gamma_s DoD^{\omega_s}, \quad \forall s \in S \tag{5.5}$$

L_s represents number of cycles of a BESS at DoD for a particular service s, γ_s and ω_s are the fitting function coefficients, where each of the flexibility services- LF, MF, and HF have their own set of parameters, which will be presented in a latter section.

After obtaining γ_s and ω_s from (5.5), the degradation cost model of the battery at time t and service s can be represented as follows [87]:

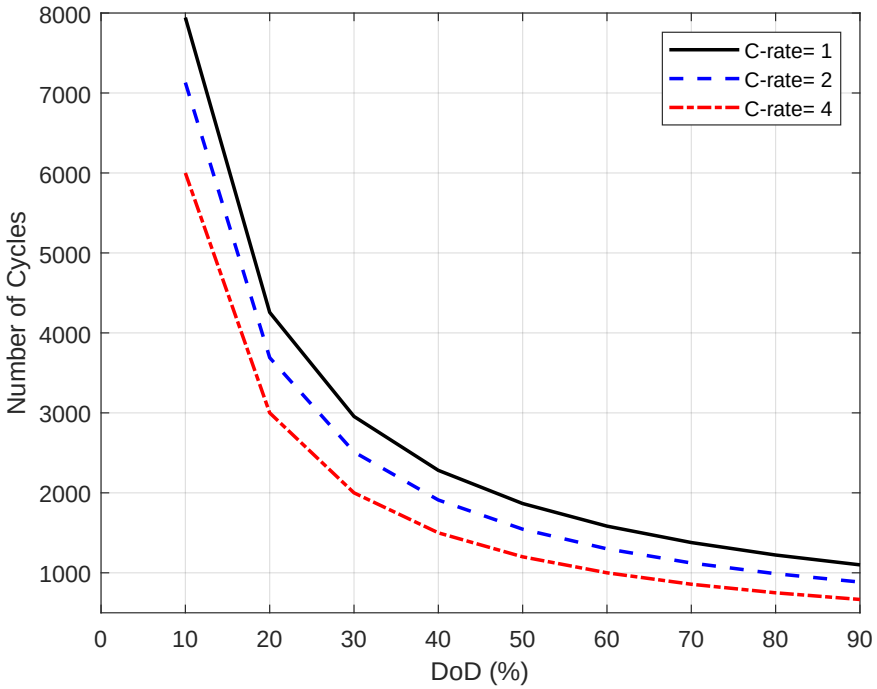

Figure 5.2: Number of cycles of BESS versus DoD at different C-Rates.

$$DGC_{t,s} = \frac{C^B}{\gamma_s} \mid ((1 - SoC_t)^{\omega_s} - (1 - SoC_{t-1})^{\omega_s}) \mid, \quad \forall\, t \in \mathcal{T}, s \in S \tag{5.6}$$

In order to take into account the impact of the change in SOC over a time interval, different values SoC_t and SoC_{t-1} are used in (5.6) to calculate $DGC_{t,s}$ for different services. Using these data, the degradation cost of the BESS for different SoC_t and SoC_{t-1} scenarios and C-Rates are plotted as shown in Figure 5.3. It is noted that higher C-Rate values (e.g. C-Rate = 4) results in a relatively high degradation cost as compared to lower C-Rate (e.g. C-Rate = 1). For instance, the discharge of BESS from an SoC_{t-1} value of 100% to SoC_t of 20% will have a degradation cost of about 2 \$/kWh. On the other hand, the maximum change in SOC within the limits of LF service will result in maximum degradation cost of 1 \$/kWh.

In order to incorporate (5.6) into an MILP problem, it can be linearized using multi-

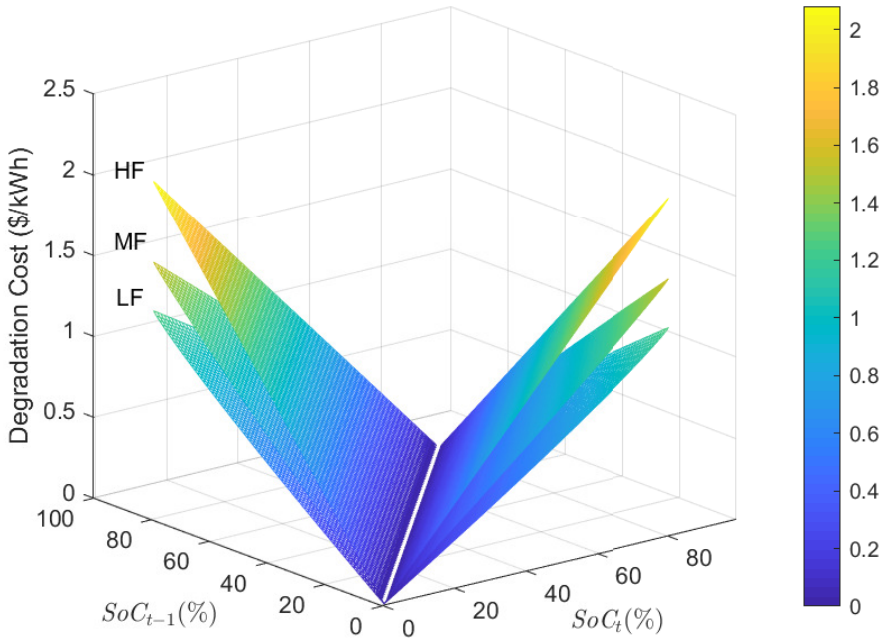

Figure 5.3: Degradation cost of BESS for different flexibility services.

linear regression as follows [87]:

$$DGC_{t,s} = a_s SoC_{t,s} + b_s SoC_{t-1,s} + c_s \Delta SoC_{t,s} \quad \forall\, t \in \mathcal{T}, s \in S \tag{5.7}$$

In (5.7), the linearized degradation cost $DGC_{t,s}$ is presented. Service LF, MF, and HF have their individual degradation cost coefficients a_s, b_s, and c_s, which gives different weights for their associated variables.

5.2.3 LDC Operations Considering BESS Flexibility Services

The distribution system accommodates several distributed BESSs which are contracted to provide any of the three previously defined flexibility services – LF, MF, and HF. It is also assumed that the LDC purchases energy from the wholesale energy market at the Hourly

Electricity Price (HEP), while its energy arbitrage with the distributed BESSs is carried out at TOU prices. The LDC is responsible for meeting the system demand while seeking to minimize its total operation cost, as given below:

$$J = \sigma^{Peak} P^{Peak} + \sum_{t}^{\mathcal{T}} \sigma_t^{\text{HEP}} P_{j,t}^{SS} - \sum_{j}^{\mathcal{J}} \sum_{t}^{\mathcal{T}} \Big(P_{j,t}^{CH} - P_{j,t}^{DCH} \Big) \sigma_t^{\text{TOU}} + \sum_{j}^{\mathcal{J}} \sum_{t}^{\mathcal{T}} \sum_{s}^{\mathcal{S}} \Big(a_s SoC_{j,t} Z_{j,t,s} + b_s SoC_{j,t-1} Z_{j,t,s} + c_s \Delta SoC_{j,t,s} \Big) \quad (5.8)$$

The objective function (5.8) comprises four components: the first component represents the demand charge paid by the LDC depending on its measured peak load during a given operating period; the second, the total cost of buying energy from the electricity market at HEP; the third, the net cost of selling / buying energy to / from the distributed BESSs at TOU prices; and the final, the degradation cost of BESS operation at different flexibility services, as discussed in Section 5.2.1 and 5.2.2. The objective function (5.8) is subject to the nodal demand-supply balance constraints for active and reactive power, as given below:

$$P_{j,t}^{SS} - P_{j,t}^{d} + P_{j,t}^{DCH} - P_{j,t}^{CH} = \sum_{k=1, k\neq j}^{\mathcal{J}} \Big(K_{j,k,1} (\delta_{j,t} - \delta_{k,t}) + K_{j,k,2} (V_{j,t} - V_{k,t}) \Big), \quad \forall t \in \mathcal{T};\ \forall (j,k) \in \mathcal{J} \quad (5.9)$$

$$Q_t^{SS} - Q_{j,t}^{d} = \sum_{k=1, k\neq j}^{N} K_{j,k,2} (\delta_{j,t} - \delta_{k,t}) + K_{j,k,1} (V_{j,t} - V_{k,t}), \quad \forall t \in \mathcal{T};\ \forall (j,k) \in \mathcal{J} \quad (5.10)$$

where,

$$K_{j,k,1} = \frac{\frac{x_{j,k}^2}{r_{j,k}^2 + x_{j,k}^2}}{x_{j,k}}, K_{j,k,2} = \frac{\frac{r_{j,k} x_{j,k}}{r_{j,k}^2 + x_{j,k}^2}}{x_{j,k}},\ \forall (j,k) \in \mathcal{J} \quad (5.11)$$

The linearized power flow equations (5.9) and (5.10) are given in [45] and adopted here to

represent the power balance equations. Additionally, the following constraints are imposed:

$$0 \leq P_{j,t}^{SS} \leq \overline{P_t^{SS}}, \quad \forall t \in \mathcal{T};\ j = 1 \tag{5.12}$$

$$P_{j,t}^{d} + P_{j,t}^{CH} - P_{j,t}^{DCH} \leq P^{Peak}, \quad \forall t \in \mathcal{T};\ j \in \mathcal{J} \tag{5.13}$$

$$0.9 \leq V_{j,t} \leq 1.05, \quad \forall t \in \mathcal{T};\ \forall (j,k) \in \mathcal{J} \tag{5.14}$$

Equation (5.12) denotes the limits on power imported by the LDC from the external grid, which is limited by the capacity of the distribution transformer. Constraint (5.13) calculates the system peak over the day. Constraint (5.14) ensures that the voltages at each bus are within predefined ranges.

The BESSs operational constraints are given below:

$$E_{j,t} = E_{j,t-1} + \tau\ \eta^{ch}\ P_{j,t}^{ch} - \tau\ \frac{P_{j,t}^{dch}}{\eta^{dch}}, \quad \forall t \in \mathcal{T}, j \in \mathcal{J} \tag{5.15}$$

$$\underline{E_j} \leq E_{j,t} \leq \overline{E_j}, \quad \forall t \in \mathcal{T}, j \in \mathcal{J} \tag{5.16}$$

$$0 \leq P_{j,t}^{ch} \leq \overline{P_j} Z_{j,t,ch}, \quad \forall t \in \mathcal{T}, j \in \mathcal{J} \tag{5.17}$$

$$0 \leq P_{j,t}^{dch} \leq \overline{P_j} Z_{j,t,dch}, \quad \forall t \in \mathcal{T}, j \in \mathcal{J} \tag{5.18}$$

$$Z_{j,t,ch} + Z_{j,t,dch} \leq 1, \quad \forall t \in \mathcal{T}, j \in \mathcal{J} \tag{5.19}$$

Equation (5.15) represents the inter-temporal changes of energy level of the BESS taking into account its charging and discharging efficiencies. Constraints (5.16) ensures that the energy levels of the BESSs are within their rated capacities. In addition, the charge and discharge decisions are limited by the rated power of the BESS, as given in (5.17) and (5.18).

The SOC of the BESS is the level of charge of the facility relative to its rated capacity, as given below:

$$SoC_{j,t} = \frac{E_{j,t}}{\overline{E_j}}, \quad \forall t \in \mathcal{T}, j \in \mathcal{J} \tag{5.20}$$

$$SoC_{j,t} = \begin{cases} SoC_{j,t-1} + \sum\limits_{s\in\{s_1,s_2,s_3\}} \Delta SoC_{j,t,s}, & if \quad t \neq \{0, \overline{T}\} \\ 0.5, & otherwise \end{cases}, \quad \forall j \in \mathcal{J} \tag{5.21}$$

$$\underline{SoC} \leq SoC_{j,t} \leq \overline{SoC}, \quad \forall t \in \mathcal{T}, j \in \mathcal{J} \tag{5.22}$$

The inter-temporal changes in SOC of the BESSs are functions of their change in SOC as given in (5.21). Constraint (5.22) limits the SOC levels within their lower and upper limits, which are assumed to be 20% and 100%, respectively, in the present work. The change in SOC of BESSs are modeled as follows:

$$0 \leq |\Delta SoC_{j,t,LF}| \leq \mathrm{CR}_{LF} Z_{j,t,LF}, \quad \forall t \in \mathcal{T}, j \in \mathcal{J} \tag{5.23}$$

$$\mathrm{CR}_{LF} Z_{j,t,MF} < |\Delta SoC_{j,t,MF}| \leq \mathrm{CR}_{MF} Z_{j,t,MF}, \quad \forall t \in \mathcal{T}, j \in \mathcal{J} \tag{5.24}$$

$$\mathrm{CR}_{MF} Z_{j,t,HF} < |\Delta SoC_{j,t,HF}| \leq \mathrm{CR}_{HF} Z_{j,t,HF}, \quad \forall t \in \mathcal{T}, j \in \mathcal{J} \tag{5.25}$$

$$Z_{j,t,LF} + Z_{j,t,MF} + Z_{j,t,HF} \leq 1, \quad \forall t \in \mathcal{T}, j \in \mathcal{J} \tag{5.26}$$

The constraints (5.23) to (5.25) denotes the limits of the changes in SOC of BESSs for service LF, MF, and HF, respectively. The $\Delta SoC_{j,t,s}$ is limited by the maximum rate of change CR_s, as discussed earlier in (5.1). Constraint (5.26) ensures that only a single service, LF, MF, or HF, can be selected at a time.

The above formulation contains some nonlinear terms, as in the objective function (5.8) and the constraints (5.23) to (5.25), which can be easily reformulated as follows [88]:

$$SoC^L_{j,t,s} \geq 0, \quad \forall t \in \mathcal{T}, j \in \mathcal{J} \tag{5.27}$$

$$SoC^L_{j,t,s} \leq SoC_{j,t}, \quad \forall t \in \mathcal{T}, j \in \mathcal{J} \tag{5.28}$$

$$SoC^L_{j,t,s} \leq Z_{j,t,s} M, \quad \forall t \in \mathcal{T}, j \in \mathcal{J} \tag{5.29}$$

$$SoC^L_{j,t,s} \geq SoC_{j,t} - M\,(1 - Z_{j,t,s}), \quad \forall t \in \mathcal{T}, j \in \mathcal{J} \tag{5.30}$$

Constraints (5.27) to (5.30) represent the linearization of the product of the two variables appearing in (5.8): the binary variable ($Z_{j,t,s}$) and the continuous variable ($SoC_{j,t}$). The linearized term is introduced as a positive variable $SoC^{L}_{j,t,s}$. The constraint (5.28) ensures that $SoC^{L}_{j,t,s}$ is less than or equal to $SoC_{j,t}$. In (5.29) and (5.30), $SoC^{L}_{j,t,s}$ is forced to be equal to $SoC_{j,t}$ if $Z_{j,t,s} = 1$; otherwise, $SoC^{L}_{j,t,s}$ equals to zero.

The term $|\Delta SoC_{j,t,s}|$ in (5.23) to (5.25) can be linearly formulated as below [88]:

$$\Delta SoC^{+}_{j,t,s} \geq 0, \Delta SoC^{-}_{j,t,s} \leq 0, \quad \forall t \in \mathcal{T}, j \in \mathcal{J} \tag{5.31}$$

$$|\Delta SoC_{j,t,s}| = \Delta SoC^{+}_{j,t,s} - \Delta SoC^{-}_{j,t,s}, \quad \forall t \in \mathcal{T}, j \in \mathcal{J} \tag{5.32}$$

$$\mathrm{CR}_{s-1}\ \overline{SoC}\ Z^{+}_{j,t,s} < \Delta SoC^{+}_{j,t,s} \leq \mathrm{CR}_{s}\ \overline{SoC}\ Z^{+}_{j,t,s}, \quad \forall t \in \mathcal{T}, j \in \mathcal{J} \tag{5.33}$$

$$-\mathrm{CR}_{s}\ \overline{SoC}\ Z^{-}_{j,t,s} \leq \Delta SoC^{-}_{j,t,s} < -\mathrm{CR}_{s-1}\ \overline{SoC}\ Z^{-}_{j,t,s}, \quad \forall t \in \mathcal{T}, j \in \mathcal{J} \tag{5.34}$$

$$Z^{+}_{j,t,s} + Z^{-}_{j,t,s} \leq Z_{j,t,s}, \quad \forall t \in \mathcal{T}, j \in \mathcal{J} \tag{5.35}$$

Two auxiliary variables are introduced to reformulate the absolute change in SOC; $\Delta SoC^{+}_{j,t,s}$ and $\Delta SoC^{-}_{j,t,s}$ converts the range of the change in SOC to two components. The boundaries of the positive and negative changes in SOC are modeled as in (5.33) and (5.34), respectively. The binary variables $Z^{+}_{j,t,s}$ and $Z^{-}_{j,t,s}$ are used to ensure that either $\Delta SoC^{+}_{j,t,s}$ or $\Delta SoC^{-}_{j,t,s}$ should be zero. Constraint (5.35) coordinates the binary variables of the linearized change in SOC and the binary variable associated with the selected service to be provided.

5.2.4 Allocation of Cost Savings

First, an LDC operations model without any BESS units is executed and the total system cost is determined. Next, the LDC operations model including distributed BESSs, presented in Section 5.2.3, is executed to find the operations cost with the flexibility service provisions from the BESS. The difference between the two system operation costs is the total contribution of the distributed BESSs to system savings.

In this work, the Shapley value criterion [89], which is well known in the literature of

cooperative game theory, is used to allocate the total system savings among the BESSs for their flexibility service provisions, on the basis of their marginal contributions to the savings. This concept provides a unique allocation strategy among the participants in a coalition game [89]. It is assumed that the LDC schedules and dispatches the distributed BESS units. In return, the LDC distributes the savings accrued among the BESSs units. The Shapley value of a cooperative game is given as follows:

$$\phi_h = \frac{1}{n} \sum_{q=1}^{n} \frac{1}{c(q)} \sum_{h \in H} v(h) \tag{5.36}$$

where,

$$v(h) = v(H) - v(H - h) \tag{5.37}$$

$$c(q) = \frac{(n-1)!}{(n-q)!(q-1)!} \tag{5.38}$$

The second summation in (5.36) represents the sum of all marginal contributions of a BESS h to all possible subsets of BESS units H, which is obtained from (5.37). The first summation calculates the number of all formed coalitions of size q that contains the BESS h, and n is the total number of BESSs, as in (5.38).

From the above discussions, the notion of contribution of the BESSs to system savings can be utilized to develop a financial compensation scheme for their flexibility service provisions. The payment for flexibility services by a BESS unit can be represented as follows:

$$\rho_h = f_h + \phi_h \tag{5.39}$$

Equation (5.39) includes two components: a fixed payment component f_h, and a variable payment component ϕ_h. The fixed payment can be payable to the BESS for participating, collaborating and providing control access to their flexible asset to the LDC. The BESSs would receive this component of payment even if the LDC keeps a BESS unit in idle mode. The variable component of payment in (5.39) would be a

function of the contribution of BESS h to the system savings, as obtained using the Shapley value criterion.

5.3 Results and Discussions

In this example, the LDC is responsible for managing a 33-bus distribution system, the same as that used in the previous chapters [90], and meeting the demand of its customers. It is assumed that three investor-owned BESS units are located at buses $j = 2,\ 23, \text{and } 30$, which is in line with the findings of optimal BESS placement from the previous chapter; they are sized 800 kW/200 kWh, 2400 kW/600 kWh, and 3200 kW/800 kWh, respectively. The LDC aims to minimize its total operation cost, given in (5.8) which includes the cost of flexible operation of the BESSs. The following scenarios have been analyzed:

- SC-1: Normal operation with a typical given HEP profile.
- SC-2: Sudden 100% increase in HEP in the interval 1-2 PM.
- SC-3: Sudden 30% increase in system demand during the interval 8-9 PM, which is close to the peak-load hour of the system.

The total system load profile and the HEP profile over an operation day of August 1, 2018, are shown in Figure 5.4 and 5.5, respectively. The system peak demand is 0.4 p.u., which is equivalent to 4 MW. Shown in Figure 5.5, the HEP varies over the day between 1.2 and 2.2 \$/kWh.

5.3.1 Calculation of Shapley Value of BESS Investors

LF Service

In this subsection only the LF service from BESSs is considered in the SC-1 (normal operation) scenario, in order to demonstrate in detail the calculation of the Shapley values from the system savings and the marginal contributions of the BESSs. First, the LDC

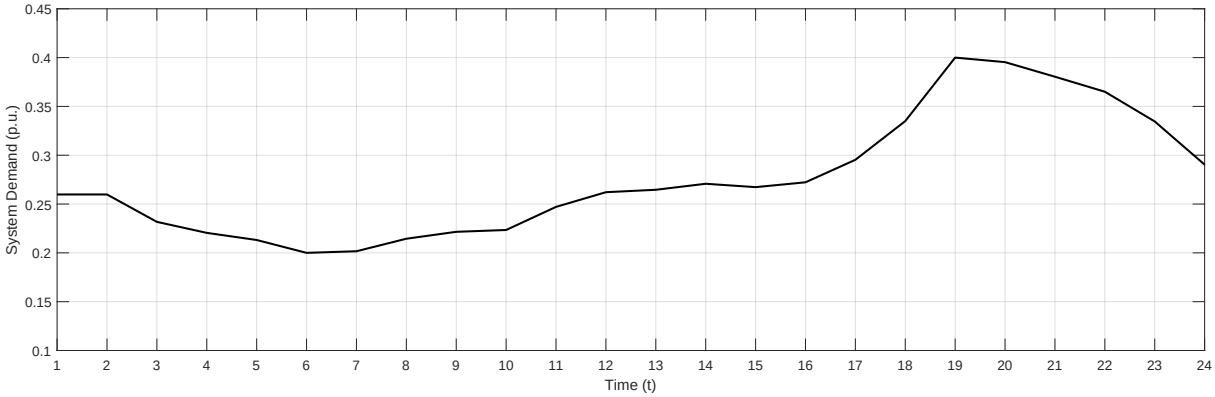

Figure 5.4: Load profile of the LDC over a day.

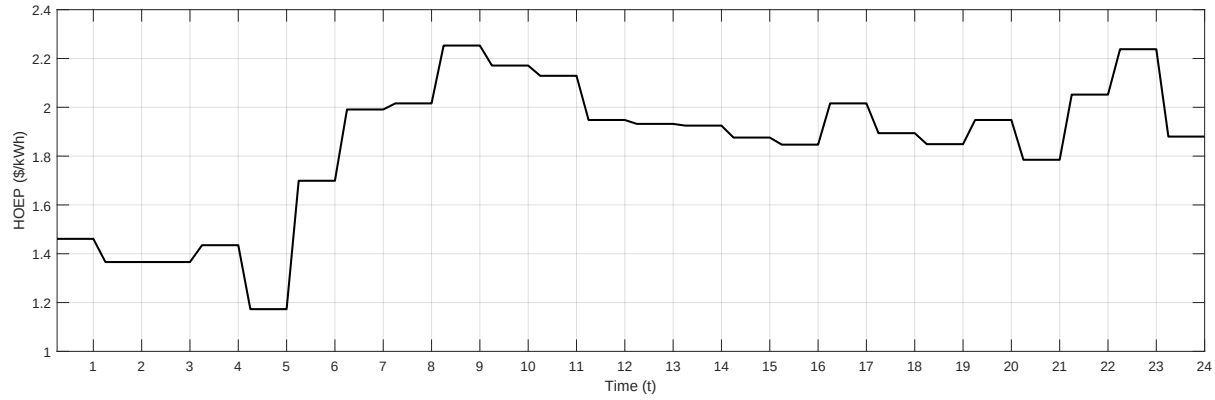

Figure 5.5: HEP profile over a day.

operations model (i.e. (5.8) to (5.35)) is executed considering all possible BESS coalitions to calculate their contribution to the total system savings. As stated earlier, three BESS units (B-2, B-23 and B-30) are participating in LF service provisions, and hence they can form one of the seven different coalitions, as presented below:

$$H = \{\text{B-2}\}\ V\ \{\text{B-23}\}\ V\ \{\text{B-30}\}\ V\ \{\text{B-2,B-23}\}\ V\ \{\text{B-23,B-30}\}\ V\ \{\text{B-30,B-2}\}\ V\ \{\text{B-2,B-23,B-30}\} \quad (5.40)$$

After executing the LDC operations model, the total system savings for each coalition is reported in Table 5.2. The savings accrued from single-facility coalitions namely, B-2, B-23, and B-30 operating independently, are \$30, \$117, and \$153, respectively. The BESS units can also form paired coalitions such as B-2, B-23, B-23, B-30, and B-30, B-2, which accrues total system savings of \$139, \$244, and \$176, respectively. Also, in the grand coalition when all BESS units are operating simultaneously, the total system savings is \$266. It should be noted that the total system savings are calculated with reference to the LDC system operation cost when there are no BESSs.

Table 5.2: Total Savings in a BESS Coalition for LF Service

Coalition (H)	Total System Savings (\$)
B-2	30
B-23	117
B-30	153
B-2, B-23	139
B-23, B-30	244
B-30, B-2	176
B-30, B2, B-23	266

From the knowledge of total system savings in each coalition, the marginal contribution of a BESS unit can be determined. Table 5.3 presents the marginal contributions of B-2 to each coalition in which it can be part of; these are obtained by subtracting the savings of

the coalition without B-2 from the savings obtained from a coalition in which B-2 is part of. The corresponding Shapley value of B-2 for the LF service is obtained as \$25. Similar to the calculations shown in Table 5.3, Shapley values can be calculated for other BESS units B-23 and B-30 as well, as shown in Table 5.4 and 5.5. It should be noted that the sum of the Shapley values of all BESS units for a given service, should be equal to the total system savings achieved in the grand coalition. For instance, the sum of the Shapley values for the three BESS units in the present example, for the LF service provisions, is \$25 + \$102 + \$139 = \$266, which is the savings accrued in the grand coalition, as noted from 5.2.

Table 5.3: Marginal Contributions and Shapley Value Calculation for BESS B-2

Coalition (H)	Marginal Contribution of B-2 in coalition H $v(h) = v(H) - v(H-h)$	Weight on H $\frac{1}{n}\frac{1}{c(H)}$
B-2	\$30 - \$0 = \$30	1/3
B-2, B-23	\$139 - \$117 = \$22	1/6
B-2, B-30	\$176 - \$153 = \$23	1/6
B-2, B23, B-30	\$266 - \$244 = \$22	1/3
Shapley Value (\$)	30/3 + 22/6 + 23/6 + 22/3 ≈ \$25	

Table 5.4: Marginal Contributions and Shapley Value Calculation for BESS B-23

Coalition (H)	Marginal Contribution of B-23 in coalition H $v(h) = v(H) - v(H-h)$	Weight on H $\frac{1}{n}\frac{1}{c(H)}$
B-23	\$117 - \$0 = \$117	1/3
B-23, B-2	\$139 - \$30 = \$109	1/6
B-23, B-30	\$244- \$153 = \$91	1/6
B23, B-2, B-30	\$266 - \$176 = \$90	1/3
Shapley Value (\$)	117/3 + 109/6 + 91/6 + 90/3 ≈ \$102	

Table 5.5: Marginal Contributions and Shapley Value Calculation for BESS B-30

Coalition (H)	Marginal Contribution of B-30 in coalition H $v(h) = v(H) - v(H-h)$	Weight on H $\frac{1}{n}\frac{1}{c(H)}$
B-30	\$153 - \$0 = \$153	1/3
B-30, B-2	\$176 - \$30 = \$145	1/6
B-30, B-23	\$244 - \$117 = \$127	1/6
B-30, B-2, B-23	\$266 - \$139 = \$126	1/3
Shapley Value (\$)	153/3 + 145/6 + 127/6 + 126/3 ≈ \$139	

MF and HF Services

This subsection discusses the provision of LF, MF, and HF services being available individually, for scenario SC-1. Table 5.6 presents the savings accrued in the grand coalition of the BESSs for each of these services, and a fourth case when all the flexibility services are available simultaneously – but only one of them is selected. It is noted that the grand coalition savings for service LF are very close to that when all services are provided simultaneously. This implies that the LF service is the most selected service while MF or HF only leads to a reduction in the total savings. Also note that when all services are available simultaneously, the grand coalition savings are the highest. Similar to the discussion presented in Section 5.3.1, Tables 5.7, 5.8, and 5.9 present the marginal contributions and allocations of savings among B-2, B-23, and B-30, respectively.

Table 5.6: Grand Coalition Savings for a given Flexibility Service

Service Provided	Grand Coalition Savings (\$)
LF Only	266
MF Only	247
HF Only	184
LF & MF & HF Available Simultaneously	267

As seen from the tables, the size of the BESS plays a crucial role in its marginal contribution. The BESS B-2, for example, represents 12.5% of the total installed BESS capacity, and receives the lowest share of savings, and correspondingly the Shapley value

Table 5.7: Allocation of Saving of BESS B-2 (800 kW/200 kWh)

Coalition (H)	Marginal Contribution of B-2 $v(h) = v(H) - v(H-h)$				Weight on H $\frac{1}{n}\frac{1}{c(H)}$
	LF ($)	MF ($)	HF ($)	ALL ($)	
B-2	30	22	18	30	1/3
B-2, B-23	23	21	23	23	1/6
B-2, B-30	23	28	27	23	1/6
B-2, B-23, B-30	22	22	18	22	1/3
Shapley Value ($)	25	23	20	25	

Table 5.8: Allocation of Saving of BESS B-23 (2400 kW/600 kWh)

Coalition (H)	Marginal Contribution of B-23 $v(h) = v(H) - v(H-h)$				Weight on H $\frac{1}{n}\frac{1}{c(H)}$
	LF ($)	MF ($)	HF ($)	ALL ($)	
B-23	117	103	64	120	1/3
B-23, B-2	109	102	69	112	1/6
B-23, B-30	91	98	82	92	1/6
B-23, B-2, B-30	90	92	73	91	1/3
Shapley Value ($)	102	98	71	104	

Table 5.9: Allocation of Saving of BESS B-30 (3200 kW/800 kWh)

Coalition (H)	Marginal Contribution of B-30 $v(h) = v(H) - v(H-h)$				Weight on H $\frac{1}{n}\frac{1}{c(H)}$
	LF ($)	MF ($)	HF ($)	ALL ($)	
B-30	153	128	85	160	1/3
B-30, B-2	145	134	93	152	1/6
B-30, B-23	127	122	102	131	1/6
B-30, B-2, B-23	126	123	97	131	1/3
Shapley Value ($)	139	126	93	144	

Table 5.10: Share of Savings Among BESSs

BESS	Shapley Value ($)			Share in Total Savings (%)			Average of the Share in Total Savings (%)
	LF	MF	HF	LF	MF	HF	
B-2	25	23	20	9.4	9.3	10.9	9.8
B-23	102	98	71	38.4	39.7	38.6	38.9
B-30	139	126	93	52.2	51	50.5	51.2

* Capacity share of B-2: 12.5%, B-23: 37.5%, B-30: 50%

of BESS B-2 approximately equals its percentage share of installed capacity within the distribution system.

Table 5.10 presents the distribution of savings among the BESS units using the Shapley value criterion for individual flexibility services. Each of the BESS unit's share in total savings for LF service is obtained by dividing the corresponding Shapley values by the savings in the grand coalition (i.e. $266), as reported in Table 5.6. Similarly, the BESS unit's share in total savings for MF and HF services are obtained by dividing the corresponding Shapley values by the savings in the grand coalition (i.e. $247 and $184, respectively), obtained from Table 5.6. The averages of the share in total savings considering all the services, for B-2 is 9.8%, for B-23 is 38.9% and for B-30 is 51.2%. It is noted that these average shares in savings are in line with their capacity shares of 12.5%, 37.5%, and 50% with reference to the total BESS capacity in the system. It may be inferred that B-30 has the highest impact on total system flexibility since it has the largest share in system savings.

5.3.2 Operational Performance of BESS Flexibility Services in Different Scenarios

Figure 5.6 shows the operation of the BESSs for different flexibility services; the changes in the SOC are presented for every 15 min operating interval. It is noted from Figure 5.6(a) that the increments/decrements in SOC with the LF service are smaller than other

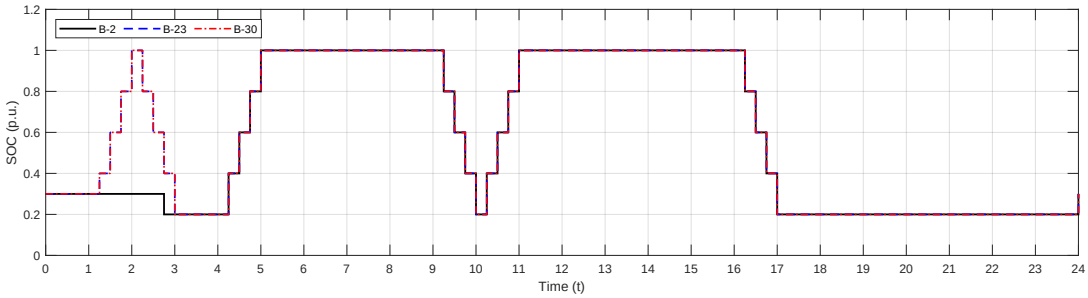

(a) LF

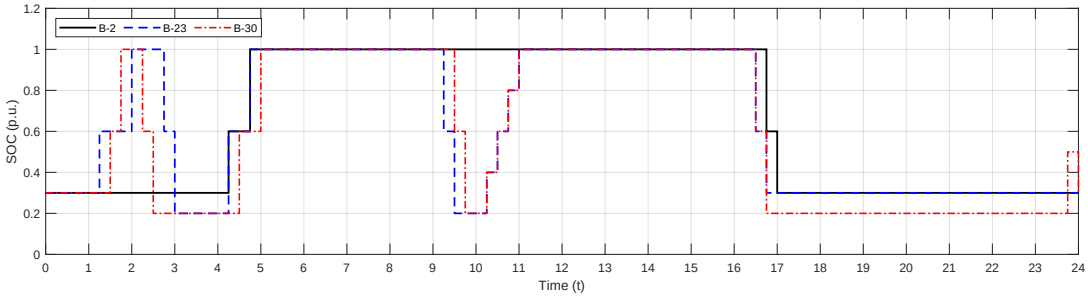

(b) MF

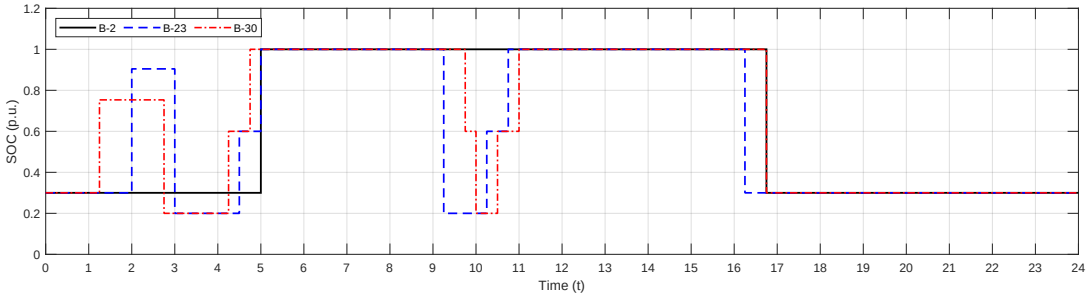

(c) HF

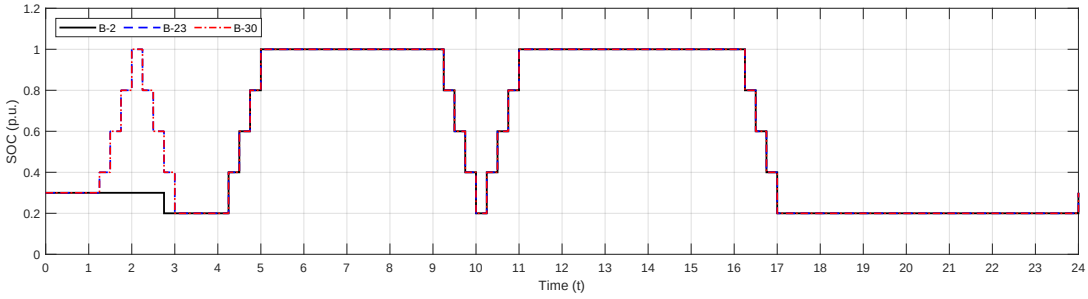

(d) All Services

Figure 5.6: SOC of BESSs providing different flexibility services in Scenario SC-1.

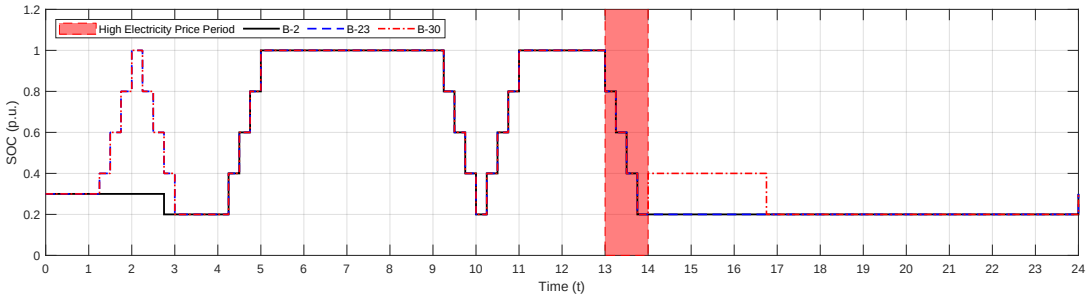

(a) LF

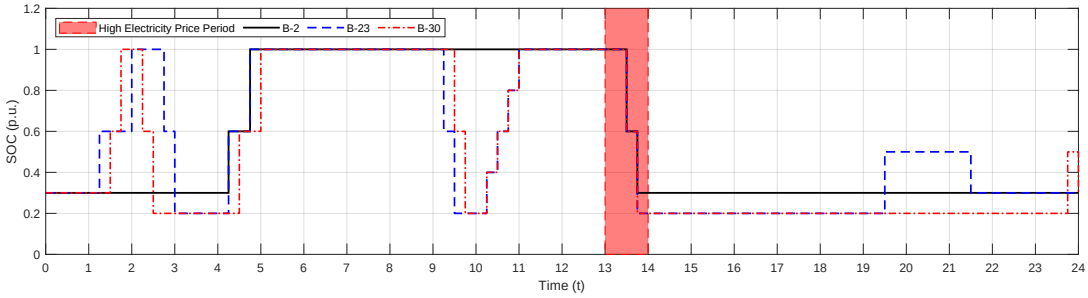

(b) MF

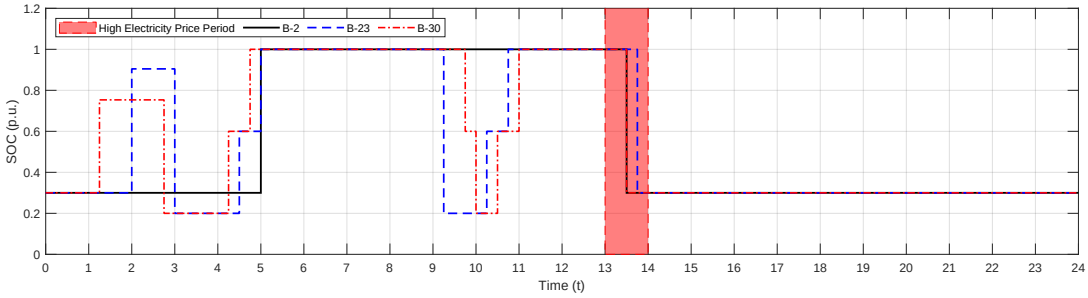

(c) HF

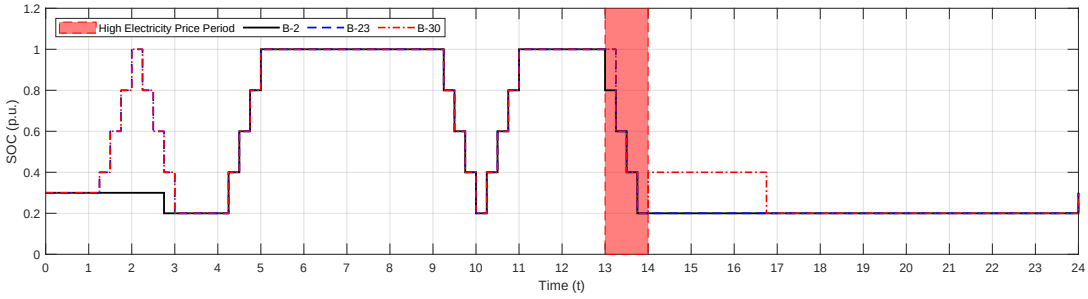

(d) All Services

Figure 5.7: SOC of BESSs for different flexibility services in Scenario SC-2.

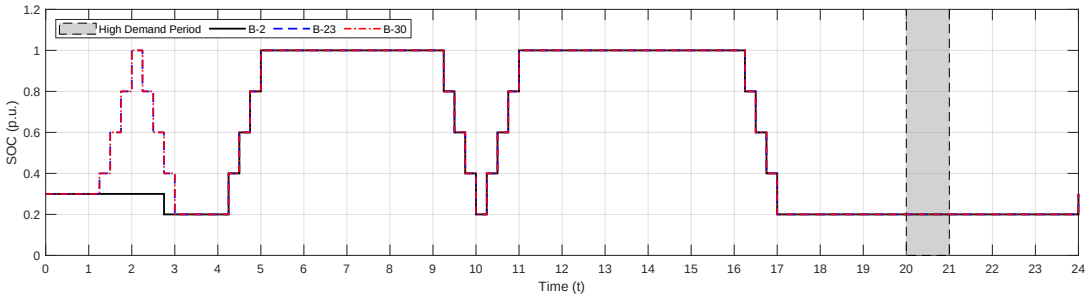

(a) LF

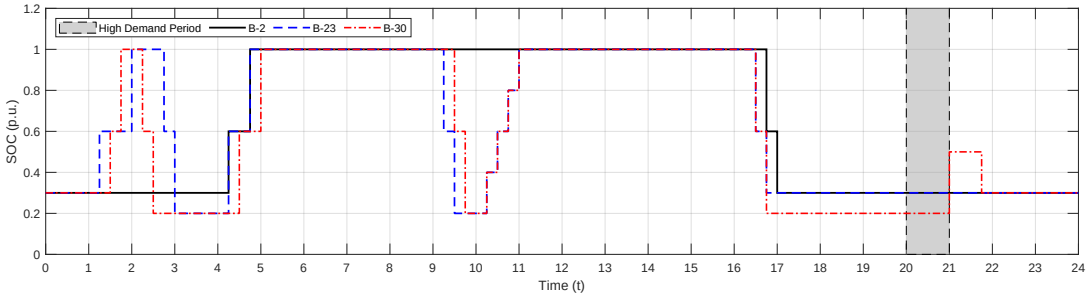

(b) MF

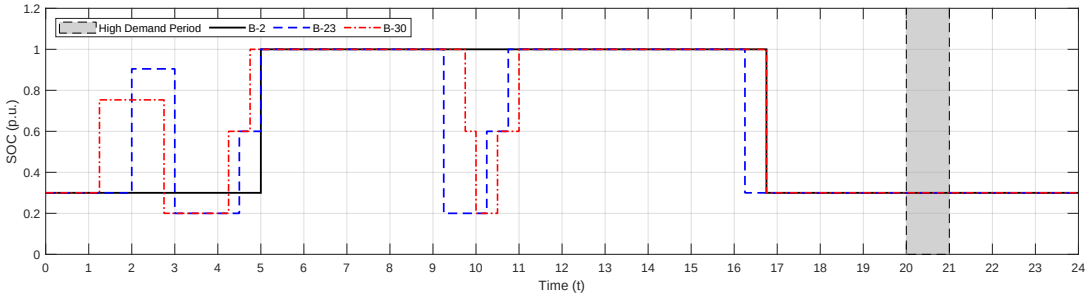

(c) HF

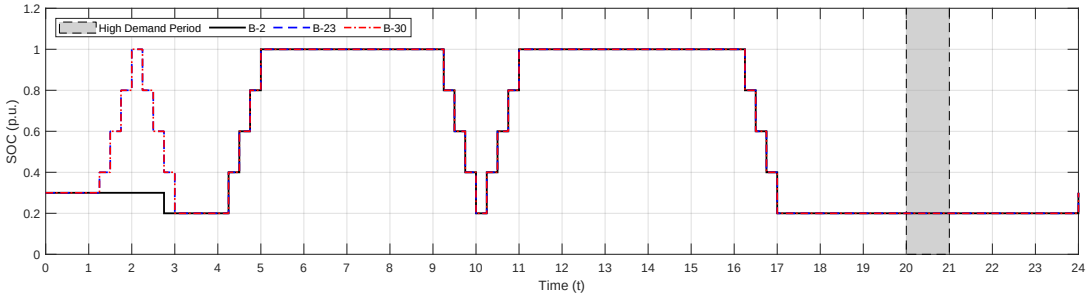

(d) All Services

Figure 5.8: SOC of BESSs for different services in Scenario SC-3.

services. For example, all the batteries require an hour to fully discharge between 9 to 10 AM when providing LF service, while B-23 and B-30 requires only 30 minutes to fully discharge, when providing MF service. The fastest response is noted in HF service, when B-23 and B-30 discharges from high to low SOC in 15 minutes (Fig. 5.6(c)). Each service impacts the total operation cost of the BESS. The need for larger changes in the SOC in a short time results in a high degradation cost of the BESS, as given in (5.8).

Figure 5.7 shows the operation of BESS B-30 in scenario SC-2 which assumes a 100% increase in the HEP between 1-2 PM, from its price reported in Fig. 5.5. The operation of the BESS units are exactly identical to scenario SC-1 until the price spike has occurred at 1 PM, after which the flexibility services come into play. It is noted that all the BESS units are discharged fully during the period of price spike in the LF service or when all services are provided simultaneously. In the case of MF service B-23 and B-30 are fully discharged, while B-2 is discharged to 30% SOC within 30 min, as noted in Fig. 5.7(b). In the case of HF service all the BESS units are discharged to 30% SOC within 15 min, as noted in Fig. 5.7(c). Finally, Figure 5.7(d) shows that when all the services are available simultaneously, 80% of the BESS stored energy is depleted during the price spike interval, and the LF service is primarily selected over the other services.

In should be noted that since the overall objective of the LDC is to minimize its system operation cost, the BESS units discharge when the price spike occurs in order to reduce the amount of power purchased from the external grid at the high price while supplying the LDC demand internally, thereby maximizing the savings.

In scenario SC-3 the LDC system demand during hour 20-21 increases by 30%. It is again assumed that the BESS operations until that point of time were identically following the base-case operation of the day-ahead, as was determined from scenario SC-1 (Figure 5.6) and that all the BESS units were at low SOC levels at hour-20. When the demand spike occurs, if the BESS units would start charging in order to discharge and meet the demand spike, it would create an instantaneous further increase in demand which would be detrimental for the system. Hence, the BESS units continue to stay idle at their low SOC levels, and do not provide any flexibility services, as shown in Fig. 5.8.

5.4 Summary

In this chapter, a novel flexibility services framework was developed based on the capabilities of BESSs in providing different C-Rate levels, namely, low flexibility (LF), moderate flexibility (MF), and high flexibility (HF). A novel mathematical model was proposed, from the perspective of the LDC, to optimally procure the LF, MF and HF services in the operations horizon. This model included a degradation cost formulation of the BESS units based on the new flexibility services definitions proposed. Thereafter, a cooperative game-theory based approach was applied wherein the Shapley value criterion was used to allocate the total system savings among the flexible BESS asset owners, and hence a pricing scheme for flexibility services was developed. The proposed approach ensured that the flexible resources were financially compensated based on their marginal contribution to the system savings.

Chapter 6

Conclusions

6.1 Summary

This thesis focused on the flexibility provisions from REHs and BESSs in operation and planning frameworks of distribution systems. Chapter-1 presented the motivation and related literature review relevant to the work presented in the subsequent chapters. In addition, Chapter-1 outlined the main research objectives and finally the overall layout of the thesis.

In Chapter-2, brief overviews of the background topics related to the research objectives were presented. The concept of REH and the mathematical model for the optimal operation of the HEMSs were discussed. The characteristics and various technologies of ESS were discussed along with their applications in smart grids. The RCA was introduced, and followed by a brief introduction on NNs. Also, a brief discussion on cooperative game theory was presented with particular focus on the concept of Shapley value criterion.

In Chapter-3, a novel two-stage scheme was proposed to coordinate the interaction between the large number of REHs and the LDC. A flexibility evaluation approach was developed to quantify the available flexibility from individual REHs. The evaluated flexibility, along with the REHs load profiles were communicated to the LDC in order to study their impact on the distribution grid operation. A new mathematical model was

proposed for the LDC system operator to determine the bus-wise PRRs, which were communicated back to the REHs based on their individual flexibility indices.

The main advantage of the proposed two-stage coordination scheme was the avoidance of a centralized optimization model which would need to optimize thousands of REHs as well as the LDC's operations, simultaneously. Therefore, the proposed scheme disaggregated and distributed the computational burden amongst each entity in the distribution grid.

In Chapter-4, a novel NN-based SoH estimator was developed considering the presence of a large cluster of REHs, as introduced in Chapter-3, and a large data set of BESS operations, simulated to mimic the LDC's behavior in controlling these units. Subsequently, the obtained structure of the NN was converted to a functional relationship, which was incorporated within a BESS planning problem. The weights and biases of the mathematical representation of the NN were updated iteratively to improve the plan decisions. The proposed approach showed high accuracy in estimating the SoH of the BESS. Different case studies were carried out to investigate the impact of neglecting calendar and cycle aging and under / over-estimation of the BESS capacity on the LDC's plan decisions. In addition, several scenarios were simulated to study the influence of the load mix and PV penetration on battery degradation.

In Chapter-5, new definitions for flexibility services from BESS units were developed, namely, low flexibility (LF), moderate flexibility (MF), and high flexibility (HF) services. The impact of each of these services on the BESS degradation cost were captured and modeled. A novel LDC operation model was proposed to optimally procure the LF, MF and HF services while taking into account the degradation cost model. Thereafter, the Shapley value criterion was applied to allocate the total system savings among the BESS units for their respective services. The proposed approach ensured that the flexible resources were financially rewarded based on their marginal contribution to the system savings.

The following conclusions can be drawn from the thesis:

- The presence of a large number of uncoordinated REHs can reshape the total load of the distribution system and might result in a high peak-to-average power ratio. Studies revealed that the procurement of flexibility from REHs significantly

enhanced the grid operational efficiency, reduced peak demand, and minimized the power system losses.

- The integration of BESSs in the distribution grid can significantly contribute to the LDC's operational flexibility. However, it is important to consider their SoH while making operational and planning decisions. The proposed novel BESS degradation model integrated within the BESS planning problem presented a very accurate estimate of the batteries' SoH. This helped the LDC in avoiding under / over-estimation of the BESSs available capacity during the operation phase, and the required rated power and energy capacity in the planning phase.

- Scenario studies were carried out to analyze the impact of load mix on the plan decisions and the degradation of BESSs. Load profiles with extended duration peaks resulted in a larger installed capacity of BESSs. The studies also revealed that the level of PV penetration significantly reduced the required rated capacity of batteries. Although the considered system load profile had a peak during the daytime, because of the presence of REHs, the system peak demand was shifted and did not coincide with the peak power generation from the PV panels, hence requiring lesser installation capacity of BESS.

- Studies revealed that BESSs can provide flexibility services to the LDC particularly during demand and price spikes. The contribution of a BESS unit to flexibility was noted to be proportional to its capacity share in total installed capacity.

6.2 Contributions

The main contributions of the research presented in this thesis can be summarized as follows:

- The mathematical model of the REH, previously reported, was extensively improved by taking into account a comprehensive set of individual appliance operation models and their optimal operation, considering the customer's preferences, behavior, and objectives.

- A new REH model was presented considering different levels of interactions in terms of power interchanges between several devices internally within the REH and externally with the LDC.
- A novel concept of residential load flexibility was proposed and hence a flexibility index was defined to quantify the available flexibility from an REH, aggregated from that provided by various appliances, ESS, and PV panel.
- A novel two-stage coordination scheme and associated novel models of the REH and LDC were proposed that took into account distinctly individual objectives of each HEMS as well as that of the LDC, seeking to enhance the grid operational efficiency, and create an aggregated flexibility provision for the system.
- A novel NN based degradation model was proposed to estimate the SoH of Li-ion batteries of an BESS by considering a large data set of BESS operations for NN training. This data set was obtained by simulating the LDC operations in controlling the BESS in the presence of a large cluster of uncoordinated REH loads.
- The proposed SoH model of the BESS was incorporated into the planning model to determine the optimal energy capacity, power rating, location and year of installation / replacement of BESSs while internalizing battery capacity degradation due to cycling and aging effects.
- A novel flexibility services framework was developed based on the capabilities of BESSs in providing different C-Rate levels, namely, low flexibility (LF), moderate flexibility (MF), and high flexibility (HF). A novel mathematical model was proposed, from the perspective of the LDC, to optimally procure the LF, MF and HF services in the operations horizon.
- A cooperative game theory based approach was applied to allocate the accrued financial benefits among the BESS units for their flexibility services. The Shapley value was applied to fairly distribute the total savings from the BESS flexibility provision based on their individual marginal contributions, and hence a new pricing scheme for flexibility services was proposed.

6.3 Future Work

Based on the work presented in this thesis, the following issues can be examined in the future:

- With the increase in PEV penetration, there is a need to consider their smart charging and how they impact the system operation. This involves optimizing the PEV charging load in the REHs to minimize the customer's cost. It is also worth investigating the effect of smart charging PEVs on the flexibility provided by an REH.
- The study of flexibility of smart loads and BESSs need be extended further to examine their impact on the reliability of the distribution system.
- The proposed SoH estimation approach can be incorporated within the bids / offers of BESS units and included within electricity market settlement models.
- The BESS flexibility service provision framework can be improved to take into account the impact of uncertainty in demand and electricity prices on the BESS operation by incorporating model predictive control approach.
- The proposed flexibility services framework can be extended to be included as products for trading within a wholesale electricity market auction model.

References

[1] International Energy Agency, "World energy outlook 2020," IEA, Tech. Rep., 2020. [Online]. Available: www.iea.org/reports/world-energy-outlook-2020

[2] Independent Electrcity System Operator, "Options for the future of peaksaverplus® residential demand response." [Online]. Available: www.ieso.ca/-/media/files/ieso/document-library/sac/2016/sac-20160210-peaksaverplus-presentation.pdf?la=en

[3] Independent Electricity System Operator, "Global adjustment (ga)." [Online]. Available: www.ieso.ca/power-data/price-overview/global-adjustment

[4] Federal Energy Regulatory Commission, "Assessment of demand response and advanced metering." [Online]. Available: www.ferc.gov/sites/default/files/2020-04/09-07-demand-response.pdf

[5] E. Lannoye, D. Flynn, and M. O'Malley, "Evaluation of power system flexibility," *IEEE Trans. Power Syst.*, vol. 27, no. 2, pp. 922–931, May 2012.

[6] N. Ruiz, I. Cobelo, and J. Oyarzabal, "A direct load control model for virtual power plant management," *IEEE Trans. Power Syst.*, vol. 24, no. 2, pp. 959–966, May 2009.

[7] P. Favre-Perrod, "A vision of future energy networks," in *2005 IEEE Power Engineering Society Inaugural Conference and Exposition in Africa*, July 2005, pp. 13–17.

[8] M. Geidl, G. Koeppel, P. Favre-Perrod, B. Klockl, G. Andersson, and K. Frohlich, "Energy hubs for the future," *IEEE Power and Energy Magazine*, vol. 5, no. 1, pp. 24–30, Jan 2007.

[9] Ontario's Independent Electricity System Operator. *IESO York Region Non Wires Alternatives Demonstration Project*. Accessed: Feb. 15, 2021. [Online]. Available: https://www.ieso.ca/en/Sector-Participants/Engagement-Initiatives/Engagements/IESO-York-Region-Non-Wires-Alternatives-Demonstration-Project

[10] Federal Energy Regulatory Commission. *FERC Order No. 2222: A New Day for Distributed Energy Resources*. Accessed: Feb. 15, 2021. [Online]. Available: https://www.ferc.gov/media/ferc-order-no-2222-fact-sheet

[11] Independent, Electricity Market Operator, "18 month outlook: An assessment of the reliability and operability of the ontario electricity system," 2018.

[12] Canadian Energy Research Institute, "Electricity storage systems: Applications and business cases," 2019. [Online]. Available: https://ceri.ca/assets/files/Study_180_Full_Report.pdf

[13] W. J. Cole and A. Frazier, "Cost projections for utility-scale battery storage," National Renewable Energy Lab.(NREL), Golden, CO (United States), Tech. Rep., 2019.

[14] K. Abdulla, J. de Hoog, V. Muenzel, F. Suits, K. Steer, A. Wirth, and S. Halgamuge, "Optimal operation of energy storage systems considering forecasts and battery degradation," *IEEE Transactions on Smart Grid*, vol. 9, no. 3, pp. 2086–2096, 2018.

[15] A. H. Mohsenian-Rad and A. Leon-Garcia, "Optimal residential load control with price prediction in real-time electricity pricing environments," *IEEE Trans. Smart Grid*, vol. 1, no. 2, pp. 120–133, Sept 2010.

[16] M. Pedrasa, E. Spooner, and I. MacGill, "Robust scheduling of residential distributed energy resources using a novel energy service decision-support tool," in *Innovative Smart Grid Technologies (ISGT), 2011 IEEE PES*, Jan 2011, pp. 1–8.

[17] J. H. Yoon, R. Baldick, and A. Novoselac, "Dynamic demand response controller based on real-time retail price for residential buildings," *IEEE Trans. Smart Grid*, vol. 5, no. 1, pp. 121–129, Jan 2014.

[18] Y. Wang, X. Lin, and M. Pedram, "Adaptive control for energy storage systems in households with photovoltaic modules," *IEEE Trans. Smart Grid*, vol. 5, no. 2, pp. 992–1001, March 2014.

[19] Y. Ozturk, D. Senthilkumar, S. Kumar, and G. Lee, "An intelligent home energy management system to improve demand response," *IEEE Trans. Smart Grid*, vol. 4, no. 2, pp. 694–701, June 2013.

[20] ——, "An intelligent home energy management system to improve demand response," *IEEE Trans. Smart Grid*, vol. 4, no. 2, pp. 694–701, June 2013.

[21] A. Anvari-Moghaddam, H. Monsef, and A. Rahimi-Kian, "Optimal smart home energy management considering energy saving and a comfortable lifestyle," *IEEE Trans. Smart Grid*, vol. 6, no. 1, pp. 324–332, Jan 2015.

[22] M. Bozchalui, S. Hashmi, H. Hassen, C. Canizares, and K. Bhattacharya, "Optimal operation of residential energy hubs in smart grids," *IEEE Trans. Smart Grid*, vol. 3, no. 4, pp. 1755–1766, Dec. 2012.

[23] A.-H. Mohsenian-Rad, V. Wong, J. Jatskevich, R. Schober, and A. Leon-Garcia, "Autonomous demand-side management based on game-theoretic energy consumption scheduling for the future smart grid," *IEEE Trans. Smart Grid*, vol. 1, no. 3, pp. 320–331, Dec 2010.

[24] T. H. Chang, M. Alizadeh, and A. Scaglione, "Real-time power balancing via decentralized coordinated home energy scheduling," *IEEE Trans. Smart Grid*, vol. 4, no. 3, pp. 1490–1504, Sept 2013.

[25] A. C. Luna, N. L. Diaz, M. Graells, J. C. Vasquez, and J. M. Guerrero, "Cooperative energy management for a cluster of households prosumers," *IEEE Trans. Consum. Electron*, vol. 62, no. 3, pp. 235–242, August 2016.

[26] T. Logenthiran, D. Srinivasan, and T. Z. Shun, "Demand side management in smart grid using heuristic optimization," *IEEE Trans. Smart Grid*, vol. 3, no. 3, pp. 1244–1252, Sept 2012.

[27] D. Wang, S. Ge, H. Jia, C. Wang, Y. Zhou, N. Lu, and X. Kong, "A demand response and battery storage coordination algorithm for providing microgrid tie-line smoothing services," *IEEE Trans. Sustain. Energy*, vol. 5, no. 2, pp. 476–486, April 2014.

[28] Y. Guo, M. Pan, Y. Fang, and P. Khargonekar, "Decentralized coordination of energy utilization for residential households in the smart grid," *IEEE Trans. Smart Grid*, vol. 4, no. 3, pp. 1341–1350, Sept 2013.

[29] G. Brusco, A. Burgio, D. Menniti, A. Pinnarelli, and N. Sorrentino, "Energy management system for an energy district with demand response availability," *IEEE Trans. Smart Grid*, vol. 5, no. 5, pp. 2385–2393, Sept 2014.

[30] Safdarian, A. and Fotuhi-Firuzabad, M. and Lehtonen, M., "A distributed algorithm for managing residential demand response in smart grids," *IEEE Trans. Ind. Informat*, vol. 10, no. 4, pp. 2385–2393, Nov 2014.

[31] A. Safdarian, M. Fotuhi-Firuzabad, and M. Lehtonen, "Optimal residential load management in smart grids: A decentralized framework," *IEEE Trans. Smart Grid*, vol. 7, no. 4, pp. 1836–1845, July 2016.

[32] N. G. Paterakis, O. Erdinç, I. N. Pappi, A. G. Bakirtzis, and J. P. S. Catalão, "Coordinated operation of a neighborhood of smart households comprising electric vehicles, energy storage and distributed generation," *IEEE Trans. Smart Grid*, vol. 7, no. 6, pp. 2736–2747, Nov 2016.

[33] B. Moradzadeh and K. Tomsovic, "Two-stage residential energy management considering network operational constraints," *IEEE Trans. Smart Grid*, vol. 4, no. 4, pp. 2339–2346, Dec 2013.

[34] K. McKenna and A. Keane, "Residential load modeling of price-based demand response for network impact studies," *IEEE Transactions on Smart Grid*, vol. 7, no. 5, pp. 2285–2294, Sept 2016.

[35] K. Hartwig and I. Kockar, "Impact of strategic behavior and ownership of energy storage on provision of flexibility," *IEEE IEEE Trans. Sustainable Energy*, vol. 7, no. 2, pp. 744–754, April 2016.

[36] J. Ponocko and J. V. Milanovic, "Forecasting demand flexibility of aggregated residential load using smart meter data," *IEEE Trans. Power Syst.*, 2018.

[37] A. Anvari-Moghaddam, H. Monsef, and A. Rahimi-Kian, "Optimal smart home energy management considering energy saving and a comfortable lifestyle," *IEEE Trans. Smart Grid*, vol. 6, no. 1, pp. 324–332, Jan 2015.

[38] O. Kilkki, A. Alahäivälä, and I. Seilonen, "Optimized control of price-based demand response with electric storage space heating," *IEEE Trans Ind. Informat*, vol. 11, no. 1, pp. 281–288, Feb 2015.

[39] V. C. Cunha, R. Torquato, T. R. Ricciardi, W. Freitas, and B. Venkatesh, "Assessing energy storage potential to facilitate the increased penetration of photovoltaic generators and electric vehicles in distribution networks," in *2017 IEEE Power Energy Society General Meeting*, July 2017, pp. 1–5.

[40] R. Li, W. Wang, and M. Xia, "Cooperative planning of active distribution system with renewable energy sources and energy storage systems," *IEEE Access*, vol. 6, pp. 5916–5926, 2018.

[41] S. Wen, H. Lan, Q. Fu, D. C. Yu, and L. Zhang, "Economic allocation for energy storage system considering wind power distribution," *IEEE Trans. Power Syst.*, vol. 30, no. 2, pp. 644–652, 2015.

[42] M. Sedghi, A. Ahmadian, and M. Aliakbar-Golkar, "Optimal storage planning in active distribution network considering uncertainty of wind power distributed generation," *IEEE Trans. Power Syst.*, vol. 31, no. 1, pp. 304–316, 2016.

[43] A. S. A. Awad, T. H. M. EL-Fouly, and M. M. A. Salama, "Optimal ess allocation for load management application," *IEEE Trans. Power Syst.*, vol. 30, no. 1, pp. 327–336, 2015.

[44] H. Hamidpour, J. Aghaei, S. Pirouzi, S. Dehghan, and T. Niknam, "Flexible, reliable, and renewable power system resource expansion planning considering energy storage systems and demand response programs," *IET Renewable Power Generation*, vol. 13, no. 11, pp. 1862–1872, 2019.

[45] H. Akhavan-Hejazi and H. Mohsenian-Rad, "Energy storage planning in active distribution grids: A chance-constrained optimization with non-parametric probability functions," *IEEE Trans. Smart Grid*, vol. 9, no. 3, pp. 1972–1985, May 2018.

[46] F. Luo, K. Meng, Z. Y. Dong, Y. Zheng, Y. Chen, and K. P. Wong, "Coordinated operational planning for wind farm with battery energy storage system," *IEEE Trans. Sustainable Energy*, vol. 6, no. 1, pp. 253–262, 2015.

[47] T. Qiu, B. Xu, Y. Wang, Y. Dvorkin, and D. S. Kirschen, "Stochastic multistage coplanning of transmission expansion and energy storage," *IEEE Trans. Power Syst.*, vol. 32, no. 1, pp. 643–651, Jan 2017.

[48] H. Alharbi and K. Bhattacharya, "Stochastic optimal planning of battery energy storage systems for isolated microgrids," *IEEE Trans. Sustain. Energy*, vol. 9, no. 1, pp. 211–227, Jan 2018.

[49] I. Alsaidan, A. Khodaei, and W. Gao, "A comprehensive battery energy storage optimal sizing model for microgrid applications," *IEEE Trans. Power Syst.*, vol. 33, no. 4, pp. 3968–3980, 2018.

[50] T. Alharbi, K. Bhattacharya, and M. Kazerani, "Planning and operation of isolated microgrids based on repurposed electric vehicle batteries," *IEEE Trans. Ind. Informat.*, vol. 15, no. 7, pp. 4319–4331, July 2019.

[51] B. Xu, A. Oudalov, A. Ulbig, G. Andersson, and D. S. Kirschen, "Modeling of lithium-ion battery degradation for cell life assessment," *IEEE Trans. Smart Grid*, vol. 9, no. 2, pp. 1131–1140, March 2018.

[52] Y. Jiang, J. Zhang, L. Xia, and Y. Liu, "State of health estimation for lithium-ion battery using empirical degradation and error compensation models," *IEEE Access*, vol. 8, pp. 123 858–123 868, 2020.

[53] X. Tan, Y. Tan, D. Zhan, Z. Yu, Y. Fan, J. Qiu, and J. Li, "Real-time state-of-health estimation of lithium-ion batteries based on the equivalent internal resistance," *IEEE Access*, vol. 8, pp. 56 811–56 822, 2020.

[54] G.-w. You, S. Park, and D. Oh, "Real-time state-of-health estimation for electric vehicle batteries: A data-driven approach," *Applied Energy*, vol. 176, pp. 92–103, 2016.

[55] C. O. Adika and L. Wang, "Non-cooperative decentralized charging of homogeneous households' batteries in a smart grid," *IEEE Trans. Smart Grid*, vol. 5, no. 4, pp. 1855–1863, 2014.

[56] H. M. Soliman and A. Leon-Garcia, "Game-theoretic demand-side management with storage devices for the future smart grid," *IEEE Trans. Smart Grid*, vol. 5, no. 3, pp. 1475–1485, 2014.

[57] W. Tushar, B. Chai, C. Yuen, S. Huang, D. B. Smith, H. V. Poor, and Z. Yang, "Energy storage sharing in smart grid: A modified auction-based approach," *IEEE Transactions on Smart Grid*, vol. 7, no. 3, pp. 1462–1475, 2016.

[58] C. P. Mediwaththe, M. Shaw, S. Halgamuge, D. B. Smith, and P. Scott, "An incentive-compatible energy trading framework for neighborhood area networks with shared energy storage," *IEEE Transactions on Sustainable Energy*, vol. 11, no. 1, pp. 467–476, 2020.

[59] H. Wang and J. Huang, "Incentivizing energy trading for interconnected microgrids," *IEEE Trans. Smart Grid*, vol. 9, no. 4, pp. 2647–2657, 2018.

[60] L. Han, T. Morstyn, and M. McCulloch, "Incentivizing prosumer coalitions with energy management using cooperative game theory," *IEEE Trans. Power Syst.*, vol. 34, no. 1, pp. 303–313, 2019.

[61] C. Feng, F. Wen, S. You, Z. Li, F. Shahnia, and M. Shahidehpour, "Coalitional game-based transactive energy management in local energy communities," *IEEE Trans. Power Syst.*, vol. 35, no. 3, pp. 1729–1740, 2020.

[62] P. Hu, R. Karki, and R. Billinton, "Reliability evaluation of generating systems containing wind power and energy storage," *IET Generation, Transmission Distribution*, vol. 3, no. 8, pp. 783–791, August 2009.

[63] C. E. P. J. CA^{3}rdova, B. Asare-Bediako, G. M. A. Vanalme, and W. L. Kling, "Overview and comparison of leading communication standard technologies for smart home area networks enabling energy management systems," in *2011 46th International Universities' Power Engineering Conference (UPEC)*, 2011, pp. 1–6.

[64] O. Alrumayh and K. Bhattacharya, "Model predictive control based home energy management system in smart grid," in *2015 IEEE Electrical Power and Energy Conference (EPEC)*, Oct 2015, pp. 152–157.

[65] O. Alrumayh, "Optimal coordination of home energy management systems in a distribution grid," Master's thesis, 2016.

[66] S. A. Hashmi, "Evaluation and improvement of the residential energy hub management system," Master's thesis, University of Waterloo, Sept. 2010.

[67] "Ieee guide for the interoperability of energy storage systems integrated with the electric power infrastructure," *IEEE Std 2030.2-2015*, pp. 1–138, June 2015.

[68] R. A. Huggins, *Energy Storage*. Springer, 2010.

[69] M. Aneke and M. Wang, "Energy storage technologies and real life applications – a state of the art review," *Applied Energy*, vol. 179, pp. 350 – 377, 2016. [Online]. Available: www.sciencedirect.com/science/article/pii/S0306261916308728

[70] C. Amzallag, J. Gerey, J. Robert, and J. Bahuaud, "Standardization of the rainflow counting method for fatigue analysis," *International Journal of Fatigue*, vol. 16, no. 4, pp. 287 – 293, 1994. [Online]. Available: www.sciencedirect.com/science/article/pii/0142112394903433

[71] R. Dufo-Lopez, J. L. Bernal-Agustín, and J. Contreras, "Optimization of control strategies for stand-alone renewable energy systems with hydrogen storage," *Renewable energy*, vol. 32, no. 7, pp. 1102–1126, 2007.

[72] E. Telaretti, M. Ippolito, and L. Dusonchet, "A simple operating strategy of small-scale battery energy storages for energy arbitrage under dynamic pricing tariffs," *Energies*, vol. 9, no. 1, p. 12, 2015.

[73] K. Gurney, *An introduction to neural networks*. CRC press, 1997.

[74] C. M. Bishop *et al.*, *Neural networks for pattern recognition*. Oxford university press, 1995.

[75] R. Myerson, "Game theory: Analysis of conflict harvard university," *Press, Cambridge*, 1991.

[76] D. Chattopadhyay, "An energy brokerage system with emission trading and allocation of cost savings," *IEEE Trans. Power Syst.*, vol. 10, no. 4, pp. 1939–1945, 1995.

[77] S. Hart, "Shapley value," in *Game Theory*. Springer, 1989, pp. 210–216.

[78] E. Castillo, A. J. Conejo, P. Pedregal, R. Garcia, and N. Alguacil, *Building and solving mathematical programming models in engineering and science*. John Wiley & Sons, 2011, vol. 62.

[79] Ontario Energy Board. *Electricity Rates*. Accessed: Dec. 15, 2020. [Online]. Available: www.oeb.ca/rates-and-your-bill/electricity-rates

[80] GAMS Development Corporation. *General Algebraic Modeling System (GAMS)*. Accessed: Dec. 15, 2020. [Online]. Available: www.gams.com

[81] O. Alrumayh and K. Bhattacharya, "Flexibility of residential loads for demand response provisions in smart grid," *IEEE Transactions on Smart Grid*, vol. 10, no. 6, pp. 6284–6297, 2019.

[82] H. Yuan, F. Li, Y. Wei, and J. Zhu, "Novel linearized power flow and linearized opf models for active distribution networks with application in distribution lmp," *IEEE Trans. Smart Grid*, vol. 9, no. 1, pp. 438–448, Jan 2018.

[83] Y. Niu and S. Santoso, "Sizing and coordinating fast- and slow-response energy storage systems to mitigate hourly wind power variations," *IEEE Trans. Smart Grid*, vol. 9, no. 2, pp. 1107–1117, 2018.

[84] B. Vatandoust, A. Ahmadian, M. A. Golkar, A. Elkamel, A. Almansoori, and M. Ghaljehei, "Risk-averse optimal bidding of electric vehicles and energy storage aggregator in day-ahead frequency regulation market," *IEEE Trans. Power Syst.*, vol. 34, no. 3, pp. 2036–2047, 2019.

[85] M. H. Beale, M. T. Hagan, and H. B. Demuth, "Neural network toolbox™ user's guide," *The MathWorks*, 2010.

[86] C. Zhou, K. Qian, M. Allan, and W. Zhou, "Modeling of the cost of ev battery wear due to v2g application in power systems," *IEEE Transactions on Energy Conversion*, vol. 26, no. 4, pp. 1041–1050, 2011.

[87] N. Padmanabhan, M. Ahmed, and K. Bhattacharya, "Battery energy storage systems in energy and reserve markets," *IEEE Trans. Power Syst.*, vol. 35, no. 1, pp. 215–226, 2020.

[88] T. S. B.A. McCarl. *Linear Programming Modeling: Nonlinearities and Approximation.* Accessed: Dec. 15, 2020. [Online]. Available: http://agecon2.tamu.edu/people/faculty/mccarl-bruce/mccspr/new09.pdf

[89] A. E. Roth, *The Shapley value: essays in honor of Lloyd S. Shapley.* Cambridge University Press, 1988.

[90] M. E. Baran and F. F. Wu, "Network reconfiguration in distribution systems for loss reduction and load balancing," *IEEE Trans. Power Del.*, vol. 4, no. 2, pp. 1401–1407, 1989.